Study of Electrostatic Charging and Particle Wall Fouling in a Pilot-scale Pressurized Gas-Solid Fluidized Bed up to Turbulent Flow Regime

by

Di Song

uOttawa

Thesis submitted to the Faculty of Graduate and Postdoctoral Studies in partial fulfillment of the requirements for

DOCTOR OF PHILOSOPHY IN CHEMICAL ENGINEERING

Department of Chemical and Biological Engineering
Faculty of Engineering
University of Ottawa

Abstract

In gas-solid fluidized beds, the generation of electrostatic charges due to continuous contacts between fluidizing particles, and the particles and the fluidization vessel wall, is unavoidable. Industrial operations, such as the production of polyethylene, are susceptible to significant operational challenges caused by electrostatics including reactor wall fouling, a problem known as “sheeting”. The formation of particle sheets can require shutdown periods for clean-up which results in significant economic losses. To gain a better understanding of the underlying mechanisms of electrostatic charging in gas-solid fluidized beds, in an attempt to eliminate or minimize this problem, a pilot-scale pressurized gas-solid fluidization system was designed and built, housing an online electrostatic charge measurement technique consisting of two Faraday cups. The system permits the study of the degree of particle wall fouling at pressures and temperatures up to 2600 kPa and 100°C, respectively, and gas velocities up to 1 m/s (covering a range including turbulent flow regime). The system also allowed, for the first time, the measurement of the fluidizing particles’ mass, net charge and size distribution in various regions of the bed, especially those related to the wall coating under the industrially relevant operating conditions of high pressures and gas velocities. Experimental trials were carried out using polyethylene resin received from commercial reactors to investigate the influence of pressure and gas velocity on the bed hydrodynamics and in turn, the degree of bed electrification.

Mechanisms for particle charging, migration and adherence to the column wall were proposed. The size distribution of the gas bubbles shifted towards smaller bubbles as the operating pressure was raised. Thus, higher pressures lead to greater mixing within the bulk of the bed and resulted in a higher degree of particle wall fouling. Moreover, the extent of wall fouling increased linearly with the increase in gas velocity and as the bed transitioned to turbulent regime, due to the increase in particle-wall contacts. Bipolar charging was observed especially within the wall coating with smaller particles being negatively charged. Overall, particle-wall contacts generated negatively charged particles resulting in a net negative charge in the bed, whereas particle-particle contacts generated positively and negatively charged particles resulting in no net charge when entrainment was negligible. The formation of the wall layer and its extent was influenced by the gravitational and drag forces balancing the image force and Coulomb forces (created by the net charge of the bed and the metallic column wall as the attraction between oppositely charged particles).

Résumé

Dans les lits fluidisés gaz-solides, la génération de charges électrostatiques due aux contacts continuels entre les particules de fluidisation, et entre les particules et la paroi de la colonne de fluidisation, est inévitable. Les opérations industrielles, telles que la production de polyéthylène, sont sensibles aux défis opérationnels significatifs causés par l'électrostatique, y compris l'encrassement de la paroi du réacteur, ce qui mène à la formation de couches. La formation de couches peut nécessiter de longues périodes de fermeture pour le nettoyage, ce qui entraîne des pertes économiques importantes. Pour mieux comprendre les mécanismes fondamentaux de la charge électrostatique dans les lits fluidisés gaz-solides et dans une tentative pour éliminer ou minimiser ce problème, un système de fluidisation gaz-solide pressurisé à l'échelle pilote a été conçu et construit, incorporant une technique de mesure de charge électrostatique en ligne, composée de deux cavités de Faraday. Le système a permis d'étudier le degré d'encrassement de la paroi de la colonne à des pressions et températures allant jusqu'à 2600 kPa et 100°C respectivement, et des vitesses de gaz allant jusqu'à 1 m/s (qui couvraient une gamme incluant le régime d'écoulement turbulent). Le système a également permis, pour la première fois, de mesurer la masse, la charge et la distribution de taille des particules dans diverses régions du lit, en particulier, celles liées au revêtement de la paroi pour des conditions d'opération industrielles à des pressions et des vitesses de gaz élevées. En utilisant des résines de polyéthylène provenant de réacteurs commerciaux, des essais expérimentaux ont été effectués pour étudier l'influence de la pression et de la vitesse du gaz sur l'hydrodynamique du lit et le degré d'électrification du lit. Des mécanismes pour la charge des particules, la migration et l'adhérence sur la paroi de la colonne ont été proposés. La distribution de taille des bulles de gaz s'est déplacée vers des bulles plus petites avec l'accroissement de la pression. Ainsi, les pressions plus élevées ont conduit à un plus haut degré de mélange dans le lit et entraînent un degré d'encrassement sur la paroi plus élevé. De plus, le degré d'encrassement sur la paroi a augmenté linéairement avec l'augmentation de la vitesse du gaz, même lorsque le lit a passé au régime turbulent, en raison de l'augmentation des contacts entre les particules et la paroi de la colonne. Une charge bipolaire a été observée notamment dans le revêtement de la paroi avec les plus petites particules chargées négativement. En général, les contacts entre les particules et la paroi de la colonne ont généré des particules chargées négativement résultant en une charge nette négative dans le lit tandis que les contacts entre les particules ont généré des particules chargées positivement et négativement, ne

résultant en aucune charge nette dans le lit lorsque l'entraînement était négligeable. Le degré de formation de la couche sur la paroi a été influencé par la force gravitationnelle et la force de traînée équilibrant la force image et la force colonne (créées par la charge nette du lit et de la colonne métallique ainsi que par l'attraction entre les particules de charges opposées).

Table of Contents

List of Tables

List of Figures

Nomenclature

Symbol	Meaning	Units
d_b	Bubble diameter	m
$d_{b,DP}$	Bubble diameter estimated by differential pressure analysis	cm
$d_{b,IOP}$	Bubble diameter estimated by incoherent part of absolute pressure fluctuations analysis	cm
D_P	The distance between the two tips of the optical fiber probe	m
e	Electric charge of an electron (constant, -1.602×10^{-19} C)	C
E	Electric field	V/m
F	Force	N
g	Gravitational constant	m/s^2
i	Stands for subscript of TH_a and TH_b	–
K	Bubble velocity coefficient	–
$m\%$	Mass percentage of the initial particles	–
q	Electrostatic charge	C
q_{99}	99%-quantile of the data in one optical fiber probe measurement	V
q/m	Net specific charge	μC/kg
r	Distance between two point charges	–
t_1, t_2	Times that the bubble nose reach the bottom and top tips of the optical fiber probe	s
t_3, t_4	Times that the bubble wake leave the bottom and top tips of the optical fiber probe	s

TH_a	Threshold defines the starting and ending points of the bubbles on the optical fiber probe signal	V
TH_b	Threshold defines whether a sudden change on the optical fiber probe signal stands for a bubble passage	V
V_C	Contact potential between the surfaces	eV
U_b	Bubble rise velocity	$\mathrm{m/s}$
U_c	Turbulent transition velocity	$\mathrm{m/s}$
U_k	The velocity that the amplitude bed pressure fluctuation levels off	$\mathrm{m/s}$
U_{mf}	Minimum fluidization velocity	$\mathrm{m/s}$
ε_{mf}	Bed voidage at minimum fluidization velocity	$-$
ε_0	Permittivity of vacuum (constant, 8.85×10^{-12})	$\mathrm{F/m}$
ρ_P	Particle density	$\mathrm{kg/m^3}$
ϕ	Work function	eV
σ_{DP}	Standard deviation of differential pressure fluctuations	Pa
$\sigma_{xy,i}$	Standard deviation of incoherent part of absolute pressure fluctuations	Pa

Acknowledgements

I owe a deep sense of gratitude towards my supervisor, Dr. Poupak Mehrani, for her keen interest on all stages of my research. She expertly guided me in my graduate study in the field of fluidization. Her support and advices greatly contributed in this thesis.

It is my privilege to thank my group members, Fahad Al Amin Chowdhury, Fawzi Salama, Johnny Matta, Marc-André Olivier Séguin, and Ye Tian, for their efforts on this project. I would also like to thank the undergraduate and M. Eng. project students that helped performing the experiments, namely, Ayoub Dayib, Yinhao Zhang, Muhammad Omair Sharif, and Vijay Nag Ellapani. Special thanks to Dr. Andrew Sowinski, who was at the final stage of his Ph.D. program when I started, but continuously contributing his thoughts and time on this project, even after his graduation.

I would also like acknowledge the help from the staff in Department of Biological and Chemical Engineering at the University of Ottawa: Louis Tremblay, Gérard Nina, Franco Ziroldo, Francine Pétrin and Sylvie Saindon for their kindness and assistance.

I would like to thank Natural Sciences and Engineering Research Council (NSERC) of Canada, Canada Foundation for Innovation (CFI), Univation Technologies, LLC (USA) for the financial contributions. Particulate Solid Research Inc., Chicago, USA, is also thanked for providing the optical fiber probe.

Finally, I am extremely thankful to my family, especially my parents and my husband, for their love, understanding, and constant support.

Chapter 1 Introduction

1.1 Introduction

Gas-solid fluidization is a process by which granular material is made to behave like a fluid by an upward flow of gas [1]. Due to excellent characteristics of providing a high degree of heat and mass transfer as well as mixing, fluidization technology has been widely employed in many industries such as petrochemical, oil and gas, food, just to name a few. One problem observed in some gas-solid fluidized beds is the generation of electrostatic charges due to continuous contacts amongst the particles, and between the particles and the fluidization vessel wall. The occurrence of electrostatic charging might lead to significant operational challenges including fluidizing particles adhesion to the reactor wall, particle agglomeration, and electrostatic discharge. One industry that has significantly suffered from negative effects of fluidized bed electrification is the petrochemical industry, where fluidized bed reactors are used for gas-phase ethylene polymerization to produce polyethylene. Commercial gas-solid fluidized bed reactors for polyethylene production are operated in turbulent flow regime at pressures of 2500-3000 kPa and temperatures of 80-110°C [2]. In such reactors, electrostatic charge generation results in catalyst and polyethylene particles to adhere to the reactor wall, causing a problem known as "sheeting" [3]. As the sheets grow thicker, they may dislodge from the reactor wall and clog the distributor plate, leading to frequent reactor shutdown for clean-up. This in turn causes significant economic losses due to the loss in production and high maintenance costs.

The presence of electrostatic charges in gas-solid fluidized beds have been reported for many decades [4] and there have been studies attempting to study this phenomenon for almost as long [5]. However, although there has been some advancement in the understanding of electrostatic charging in fluidized beds and several proposed solutions, the problem persists. The fundamental mechanisms of charge generation and dissipation in gas-solid fluidized beds are poorly understood, particularly when the fluidized particles are insulators, such as polyethylene. This is partly due to complex nature of the fluidization process and that of the electrostatic phenomenon, as well as the current lack of understanding of the fundamental processes underlying electrostatic charging in insulators.

The overall goal of this thesis is to gain a better understanding of the mechanisms of electrostatic charging in gas-phase fluidized bed reactors. To achieve this goal, the focus of this thesis is to carry out an experimental program in relation to polyethylene fluidized bed reactors to study the degree of charge generation and the extent of charged particles wall coating at industrially relevant operating conditions. Although the thesis main focus is on polyethylene gas-solid fluidized bed reactors, the fundamental knowledge gained can be applied to any gas-solid fluidization process found in various industries as well as other gas-solid process such as pneumatic transport that suffer from electrostatic charging.

1.2 Gas-solid fluidization

Gas-solid fluidization is a process commonly employed in many industries for variety of applications such as gas-solid catalytic reactions, mixing, drying, etc. The schematic of a typical gas-solid fluidized bed is shown in Figure 1.1. The fluidizing gas is introduced from the bottom of the bed where it passes through a distributor plate before it reaches the bed of particles. If during the fluidization process, the terminal velocity of particles is lower than the fluidizing gas velocity, these particles will entrain from the fluidization column. Thus, an expanded section is generally added at the top of the fluidization column to reduce the fluidization gas velocity and allowing most of the entrained particles to fall back into the column.

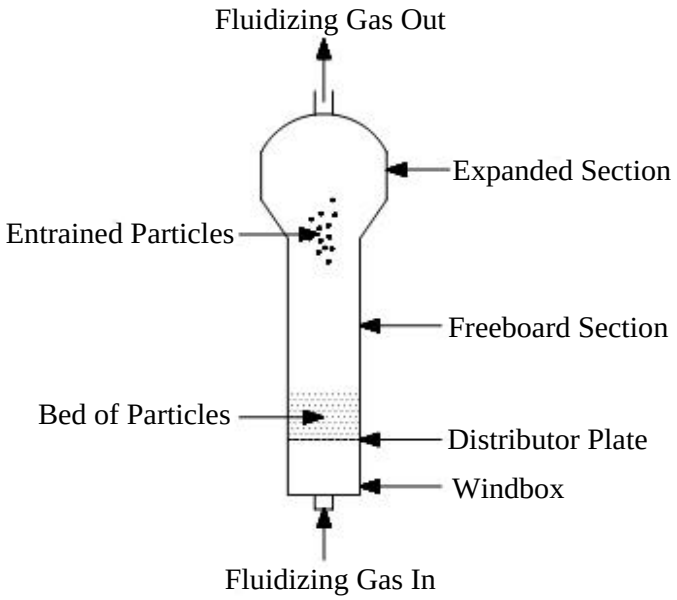

Figure 1.1: Schematic of a typical gas- solid fluidized bed.

In gas-solid fluidized beds while the gas is passed upwards through a bed of particles, the force of gravity will counter act drag and buoyant forces. When the gas velocity is high enough so that the drag and buoyant forces balance the gravitational force, the particles enter a fluidized state. This is the point of minimum fluidization, and the superficial gas velocity at this point is referred to as minimum fluidization velocity, U_{mf}. To determine U_{mf}, pressure drop across the bed of solids is measured and plotted versus the gas superficial velocity. At velocities below U_{mf}, the pressure drop increases linearly with the rise in gas velocity. However, at the onset of minimum fluidization and above, the pressure drop across the bed remains constant.

As the gas velocity is increased beyond minimum fluidization, various fluidization flow regimes are achieved as presented in Figure 1.2. At first, the excess gas beyond the minimum fluidization forms bubbles at the distributor plate. Then the bubbles grow, rise to the bed surface, and burst. If the gas velocity is raised even higher, the bubble dimeters can approach or be equal to the fluidization column resulting in slugging flow regime [6]. Slugging usually happens in fluidized beds with the ratio of static bed height and the column diameter larger than 2 [1]. Beyond slugging, turbulent fluidization is reached when the fluidization gas velocity is large enough that the top surface of the bed becomes difficult to detect and the entrainment becomes significant [1]. Finally, at very high gas velocities, and especially for those cases with very small particles, fast fluidization and pneumatic transport regimes are attained.

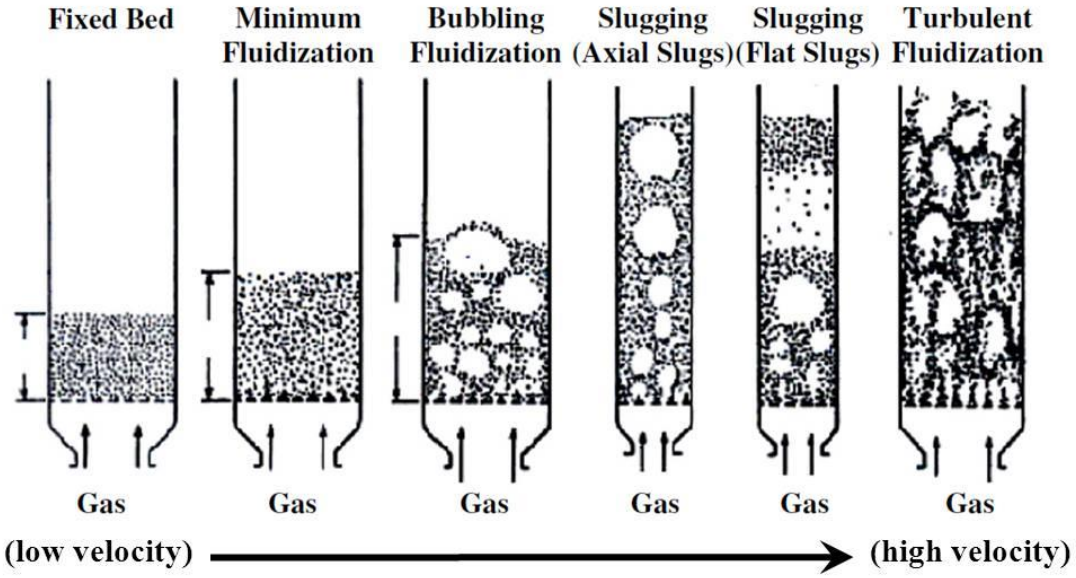

Figure 1.2: Fluidization flow regimes as fluidizing gas velocity increased [6].

Depending on the properties of the fluidizing gas (density) and particles (size and density), some particles are known to be easy to fluidize while others are cohesive and difficult to fluidize. As can be seen in Figure 1.3, Geldart [7] classified the behavior of solids fluidized by a gas into four clearly recognizable groups characterized based on the density difference between the particles and the fluidizing medium, and the mean particle size. Table 1.1 summarizes some of the key differences between each group of particles.

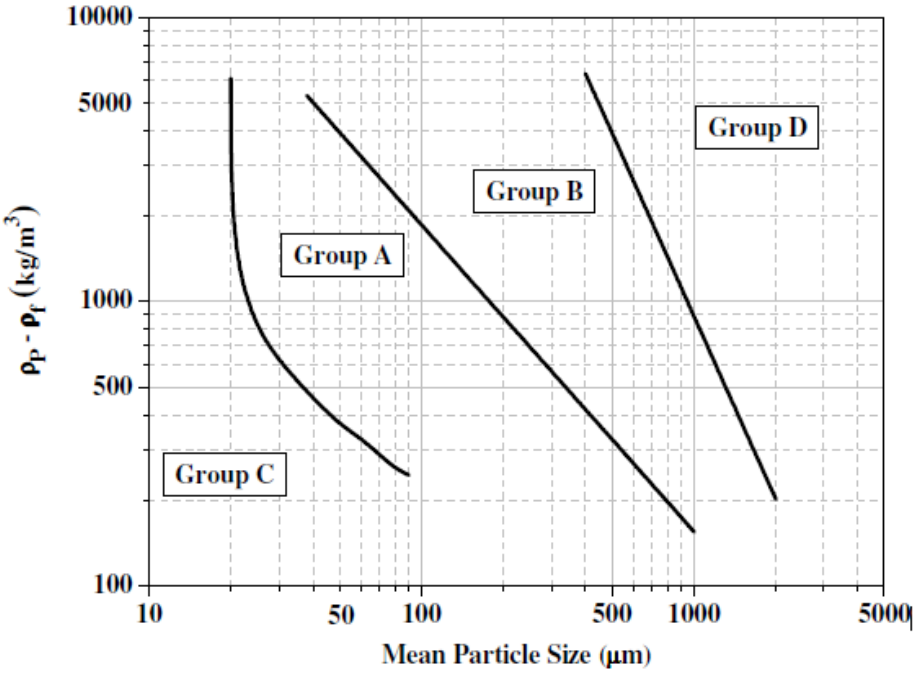

Figure 1.3: Geldart classification of powders fluidized by air at ambient conditions [7].

Table 1.1: Geldart particles classification[1,7].

Geldart Group	Particle Size (μm)	Particle Density (g/cm^3)	Description
A	20 - 100	Less than 1.4	Aeratable
B	40 - 500	1.4 - 4	Sandlike, easy to fluidize
C	Less than 60	Less than 1.4	Very fine, cohesive, difficult to fluidize
D	Above 600	Above 1.4	Spoutable, large and/or dense, difficult to fluidize

1.2.1 Detection of turbulent fluidization flow regime

According to Grace [1], the most visible feature of turbulent flow regime is the wide dispersion of solid particles in gas, as the gas travels up in the fluidization column. In addition, the surface between the bed and the freeboard in turbulent flow regime is less distinct than that in the

bubbling flow regime, since the turbulent bed frequently fluctuates up and down in the column [8].

As shown in Figure 1.4, in the bubbling flow regime, as the fluidizing gas velocity is increased, the bubbles become larger, resulting in bed pressure fluctuations amplitude to increase. However, beyond a certain superficial gas velocity, known as U_c, the amplitude of pressure fluctuations begins to decrease and the large voids in the bed begin to disappear until U_K is reached where the amplitude of pressure fluctuations levels off [9]. It is widely accepted that U_c marks the onset of turbulent flow regime [10]. The most accurate method to obtain U_c is known to be by experimental measurement (this method was used in this thesis to detect the transition to turbulent flow regime). Technics used to determine the transition from bubbling or slugging to turbulent flow regime, besides the measurement of bed pressure fluctuations, include visual observation, local voidage fluctuations determination based on signals of capacitance and optical fiber probes, and bed expansion measurements [10]. Based on the bed pressure drop fluctuation measurement method, several empirical correlations have been developed to predict the turbulent transition velocity for various particle groups [9,11–13].

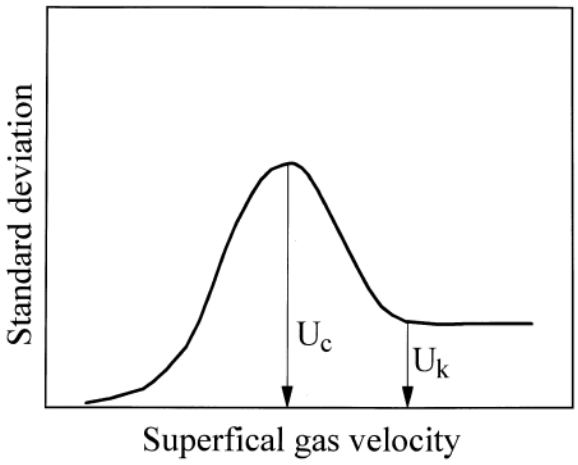

Figure 1.4: Detection of transition velocities, U_c and U_k, based on standard deviation of bed pressure fluctuation [10].

1.2.2 Gas bubble characterization

In gas-solid fluidized beds, the rising gas bubbles are the source of creating particles motion, which clearly intensifies the solids mixing. According to Davidson and Wallis [14], at the point of fluidization, voids act as a bypass for the fluidizing gas. Bubbles are then formed by the drag

force which is generated by the gas flowing though the voids. The drag forces form the roofs of the bubbles prevent the particles on the roof from falling. In bubbling flow regime, bubbles are generated at the distributor plate, rise upwards, and burst at the bed surface. As bubbles rise, their size increases due to bubble coalescence (Figure 1.5).

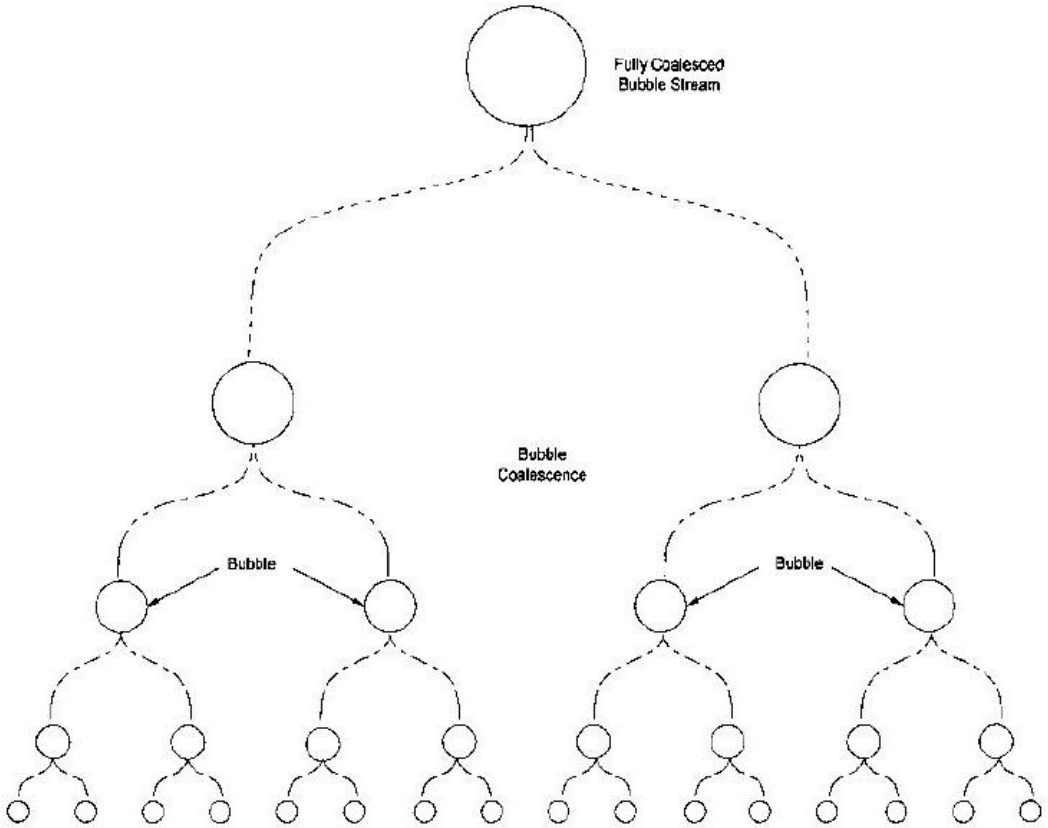

Figure 1.5: Darton's bubble coalescence moving path [15,16]

Measurement techniques employed for gas bubble characterization can be divided into two categories: intrusive methods including optical fiber probe [17–22] and capacitance probe [23–26]; and non-intrusive techniques including visual observation [27,28], pressure signal analysis [13,20,29] and X-ray and capacitance tomography [29–31]. Visual observation can only be used in 2-D gas-solid fluidized beds with transparent column walls. X-ray photography can be applied in 3-D gas-solid beds but the fluidization column has to have a relatively thin or transparent column wall, in order to detect the bubbles movement inside, and thus cannot be applied in large industrial units [20]. In this thesis, optical fiber probe as well as differential pressure signal analysis methods were employed to evaluate the gas bubble dynamics.

Differential pressure fluctuation analysis is a method utilized for estimating bubble size in fluidized beds [17,20,32]. Average bubble size can be estimated based on the standard deviation of the differential pressure (DP) signal measured at any axial position in a fluidized bed [20]. It was proposed by van der Schaaf *et al.* that the powder spectral density of absolute pressure signals can be separated into two parts, a coherent component (COP) and incoherent component (IOP) [33]. The incoherent component was related to the gas bubble diameter (d_b):

$$d_{b,IOP} \propto \frac{\sigma_{xy,i}}{\rho_P g(1-\varepsilon_{mf})} \quad [1.1]$$

where $\sigma_{xy,i}$ is the standard deviation of IOP, ρ_P is the particle density, and ε_{mf} is the bed voidage at minimum fluidization velocity.

This relation was then modified by Liu *et al.* [20] to employ differential pressure signals instead of absolute pressure signals. Based on this method, the gas bubble diameter was estimated by

$$d_{b,DP} \propto \frac{\sigma_{DP}}{\rho_P g(1-\varepsilon_{mf})} \quad [1.2]$$

where σ_{DP} is the standard deviation of the differential pressure signal. A proportionality constant of one is typically applied when using this equation.

Differential pressure fluctuation signal analysis is a non-intrusive method that can be applied in both laboratory and commercial-scale fluidization units. However, it can only provide the global average bubble size at the axial location where the measurement is conducted.

Optical fiber probes have been widely used to detect rising bubbles in atmospheric fluidized beds since 1950s [34,35]. An optical fiber probe contains two tips which are vertically arranged and separated by a certain distance. Each tip contains two bundles of optical fibers, one bundle emitting light into bed and one bundle receiving light reflected by particles. The reflected light collected by the fibers can be recorded and analyzed to obtain the bubble size, rise velocity, and frequency. When a bubble passes the probe, t_1 and t_2 represent the times when the nose of the bubble reaches the bottom and top tips, respectively. t_3 and t_4 are the times when the bubble wake leaves the two probe tips. It is clear that the time spent by a bubble passing bottom and top

tips are (t_3- t_1) and (t_4- t_2), respectively. Thus, the bubble rise velocity, U_b, and bubble diameter, d_b, could be calculated by

$$U_b = \frac{D_p}{\frac{(t_2 - t_1) + (t_4 - t_3)}{2}} \quad [1.3]$$

$$d_b = U_b(t_3 - t_1) \quad [1.4]$$

where D_p is the center-to-center distance of the two tips of the probe [20]. More information on the optical fiber probe data analysis is shown in Appendix A.

In comparison to other measurement technics, optical fiber probes have advantages of being less expensive and applicable in large fluidized beds, especially in cold and non-reactive systems [35]. Additionally, optical fiber probes can measure properties of both bubble and dense phases locally, allowing the investigation of local bubble properties at different radial and axial positions. Moreover, unlike analyzing pressure signals which is only able to give an average bubble size, optical fiber probes provide the entire distribution of bubble properties at the measurement location [20,35].

With all measurement techniques, due to the bubble coalescence, it is important to notice the location that the measurement of bubble size is taken with respect to the distributor plate.

1.2.3 Effect of pressure on gas-solid fluidized bed hydrodynamics

In gas-solid fluidization, particles are held by upward flow of gas. Thus, fluidized bed hydrodynamics, including transition velocities between fluidization regimes, bubble size and rise velocity, terminal velocity of single particle, etc., are influenced by the physical properties of fluidized gas such as density and viscosity, which are effected by operating pressure and temperature. This section will discuss some of the effects of operating pressure on fluidized bed hydrodynamics.

1.2.3.1 Effect of pressure on U_{mf}

For Geldart group A particles, pressure has almost no effect on U_{mf} as flow around the small particles is laminar which means that the fluid-particle interaction force is dominated by the gas

viscosity, which is a weak function of pressure [36]. For Geldart group B and larger particles, the interaction force of fluid-particle is dominated by inertial forces (which are sensitive to pressure) instead of viscous forces. Yates [36], who conducted a review of works presenting effect of pressure on minimum fluidization velocity, indicated that there is a sharp decrease of U_{mf} along with pressures up to 2,000 kPa and a more gradual decline thereafter. Similar results can be seen in Figure 1.6, in which illustrates the experimental results from Rowe [37]. More experimental results from other works confirm the finding as well [24,38–41].

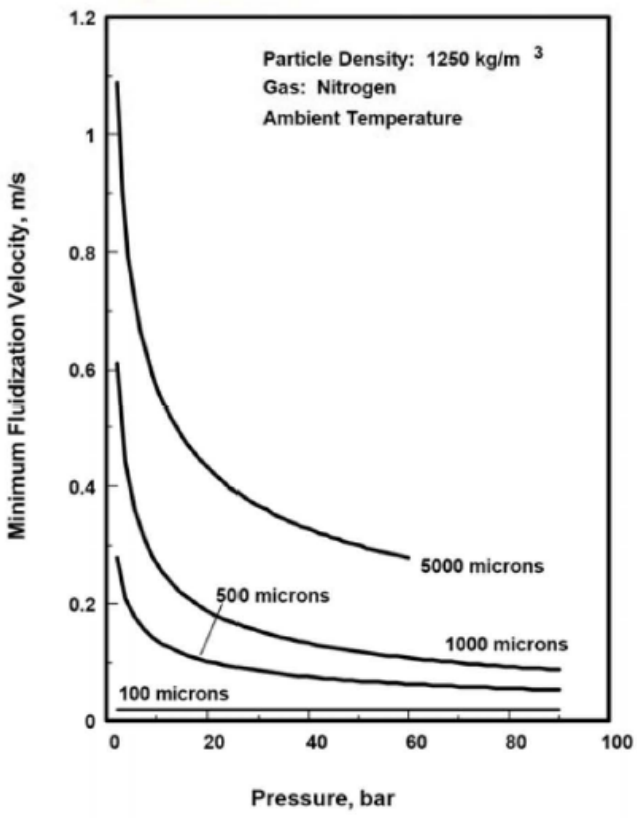

Figure 1.6: Effect of pressure on minimum fluidization velocity [37].

1.2.3.2 Effect of pressure on gas bubble dynamics

Hoffman and Yates [42] believed that both bubble coalescence and splitting increase with the increase in pressure. They suggested that bubbles are almost evenly distributed across the bed at atmospheric condition, while at higher pressure the bubble flow tends to concentrate around the vertical axis of the bed and form a 0.05-0.1 m central channel in which the resistance to gas flow would be lower. This then results in an increase in bubble coalescence, which exhibited as an

increase in bubble size. Additionally, they indicated that the stability of the bubbles decreases with the rise of pressure. Thus, the bubbles tend to break up into smaller units, leading to bubble splitting.

The influences of pressure on bubble dynamics, such as bubble size, rise velocity, and bubble frequency, have been investigated experimentally by many researchers. However, no conclusive point has been made due to the variation in results reported.

With Geldart group B particles (which are used in this thesis), Hoffman and Yates [42] experimentally measured the average bubble diameter and rise velocity in a freely-bubbling bed of alumina powder by using X-ray tomography at 0.4 m above the distributor plate. A rectangular vessel made of duralumin with cross section of 0.178 m × 0.127 m and height of 1 m was placed in a 2 m high cylindrical duralumin pressure vessel with 0.3 m I.D. Nitrogen gas from cylinders was used as fluidizing gas. Measurements were made at the operating pressure range of 101 to 6,100 kPa, and with the excess fluidizing gas velocities of 0.028 and 0.039 m/s. The results showed that the diameter of bubbles slightly increased when pressure was increased from 101 to 1,100 kPa and then decreased thereafter up to 6,100 kPa. Similar results for the effect of pressure on the bubble size have been observed by others [23,24,31,43]. However, in experiments conducted by few other researchers [25,41,44,45], bubble size was found to continuously decline with the increase of pressures, and the initial increase in bubble size at lower pressures reported by Hoffmann and Yates [42] was not observed. For example, Orta *et al*. [45] examined the effect of bed hydrodynamics by X-ray fluoroscopy technique under pressures of 200 – 2900 kPa by fluidizing polyethylene particles at 1.5 times of minimum fluidization velocity (bubbling flow regime). They found that the average bubble diameter decreased with the increase of pressure.

The experimental results from the same work by Hoffmann and Yate [42] showed that bubble rise velocity (U_b) was related to bubble size (d_b) for Geldart group B particles by

$$U_b = K(\frac{g d_b}{2})^{1/2} \qquad [1.5]$$

where K is the bubble velocity coefficient.

Figure 1.7 shows the *K* values obtained by Hoffmann and Yate [42] The coefficient decreased slightly between 101 and 2,000 kPa, and increased remarkably thereafter. Their results indicated that bubble rise velocity is not proportional to the bubble diameter pressure is increased.

Olowson and Almstedt [24] measured the effect of pressure on bubble rise velocity with silica sand (Geldart group B) for a pressure range of 101 – 1,600 kPa and excess gas velocities from 0.1 to 0.6 m/s. A capacitance probe was used in their experiments. They found that U_b increased with the increase in pressure, although the influence of pressure was smaller at elevated pressures. This means that at pressures below 1,600 kPa, the decrease of *K* value coupled with the increase in bubble diameter resulted in an increase of bubble rise velocity. Rowe *et al*. [31] and Wiman and Almstedt [46] reported similar trend at various operating pressures. On the other hand, Chan *et al*. [44] fluidized five different solids of Geldart group A and B with average particle sizes of 100 – 400 μm in a 0.4 m (15 inches) I.D. carbon steel column with nitrogen gas. Average bubble rise velocities were measured at pressures up to 3200 kPa and with the excess gas velocity of 0.1 m/s. They observed that bubble rise velocity decreased with the increase of pressure. Moreover, the previously mentioned Orta *et al*. [45], who used polyethylene particles, concluded that the operating pressure did not influence bubble rise velocity.

In relation to bubble frequency, a few works have reported that the bubble frequency increases with elevation in pressure from 101 to 3200 kPa [24,31,44]. One the other hand Chitester and Kornosky [43] reported a decline in frequency at pressures of 3242 to 6485 kPa. They observed the trend in the experiments fluidizing coal and char in a 0.16 × 0.19 m two-dimension Plexiglas column with nitrogen gas at pressures up to 6485 kPa. The coal and char particles had wide size distributions, and had average sizes of 195 and 203 μm, respectively.

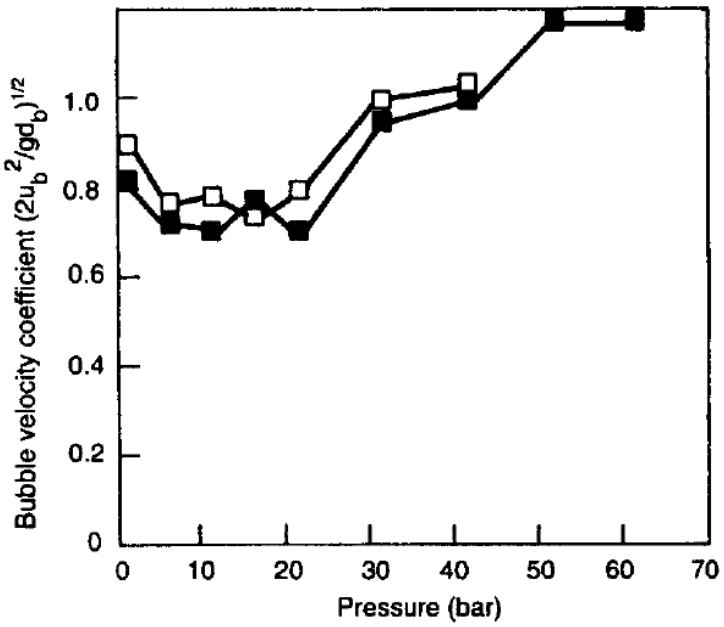

Figure 1.7: Effect of pressure on bubble velocity coefficient measured 0.4 m above the distributor plate for Geldart group B particles. U-U_{mf}: 0.028 m/s (■); 0.039 m/s (□) [42].

1.2.4 An industrial example of gas-solid fluidization process: Gas-phase ethylene polymerization

In petrochemical industry, fluidized bed reactors were adopted for gas-phase ethylene polymerization to produce polyethylene as early as 1950s [6,47], in which was first commercially constructed by Union Carbide in 1968. Figure 1.8 shows the schematic of the Union Carbide gas-phase ethylene polymerization process, the UNIPOL^{TM} process [48,49]. In this process, the fluidizing ethylene gas, along with some commoners, is fed from the bottom of the reactor and well distributed by the distributer plate. The catalyst (namely Ziegler-Natta or Metallocene) is introduced at the middle of the bed by nitrogen gas. Polymerization reaction occurs on the surface of the catalyst and as the polyethylene chains grow the catalyst particle is embedded within the resin. As the polyethylene resin grows, gets heavier and settles to the bottom of the reactor, close to the distributor plate, where it is discharged as a product. An expanded portion of the column reduces the gas velocity and reduces the entrainment from the bed. If entrained, polyethylene and catalyst particles are separated from unreacted ethylene gas in a cyclone. Then the ethylene gas is compressed, and cooled in a heat exchanger, before being recycled back to the reactor. In the later designs of the UNIPOL^{TM} technology, the entrained particles along with the gas are recycled back to the column without separation and usage of

cyclone. Heat removal is necessary because the polymerization reaction is highly exothermic with an adiabatic reaction temperature of almost 1500°C. Companies including ExxonMobil (USA) and Dow Chemical Company (USA) and many others use the UNIPOL™ later design while other companies such as Nova Chemicals (Alberta, Canada) use reactors with cyclones. Polyethylene reactors are usually operated at turbulent flow regime, due to its high gas-solids contact efficiency [10,13,50], and at pressures and temperatures up to 3,500 kPa and 100 °C, respectively [2].

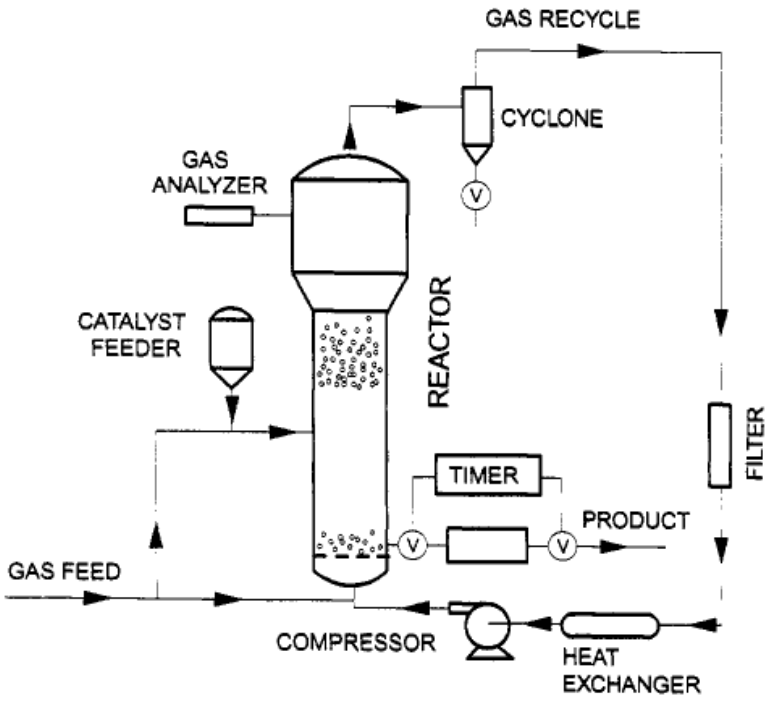

Figure 1.8: UNIPOL™ gas-phase ethylene polymerization process [48,49].

1.3 Electrostatic Charge Generation

Electrostatic charge resulting from a loss or gain of electrons on the surface of an object makes the object to be positively or negatively charged, respectively. The charge generation could be due to various mechanisms with most dominating to include contact, frictional, and induction charging (Figure 1.9).

Contact and frictional charging can be generated by simple contact between any two materials. In contact charging (Figure 1.9a), the exchange of charge from one surface to another occurs due to the difference in the surface energies. Electrons can also transfer by more energetic contact

generating friction between the surfaces in which generates thermal energy [51]. This method is known as frictional charging (Figure 1.9b). In practice, it is often impossible to distinguish these two methods of charging. Therefore, the contact and frictional charging are generally grouped together and referred to as triboelectrification (or triboelectric charging). Induction charging, as shown in Figure 1.9c occurs when a charged object approaches a conductor. The field from the charged object then redistributes electrons and protons on the conductor's surface, making it polarized. In the case shown in Figure 1.9c, the object is positively charged. As the surface of the conductor polarizes, electrons are accumulated on the side closer to the charged object, making it negatively charged, while leaving the farther side positively charged. Induction charging leads to an attractive force generated between the charged object and its image on the conductor that is referred to as the "image force". If the farther side of conductor is grounded, the charge on that side will be dissipated. Thus, upon the removal of the charged object, the conductor is left to be negatively charged.

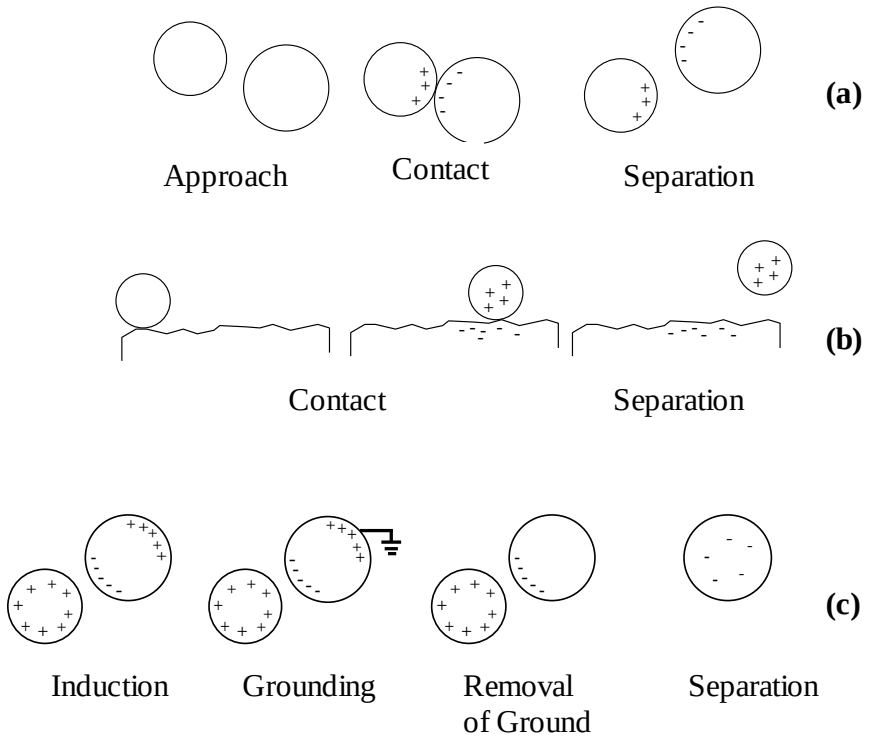

Figure 1.9: Electrostatic charge generation mechanisms: (a) contact, (b) frictional, and (c) induction charging.

Coulomb's law describes the electrostatic force between any two point charges at a distance apart:

$$F = \frac{1}{4\pi\varepsilon_0}\frac{q_1 q_2}{r^2} \quad [1.6]$$

where F is the electrostatic force, ε_0 is the permittivity of free space (a constant with a magnitude of 8.85×10^{-12} F/m), q_1 and q_2 are the two charges, and r is the distance between the two points.

The electric field (E) generated due to the electrostatic force is then defined as electrostatic force per unit charge:

$$E = \frac{F}{q} \quad [1.7]$$

Combining Equations 1.6 and 1.7 defines the electric field due to a point charge q as

$$E = \frac{q}{4\pi\varepsilon_0 r^2} \quad [1.8]$$

Materials can be arranged based on their charging tendency in series known as "triboelectric series" such as the two presented in Table 1.2. In such series, materials acquire a positive charge when contacted with a material located lower down in the series [52]. Triboelectric series are completely experimental and at times not reproducible. The irreproducibility is because of the differences, even minor, in the experimental conditions (such as humidity) and material properties (such as impurity states at the surface) at the time of generating the series. Another reason is the lack of understanding of the fundamental mechanism of triboelectrification. Depending on the surface electrical properties of solids, their underlying triboelectrification charging mechanism could be different.

Table 1.2: Triboelectric series [51,53,54].

More (+)	Plexiglass
	Bakelite
	Cellulose acetate
	Silicon wax
	Glass, mica
	Nylon
	Wool
	Human hair
	Silk
	Paper, cotton, wood
	Amber, resins (natural or synthetic)
	Styrofoam, polyurethane
	Polyethylene
	Rubber
	Rayon, Dacron, Orlon
	PVC
More (−)	Silicon

(a)

	Material	Polymer type
+	Wool	
	Nylon	
	Viscose	Cellulose
	Cotton	
	Silk	
	Acetate rayon	Cellulose acetate
	Lucite or Perspex	PMMA
	Polyvinyl alcohol	
	Dacron	Copolyester of ethylene glycol and terephthalic acid
	Orlon	Polyacrylonitrile
	PVC	
	Dynel	Copolymer acrylonitrile/vinyl chloride
	Velon	Copolymer vinylidene chloride/vinyl chloride
	Polyethylene	
−	Teflon	PTFE

(b)

1.3.1 Electrostatic charging in conductors

It is generally agreed that electrons are transferred between two contacted conductors to bring the surfaces, at the point of contact, to thermodynamic equilibrium [55]. The amount of charge transferred during contact depends on the work functions of the two surfaces. Work function (ϕ, commonly measured in electron volts), which depends only on the nature of material at its surface but not the bulk, is defined as the minimum energy required to remove an electron from

the Fermi level, which is the highest occupied molecular level at equilibrium, to just outside the metal surface. As shown in Figure 1.10, as two metal surfaces are brought into contact, the metal with lower work function, whose valance electrons are at higher energy levels, will lose some of the electrons to the other metal. Thus, the metal with lower work function becomes positively charged while the other metal is negatively charged.

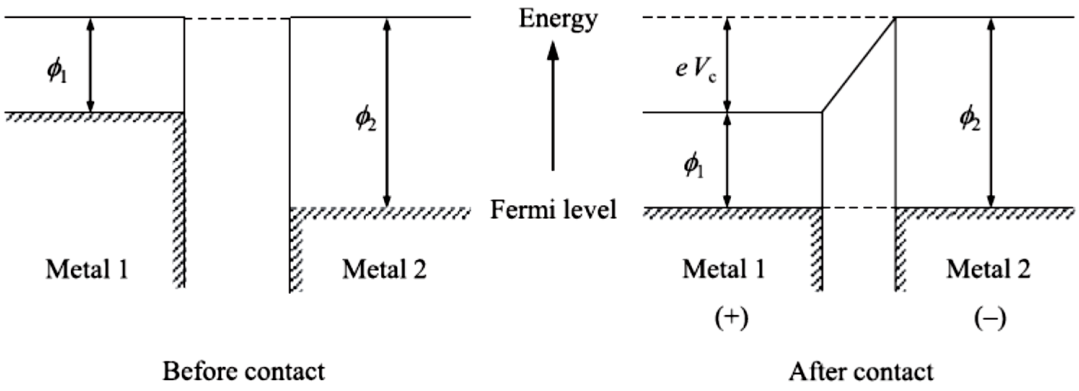

Figure 1.10: Electron potential energy for metal-metal contacts [56].

During the contact of two conductor surfaces, the contact potentials between the two surfaces is:

$$V_c = \frac{(\phi_B - \phi_A)}{e} \qquad [1.9]$$

where V_C is the contact potential between the surfaces, ϕ_A and ϕ_B are the surface work functions, and e is the electric charge of an electron (-1.602 × 10^{-19} C). As the two surfaces separate, electrons tend to tunnel across the interface so as to maintain thermodynamic equilibrium. This reduces the final charge left on the surface.

Table 1.3 lists the work functions of various materials found by Tanoue and Masuda [57]. Most of such measurements were normally done under vacuum, but inconsistent results on work functions of metals and polymers have still been reported [51].

Table 1.3: Work functions of various materials [57].

Material	Work Function (eV)	Material	Work Function (eV)	Material	Work Function (eV)
Zn	3.63	BaO	1.1	Polyethylene	5.24 ± 0.24
C	4	CaO	1.60 ± 0.2	Polyethylene	6.04 ± 0.47
Al	4.06 – 4.26	Y_2O_3	2	Polypropylene	5.43 ± 0.16
Cu	4.25	No_2O_3	2.3	Polypropylene	5.49 ± 0.34
Ti	4.33	ThO_2	2.54	Polystyrene	4.77 ± 0.20
Cr	4.5	Sm_2O_3	2.8	Polyvinyl chloride	4.86 ± 0.73
Ag	4.52 – 4.74	UO_2	3.15	Poly carbonate	3.85 ± 0.82
Si	4.60 – 4.91	FeO	3.85	PMMA	4.30 ± 0.29
Fe	4.67 – 4.81	SiO_2	5	Polytetrafluoroethylene	6.71 ± 0.26
Co	5	Al_2O_3	4.7	Polyimide	4.36 ± 0.06
Ni	5.05 – 5.35	MgO	4.7	Polyethylene Terephthalate	4.25 ± 0.10
Pt	5.12 – 5.93	ZrO_2	5.8	Nylon66	4.08 ± 0.06
Au	5.31 – 5.47	TiO_2	6.21	Pylex7740	4.84 ± 0.21

1.3.2 Electrostatic charging involving insulators

Unlike in conductors, electrons are not likely to be able to move in insulators. This therefore makes contact charging involving insulators a more complicated phenomenon. Thermodynamic equilibrium concept is not applicable in contact charging involving insulators and charging becomes a local phenomenon. Contact charging in insulators depends on not only properties of materials such as surface roughness, size, and geometry, but also surface properties like impurity and oxidization [58,59]. To date, the mechanism of contact charging involving insulators is not yet well understood. As Williams [60] suggested, this could be due to factors including involvement of many variables in charge exchange determination, difficulties of investigating the effect of surface properties on contact charging, and failure to essentially understand the nature of contact. Lacks [61] even suggested that electrostatic charging in insulators may never be predicted because of the completely opposite results from some carefully controlled experiments.

As early as 1967, main ways in which charge could transfer from one body to another had been proposed to be not only due to electron transfer, but also ions and material transfer [62].

1.3.2.1 Electron transfer

In insulators, for example a polymer, the conduction band is about 4 eV above the Fermi level [55], so that the electron movement is extremely difficult and slow. In fact, however, contact

electrification for insulators happens quite fast. This then indicates that charge generation involving insulators could not be due to electron transfer of pure insulator. In this case, Bauser *et al*. [63] suggested that the charge must be on surface rather than the bulk states. Lowell and Rose-Innes [55] described the insulator-metal contact charging by the surface states theory. This theory assumes that states lay very close to the surface of the insulator can communicate with the contacting material. According to this theory, Lowell and Rose-Innes [55] suggested that the contact charge involving insulator-metal or insulator-insulator was determined by the difference in energy between the metal Fermi level and an "effective" Fermi level of the insulator, or in the latter case that between the "effective" Fermi levels of the insulators. In other words, the contact charging between insulator-metal surfaces depends on the difference of the work function of the metal surface and the "effective" work function of the insulator surface. Similarly, as two insulators contact with each other, the contact charging is determined by the difference of the "effective" work functions of the two surfaces. During insulator-conductor contact, there is experimental evidence that the contact charge density varies linearly with the work function of the metal [55,64–66].

Experimental work showed that pure samples of crystalline insulators did not charge when contacted with metals [51]. This then indicates that for cases involving insulators in which contact charging occurs, factors including impurity states, such as side groups, surface impurities, and ends of molecular chains, must be contributing to the charging.

1.3.2.2 Ion and material transfer

To explain the charging of two identical materials during contact, Kornfeld [67,68] suggested that ions are transferred because different surfaces have different affinities for a given ion. Kornfeld's mechanism was not widely accepted as the usual cause of contact electrification. According to Lowell and Rose-Innes [55], "none of his experiments could justifiably be said to provide a critical test of his model". Harper [62,69] attributed the charge transfer between quartz surfaces to a thick layer of –OH ions, which were presented on the surfaces from the way the quartz surfaces were cleaned before experiments. On the other hand, Wagner [70] considered the charging of quartz contacting with metals (nickel, platinum, and copper) as a result of electron transfer because of the difference of work functions between the two materials.

In early works, such as those by Salaneck *et al*. [71], material transfer was not considered as a primary mechanism of contact electrification. In their work, they investigated the contact charging of metal-polymer contact, they found that because large amount of material only transfer at the first contact, while at the meantime the same region of polymer could be repeatedly charged by further contacting the metal, indicating that other mechanism than material transfer would be involved.

However, Apodaca *et al.* [72] observed that essentially identical pieces of the same material can acquire charge when contacted suggesting that microscopic variations in the surface composition can cause macroscopic changes in charging properties. Later, other researchers [73–76] investigated the surface composition of charged surfaces with nanoscopic resolution and proposed that material transfer occurs in contact charging. Baytekin *et al*. [73] performed contact electrification experiments with PDMS (polydimethylsiloxane) and PTFE (polytetrafluoroethylene) where their surfaces before and after contacts were observed by CRS (confocal Raman spectroscopy) and XPS (X-ray photoelectron spectroscopy). They found that the surfaces after contact charging were composed of "mosaics" which were nanoscale pieces with randomly charge polarities of positive and negative (Figure 1.11). They found that the charge density of mosaics per unit area was much higher than which was expected, while the net charge of the material was relatively low because of the compensation between the positive and negative regions. They concluded that contact electrification is a, "complex process of bond cleavage, chemical changes, and material transfer within distinct patches of nanoscopic dimensions."

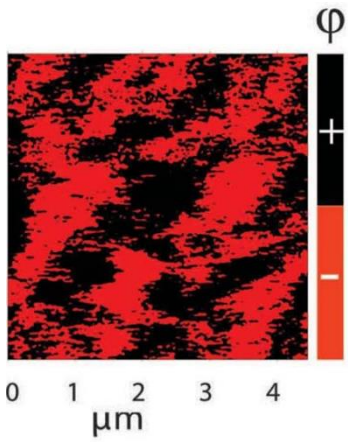

Figure 1.11: Mosaic of surface charge [73].

Burgo *et al.* [77] while contacting the surfaces of PTFE and PE (Polyethylene) observed the formation of microscopic regions of opposite charge. Analysis of the regions showed that the positively charged region on PTFE was formed by species derived from PE and that the negatively charged region on PE was formed by species derived from PTFE. This indicated that charge transfer is related to material transfer. They hypothesized that as the two surfaces were brought into contact, mechanical shear was concentrated in a fraction of the surfaces causing temperature peaks in some zones. Extensive chain breakdown occurs in these zones causing the formation of radical species. Electrons transfer from the hydrocarbon to the fluorocarbon due to the high electronegativity of the fluorine atoms, forming hydrocarbon cations and fluorocarbon anions. These species, according to Burgo et al, are the charge carriers.

In summary, the role of ion and material transfer in triboelectrification involving insulators is still not well understood and thereby more work is required on this topic.

1.3.3 Charging in a granular system

Investigation of electrostatic charging in granular systems poses challenges due to the lack of knowledge of the fundamental mechanism of triboelectrification in such systems. Additionally, the presence of numerous particles makes the study of electrostatic charging, and its measurement and control of each single particle more challenging and almost impossible.

The mechanisms of charging in particulates have been proposed and described by two models: the condenser model [78] and the charge relaxation model [79,80]. The condenser model assumes that electrons transfers between contact surfaces. Thus, as stated previously, in 1.2.2.1the magnitude of the transferred charge depends on the “effective” work function of the surfaces. The charge relaxation model assumes that after the charge transfer during contact, the charge relaxation occurs during the surface separation process due to breakdown of the gas in atmosphere. Thus, the magnitude of the observed transferred charge is larger than the initial transferred charge. In this case, the magnitude of the transferred charge depends on the gas breakdown voltage, which for air is approximately 3.0×10^6 V/m [51], and the particle diameter. The two models have been successfully applied in powders pneumatic transport in metal pipes. They could also be applied in more complex systems such as dust devils, sand storms, powder flow in insulating tubes, and fluidized beds.

1.3.3.1 Bipolar charging

A unique and important phenomenon observed in granular systems is "bipolar" charging. Researchers have noticed that in contact charging of granules made of identical material, but having different sizes, particles tend to charge oppositely. Several authors [81–84] have reported that in bipolar charging the smaller particles charge negatively and larger particles charge positively, although contradicting results were obtained by others [85–89].

Lacks and Sanakaran [74] explained the "particle-size-dependent" charging with the high energy state electron theory proposed by Lowell and Truscott [90]. The Lowell theory assumes that the electron transfer between the donor and the accepter is a "one-way trip". When particles made of identical material contact with each other, larger particles, which have smaller specific surface areas, are more possibly to contact other particles with different points. Therefore, electrons accumulate on the surface of smaller particles, making the smaller particles to be negatively charged. Moreover, Zhao *et al.* [84] proposed that the bipolar charging can be a result of the difference in the inherent work functions, microscopic surface structures, specific areas and consequently contaminant absorption, or surface energies. Although multiple mechanisms of the bipolar charging have been proposed, the exact mechanism is still unclear due to the lack of the experimental evidence.

1.4 Electrostatic charge generation in gas-solid fluidized beds

In any gas-solid fluidized bed, generation of electrostatic charges is unavoidable due to continuous contacts between particles, and particles and the fluidization vessel wall. The extent of fluidized bed electrification, however, would depend on the surface nature of fluidizing particles and those of the fluidization column wall, as well as the fluidization operating conditions. As early as 1940s, researchers had observed that the fluidization condition was influenced by the adhesion of particles on the column wall which was attributed to electrostatic charging [91–95].

Problems associated with fluidized bed electrification can be categorized as: particle-wall adhesion, particle agglomeration, and electrostatic discharge. Particles agglomeration and adherence to the fluidizations column wall would potentially change the fluidization hydrodynamics because of deviations from the conditions such as particle size. The adhesion of

particles to the fluidized bed wall and other surfaces can necessitate process shutdown for clean-up, which is a significant nuisance in industrial processes such as polyethylene production. Overall, both contact and frictional charging amongst the fluidizing particles and between the particles and the fluidization column wall would account for fluidizing particles charging.

1.4.1 Electrostatic charging in polyethylene reactors

Polyolefin industry significantly suffers from fluidized bed reactor electrification especially in production of polyethylene. During the gas-phase ethylene polymerization, as the polyethylene resin and catalyst particles are fluidized, they may become electrostatically charged resulting in their adherence to, or foul, the reactor wall. The fouling of particles on the column wall negatively affects the heat dissipation of the exothermic polymerization reaction, causing the particles to fuse together and form sheets. When these sheets become significantly heavy, they detach from the reactor wall and potentially block the distributor plate and the product discharge pipes, thus requiring reactor shutdown for clean-up. Sheeting has been observed to be most prominent in processes using catalysts of Ziegler-Natta, some bimodal catalyst, and particularly metallocene catalysts [96]. Depending on the severity of sheeting, the sheets could be a few square centimeters to a few square meters large [3]. They could have thicknesses from 0.00635 to 0.0127 m, widths of 0.0762 m to 0.457 m, and lengths of 0.305 m to 1.52 m [97]. They could typically be found at about half the diameter of the reactor above the distributor plate, where the drag forces along the column wall are at minimum [97]. Typical locations of sheeting in polyethylene reactor are shown in Figure 1.12. Sheeting can be categorized into wall and dome sheeting based on their locations [3]. Dome sheeting, which is also referred as drooling, happens when sheets adhere to the dome of the reactor while wall sheeting occurs when particles adhere to the reactor wall.

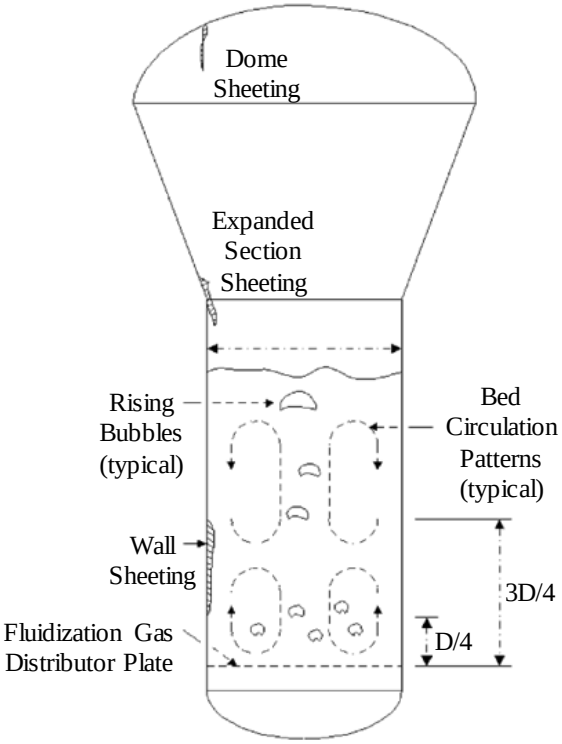

Figure 1.12: Typical sheeting formation in industrial polyethylene reactors [3]

A common method of detecting the onset of sheeting is monitoring the reactor skin thermocouple signals for minor variations. According to Song *et al*. [98], a common sign of the onset of sheeting is that the temperature of reactor wall and that of the reactor bed differs for more than 20°C. However, it is usually too late to take any steps by then. Sheeting can occur as soon as half a day past operation [99] or after the reactor produces 6 to 10 times of the bed weight of polyethylene [96]. In pilot-scale polyethylene producing experiments conducted by Goode *et al*. [97], the reactor had to be shut down after operation of only 59 hours due to the reactor wall sheeting.

The reactor shut-down and clean-up process could take from two to three days, in some sever cases, to even more than a month. There are about 100 gas-phase polyethylene plants worldwide with an average annual production capacity of approximately 200 million metric tons. A rough estimate of economic loss due to sheeting was conducted for a Dow Chemical Company polyethylene plant in Prentice, Alberta, Canada with an annual production rate of 750,000 metric tons. The approximate marginal economic loss estimation for this plant was found to be close to 2 million dollars per day. This signifies the severity of the challenge that the polyolefin industry is facing from fluidized bed reactor electrification.

1.4.2 Charge controlling in gas-solid fluidized beds

A few approaches of controlling electrostatic charge generation in commercial polyethylene reactors have been tested for the purpose of minimizing or eliminating the particles reactor wall fouling. According to Hendrickson [3], the main mechanisms of controlling the charge generation include demoting the charge generation, improving the charge dissipation, and neutralizing the existed electrostatic charge.

1.4.2.1 Treatment of the inner column wall

Fulks *et al.* [100] reported that coating the reactor wall with a polymer film prior to polymerization reduced wall sheeting in industrial reactors. Similarly, Hagerty *et al.* [96] reported that coating the reactor wall with polyethylene reduced the electrostatic charge generation. However, the mechanism of the electrostatic charge reduction when coating the inner column wall is unknown. Additionally, although treating the inner surface of the column wall reduced the degree of electrostatic charge in bed, it cannot fully prevent the generation of sheets. In this case, as the sheets necessitate the reactor shut-down for cleaning, the layer coated on the column wall might be removed during the cleaning process.

1.4.2.2 Additive injection

Various additives have been tested to reduce the electrostatic charge generation, to maintain the electrostatic level in the reactor at a neutral level, or to increase the conductivity of the particles thus providing a path for charge discharge [96–98,101]. The additives injected into the reactor can be gas, liquid, or solid. It should be noted that any additives injected into commercial reactors must not act as a poison to the reaction, or "adversely affect the quality of the product" [97].

Most of the charge controlling research has been done with solid additives. The additive particles typically have an average size of 10 to 100 μm. They can be handled as single particles (with size less than 1 μm) or as particles agglomerates (in size range of 0.01 to 200 μm). They can be introduced to the reactor independently, or along with other components employed in the reaction. Song *et al.*[98] claimed that adding sufficient amount of chemical additives such as MgO, ZnO, Al_2O_3, CuO alone or in mixture when negative electrostatic charges were detected, as well as adding sufficient amount of additives such as V_2O_5, SiO_2, TiO_2, Fe_2O_3 when positive

electrostatic charges were detected effectively maintained the "essential neutral static level" in bed. Song *et al.* [98] also concluded that carbon black effectively reduced negative charge in a gas phase polymerization reactor. However, carbon black can only be applied at the beginning of the fluidization, since carbon black is black and cannot be used to make colorable products.

Although a few works have been reported to control the electrostatic charge in gas solid fluidized bed, especially some works have shown to have some success with additive injection, it is common for one additive to work well in one system but not well in another with a different catalyst, or to find some additives to be effective for the first few days of reactor operation but not for longer [102]. This is attributed to the lack of understanding of the actual mechanism for additives to reduce the electrostatic charging, which has caused most of the studies focusing the electrostatic charge control being performed by trial and error. Finally, it should be noted that with all abovementioned works, electrostatic probes (current or voltage type probes) have been used to detect the degree of bed electrification. Thus, although injecting an additive into a reactor may have maintained the bed electrostatic level to be zero, it may not have removed or prevented wall sheeting.

For the purpose of developing more universal methods to control the particles electrification in gas-solid fluidized bed, and to find a way to minimize or eliminate the sheeting problem in industrial, more work is undoubtedly required to gain better understanding of the mechanisms of bed electrification and dissipation, as well as the mechanism of particles migrate and adhere to the column wall.

1.4.3 Electrostatic charge measurement techniques

Faraday cup and electrostatic probe are the two most common electrostatic charge measurement techniques used in fluidized beds.

1.4.3.1 Faraday cup technique

As shown in Figure 1.13, a Faraday cup consists of two concentric metal cups. The two cups are electrically isolated from each other with a piece of insulating material. The outer cup is grounded to shield the inner cup from the electric fields from the environment while the inner cup is connected to an electrometer. When a charged object is placed inside the inner cup, the object charge induces an equal and opposite charge on the cup. The inner cup is connected to an

electrometer in which measures the charge on the cup. In other words, the electrometer measures the same polarity and magnitude of charge as that of the charged object [51]. It should be noted that a Faraday cup measures the net charge of the objects placed inside its inner cup. Therefore, if both positively and negatively charged objects are present, only their net charge is measured.

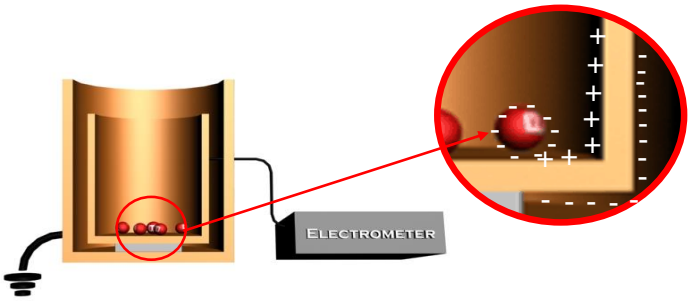

Figure 1.13: Faraday cup technique.

Majority of applications of Faraday cup in fluidized bed have involved sampling of fluidizing particles and placing them into an external Faraday cup. Such procedure requires handling of the particles that alters the particles true electrostatic charge. From the literatures, sampling methods used in previous works include using a vacuum pump [103,104], placing sampling ports with locking mechanism along the column wall [105,106], or manually removing particles with a scooper after the completion of fluidization [83] (see Appendix B Figure B.1). Steps were taken by some researchers to minimize the alteration of particle charge that could occur by handling. For example, Sharmene Ali *et al*. [83] coated the scooper used for particles sampling with the same type of particles to be handled. Nevertheless, as discussed previously, even contact between similar surfaces generates electrostatic charge. Therefore, this method still cannot avoid the effects of particle handling. In addition, the aforementioned methods only enabled a local measurement. A single sample cannot be representative of the electrostatic charging within the entire fluidized bed, since particles in different regions of the beds could be of different charge density and even charge polarity. To avoid particle handling, Mehrani *et al*. [87] developed a system that consisted of a metallic fluidized bed acting as a Faraday cage by being contained within an outer grounded column. However, this system limited to only measure the charge of entrained particles.

To overcome the challenges of using Faraday cups in works reported, a novel online method was developed in this research team by Sowinski *et al*. [88,107]. The Faraday cup method was implemented in a unique way, allowing the simultaneous measurement of particles specific charge, mass and size distribution in three different regions of the fluidized bed, including particles in bulk, those adhered to the column wall, and those entrained, without particles handling. In addition, this method for the first time allowed the measurement of the magnitude of fouling of particles on the fluidization column wall due to electrostatic charges. As shown in Figure 1.14a, two removable Faraday cups (referred to as top and bottom Faraday cups) were implemented at the top and bottom of a 0.10 m (4 inch) fluidization column made of carbon steel. The picture of the Faraday cup system is shown in Appendix C, Figure C.8. The exit of the column was fitted with a filter bag placed inside the copper top Faraday cup to captures the entrained fines during fluidization. The top Faraday cup was connected to a Keithley digital electrometer Model 6514 to measure the net cumulative charge of the entrained particles. The bottom Faraday cup was also made of copper and its outer cup acted as windbox while its inner cup was connected to a Keithley digital electrometer Model 6514 to measure the net charge of the bed particles. The conventional distributor plate was replaced with a knife-gate valve that its blade was modified to act as a perforated plate. The fluidization column was operated at atmospheric condition.

As illustrated in Figure 1.14b, the electrostatic charge measurement consisted of the following steps:

- During the fluidization process, the top Faraday cup measured the electrostatic charge of entrained fine particles (referred to as “fines”) which were trapped by the filter bag placed in the top Faraday cup.
- After the completion of the fluidization period, the knife-gate valve was opened, allowing the particles in the bulk of the bed (referred to as “dropped”) to drop into the bottom Faraday cup to measure their net charge. By the cup removal, then particles mass and thus charge-per-mass would be measured.
- Opening the knife gate valve and the removal of the bottom Faraday cup also enabled the inspection of the inner column wall from the bottom of the column for the degree of

particles-wall fouling. If any wall fouling would be observed, the bottom Faraday cup would be assembled again and the fouled layer (referred to as "wall") would be discharged into the cup for the measurement of particles charge, as well as their mass. The wall particle removal was achieved by pass extra dry air through the column from the top and through a narrow tube.

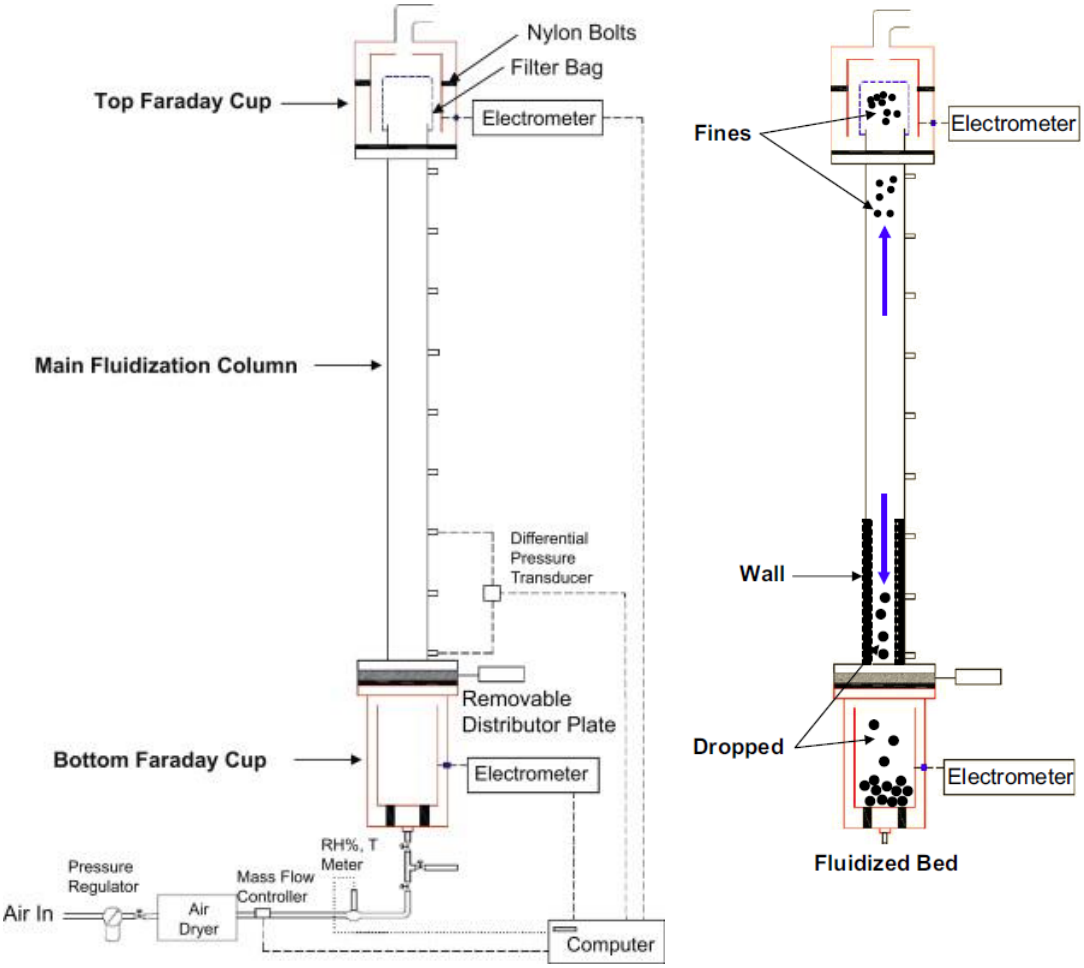

(a) (b)

Figure 1.14: (a) Fluidization system containing online Faraday cup measurement method, and (b) the charge measurement locations [107].

1.4.3.2 Electrostatic probe technique

As presented in Figure 1.15, an electrostatic probe consists of an inner conductive bar or wire, a middle insulating layer, and a grounded outer conductive layer. The conductive layers could be made of carbon steel, stainless steel, titanium, platinum, nickel, copper, or aluminum [96]. The

fundamental principle of the measurement technique is that when a charged object is brought to the proximity of tip of the probe, the object induces a charge on the probe. The other end of the probe is connected to an electrometer to measure the induced charge. The measured signal can be of electric potential, field, or current (charge).

The electrostatic probe technique has widely used in gas-solid fluidized beds. The probes are placed either vertically (parallel to the column axis) [5,59,108,109] or horizontally (perpendicular to the column axis) [105,106,110] within the fluidized beds (examples are illustrated in Appendix B, Figure B.2). They can be located at the wall of the column, near the center of the bed, or at the distributor plate; they can be located below or above the bed level.

In industrial polyethylene reactors, current probes have in some cases been used by locating them at a height of approximately half of the reactor diameter above the distributor plate [96]. The probe signal is continuously monitored during operation and the onset of sheeting is detected when deviation from the baseline signal occurs. However, the utility of such probes, as a method of detecting sheeting, is not particularly reliable. This is partly because the mechanism contributing to the measured signal as particles come into contact with the probe are poorly characterized. In other cases static probes have also been placed at the exit of the reactor to measure static from elutriated fines [96].

In academic settings, current probes have been used in most cases to detect the local column wall static conditions. However, as stated previously, current probes cannot accurately measure the charge of particle. Moreover, fouling of particles on the tip of probe such as polyethylene, would limit further particle-probe contacts, which affects the probe measurement. For these reasons, although convenient to use, electrostatic probes are not reliable in measuring electrostatic charge in fluidized beds.

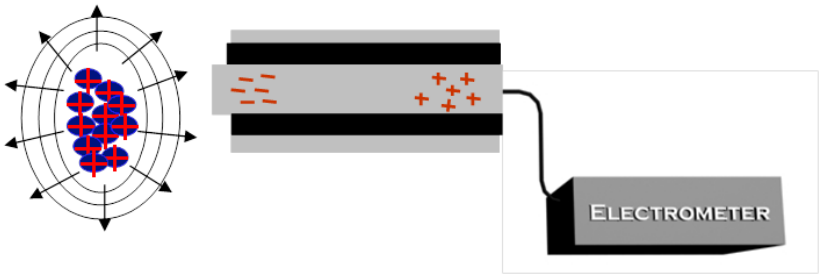

Figure 1.15: Electrostatic probe technique.

1.4.4 Electrostatic charging in gas-solid fluidized beds at elevated pressures

Since the fluidization pressure affects the hydrodynamics of a fluidized bed, it is expected that the electrostatic charge generation at elevated pressures to be different from that in an atmospheric bed. Moreover, industrial fluidized beds such as those used in polyethylene production are typically operated at pressures up to 3,000 kPa. To be able to better understand industrial fluid bed electrification and consequently assisting the industry in eliminating or reducing reactor fouling, it is essential to study electrostatic charge generation under industrially related operating conditions.

In relation to the effects of operating pressure, only two works are found in open literature focused on charge generation in high-pressure gas-solid fluidized beds, namely works by Moughrabiah *et al*. [105] and Liu *et al*. [86], both from the same research group at the University of British Columbia (BC, Canada). Moughrabiah *et al*. [105] conducted a series of experiments with polyethylene and glass beads at pressures up to 724 kPa. They used electrostatic probes mounted at various axial locations along a stainless steel fluidized bed with inner diameter of 0.150 m and height of 2.0 m. The electrostatic charge generated on the probes was recorded for only 500 s and used as a measure of bed electrification. Their results concluded that increasing pressure increased bed electrification. Although they did not measure gas bubble size, rise velocity or frequency, they attributed the observed results to an increase in these parameters. In contrast, Liu *et al*. [86] using the same experimental setup showed that operating pressure does not have consistent influence on the charging behaviour of polyethylene resin. Their experiments were conducted with five types of polyethylene particles and at limited to pressures up to 621 kPa. The authors concluded that the complex influence of pressure on bed hydrodynamics and the resin properties on electrification make it difficult to evaluate particle charging. It is important to note that their contradictory results from the same system could be due to the type of measurement technique used. As discussed previously there are issues in using electrostatic probes.

1.4.5 Electrostatic charging in gas-solid fluidized beds at elevated gas velocities

A few works have studied electrostatic charge generation in bubbling [5,86,101,105,108,111–115] and slugging [59,110,111,116] gas-solid fluidized beds. Bafrnec and Bena [108] suggested

that this could be because of the increase of charge generation, decrease of charge dissipation, or both during the increase of gas velocity.

Ciborowki and Wlodarski [5] fluidized multiple types of particles with size range of 300 – 500 μm in a 0.049 m in diameter glass column at superficial gas velocities of 0.08 – 0.5 m/s. The authors measured the potential of the bed with an electrode and showed that the electrode potential increased with the increase of fluidizing gas velocity. Revel *et al*. [112] fluidized polyethylene particles with an average size of 3000 μm in a 0.1 m in diameter acrylic column at gas velocities of 1.7 to 2.5 times U_{mf}. Air at room temperature with a relative humidity of less than 5 % was used as the fluidizing gas. They showed that the net specific charge (q/m) of particles sampled at 0.035 m above the distributor plate increased with the increase of fluidizing gas velocity. Liu *et al*. [86] studied the effect of fluidizing gas velocity on the degree of electrostatic charge generation in a 0.15 m in diameter carbon-steel gas-solid fluidization column. Polyethylene particles with an average size of 646 μm were fluidized at 138 kPa and at excess gas velocities of 0.05, 0.10, 0.15, 0.20 m/s. Air at room temperature with a relative humidity of 8 – 11% was used as the fluidizing gas. The measurements from three current collision probes located at different radial and axial positions in the column showed that the electrostatic charge increased with the increase of fluidizing gas velocity. Alsmari *et al*. [115] used the same apparatus as Liu *et al*. [22] and conducted free-bubbling experiments. They fluidized a binary mixture of large glass beads (425 – 600 μm) and 5 wt% fine glass beads (25 – 50 μm) at 207 kPa and a range of gas velocities of 0.2 – 0.6 m/s (1 – 3 times minimum fluidization velocity). Air at 20°C with a relative humidity of 12% was used as the fluidizing gas. The particles charge densities were determined by current collision probes. The results showed that as the superficial gas velocity increased, the degree of electrostatic charge measured locally at the probe tip increased.

Gajewski [111] glued copper rings connected to a microammeter on the inner surface of a 0.25 m in diameter glass column to measure the electrical current inside the bed. Polypropylene particles with diameter of 2000 μm were fluidized under gas velocities of 0.1 – 0.5 m/s while air at 40 °C and relative humidity of 35% was used as the fluidizing gas. Their results showed that the electrostatic potential above the static bed height increased with the increase of fluidizing gas velocity. The electrostatic potential reached a peak at a gas velocity of 0.35 m/s, and then started

to decrease. Sowinski *et al*. [88,89] conducted many tests with polyethylene resin (Geldart Group B) in the system described in the previous section and illustrated in Figure 1.14 and studied the effects of gas velocities in the bubbling and slugging flow regimes. They concluded that the charge-to-mass ratio of particles adhered to the wall was higher in bubbling flow regime than in slugging flow regime, and there were more particles adhered to the wall in bubbling flow regime than in slugging flow regime.

Although quite a few works on the effect of fluidizing gas velocity have been reported in literature, no work has been carried out to investigate the electrostatic charge generation in turbulent flow. As introduced in Section 1.1.4, the commercial gas-solid reactors to produce polyethylene resins are operated in turbulent flow regime. Therefore, more study should be conducted to investigate degree of electrostatic charge generation in turbulent flow, which is a industrial related condition, and its comparison with pre-turbulent flow regime

1.5 Thesis objectives

The mechanisms of charge generation in gas-solid fluidized beds are poorly understood, particularly when the fluidizing particles are insulators such as polyethylene. This is partly due to the complex nature of the fluidization process, the complex nature of the electrostatic phenomenon, and the current lack of understanding of the fundamental processes underlying electrostatic charging in insulators. The ultimate goal of research in this area is to assist industry, particularly the polyolefin industry, in diminishing or eliminating the adverse effects of fluid bed reactor charging which results in significant operational challenges. In order to achieve this, the aim of this thesis is to gain a better understanding of the mechanisms of electrostatic charging that result in wall fouling in gas-solid fluidized beds, particularly in the industrial gas-phase polyethylene fluidized bed reactors.

The current state of research in this area has mainly involved investigations carried out in small-scale fluidized beds that are mostly made of non-conductive columns (e.g., Plexiglas) and are operated at atmospheric or significantly low operating pressures and at low gas velocities. However, such conditions are not representative of the operation of real systems. For instance, industrial polyethylene reactors are operated at elevated pressures, temperatures as well as gas velocities in turbulent fluidization regime. Therefore, in this thesis the particles charge

distributions within the fluidized bed and the extent of fluidized bed wall fouling were studies in a system capable of operating at conditions similar to industrial operation.

The specific objectives of this study were to:

1. Design and build a pilot plant pressurized gas-solid fluidization system that would allow the study of bed electrification at pressures up to 2600 kPa (abs) and gas velocities up to 1 m/s (turbulent flow regime), similar to those used in industrial polyethylene reactors. The system was to contain the previously developed online Faraday cup charge measurement technique described in Section 1.3.2.1. In addition, the fluidization column to have a column dimeter equal to diameters of pilot-scale industrial reactors, making the generated results more relevant to industrial operations.
2. Perform tests to study the effect of operating pressure and fluidization flow regime on the degree of electrostatic charge generation of linear low-density polyethylene (LLDPE) resins directly received from commercial reactors and the extend of the resins wall coating. The operating conditions of interest included pressures ranging from 101 kPa to 2600 kPa (abs) and the fluidizing gas velocities ranging from 1.5 to 7.5 times the minimum fluidization velocity, covering the transition to turbulent flow regime.
3. Evaluate the influence of operating pressure on gas bubble dynamics and its relation to the extent of bed electrification.
4. Propose possible mechanisms underlying particles charging and their migration and adherence to the column wall.

1.6 Thesis outline

The thesis is divided into seven chapters from which five chapters are prepared in manuscript form for publication in refereed journals.

The second chapter describes the newly designed pilot plant pressurized gas-solid fluidization system that enables operations at pressures up to 2600 kPa (abs) and houses the online Faraday cup technique that was previously developed by Sowinski *et al.* [107]. This chapter is a manuscript published in Powder Technology journal *(Song, D., Salama, F., Matta, J., Mehrani,*

P., Implementation of Faraday Cup Electrostatic Charge Measurement Technique in High-Pressure Gas-Solid Fluidized Beds at Pilot-Scale. Powder Technol., 290, 21–26, 2016.).

The third chapter presents the effect of operating pressure on the gas bubble dynamics, measured by utilizing an optical fiber probe and a differential pressure signal analysis method, while fluidizing two types of particles, glass beads and polyethylene resin. This chapter is a manuscript prepared for journal publication.

The fourth chapter presents the effect of operating pressure on the electrostatic charge generation and the degree of wall coating when fluidizing polyethylene resin. This chapter is a manuscript submitted to the journal of Chemical Engineering Science for publication *(Song D., Mehrani, P., Effect of Pressure on Electrostatic Charge Generation in a Pilot Scale Gas-solid Fluidized Bed of Polyethylene Particles, Manuscript ID: CES-D-16-02164, 2016)*

The fifth chapter presents the results of investigating the effect of gas velocity and the transition to turbulent flow regime on the degree of electrostatic charge generation and wall coating while fluidizing polyethylene resin. This chapter is a manuscript prepared for journal publication.

The sixth chapter discusses a proposed mechanism for polyethylene particles charging and the particles migration and coating the fluidization column wall. This chapter is a manuscript published in Powder Technology journal *(Song, D., Mehrani, P., Mechanism of Particle Build-up on Gas-solid Fluidization Column Wall due to Electrostatic Charge Generation, Article in press, 2017).*

The final chapter, chapter seven, presents the overall conclusions of this research and recommendations for future work.

Additional supporting information are presented in the appendices.

References

[1] J.R. Grace, Fluidized bed hydrodynamics, in: G. Hetsoroni (Ed.), Handb. Multiph. Syst., Hemisphere, Washington, DC, 1982: p. Chapter 8.1.

[2] S. Beret, J.M. Jenkins, T.M. Jones, R.L. Jones, Method for fluidized bed polymerization, US4588790 A, 1986.

[3] G. Hendrickson, Electrostatics and gas phase fluidized bed polymerization reactor wall sheeting, Chem. Eng. Sci. 61 (2006) 1041–1064.

[4] W.K. Lewis, E.R. Gilliland, W.C. Bauer, Characteristics of Fluidized Particles, Ind. Eng. Chem. 41 (1949) 1104–1117.

[5] J. Ciborowski, A. Wlodarski, On electrostatic effects in fluidized beds, Chem. Eng. Sci. 17 (1962) 23–32.

[6] D. Kunii, O. Levenspiel, Fluidization Engineering, illustrate, Butterworth-Heinemann, Oxiford, 1991.

[7] D. Geldart, Types of gas fluidization, Powder Technol. 7 (1973) 285–292.

[8] S. Crescitelli, G. Donsi, G. Russo, R. Clift, High velocity behaviour offluidized beds: slugs and turbulent flow, in: Chisa Conf. Prague, 1978: pp. 1–11.

[9] J. Yerushalmi, N.T. Cankurt, Further studies of the regimes of fluidization, Powder Technol. 24 (1979) 187–205.

[10] H.T. Bi, N. Ellis, I.A. Abba, J.R. Grace, A state-of-the-art review of gas-solid turbulent fluidization, Chem. Eng. Sci. 55 (2000) 4789–4825.

[11] W.-C. Yang, MECHANISTIC MODELS FOR TRANSITIONS BETWEEN REGIMES OF FLUIDIZATION., AIChE J. 30 (1984) 1025–1027.

[12] G.S. Lee, S.D. Kim, Pressure fluctuations in turbulent fluidized beds, J. Chem. Eng. Japan. 21 (1988) 515–521.

[13] P. Cai, S.P. Chen, Y. Jin, Z.Q. Yu, Z.W. Wang, Effect of operating temperature and pressure on the transition from bubbling to turbulent fluidization, AIChE Symp. Ser. 85 (1989) 37–43.

[14] J.F. Davidson, Symposium on fluidization: discussion, Symp. Fluid. Discuss. 39 (1961) 230.

[15] R. Darton, R. LaNauze, J. Davidson, D. Harrison, Bubble growth due to coalescence in fluidised beds, Transcr. Inst. Chem. Eng. 55 (1977) 274–280.

[16] W.C. Yang, Bubbling Fluidized Beds, in: W.C. Yang (Ed.), Handb. Fluid. Fluid-Particle

Syst., CRC Press, 2003: p. 99.

[17] B. Bai, S. Gheorghiu, J.R. van Ommen, J. Nijenhuis, M.-O. Coppens, Characterization of the void size distribution in fluidized beds using statistics of pressure fluctuations, Powder Technol. 160 (2005) 81–92.

[18] L.R. Glicksman, W.K. Lord, M. Sakagami, Bubble properties in large-particle fluidized beds, Chem. Eng. Sci. 42 (1987) 479–491.

[19] R. Andreux, J. Chaouki, Behaviors of the bubble, cloud, and emulsion phases in a fluidized bed, AIChE J. 54 (2008) 406–414.

[20] M. Liu, Y. Zhang, H. Bi, J.R. Grace, Y. Zhu, Non-intrusive determination of bubble size in a gas–solid fluidized bed: An evaluation, Chem. Eng. Sci. 65 (2010) 3485–3493.

[21] S. Guet, R. V Fortunati, R.F. Mudde, G. Ooms, Bubble Velocity and Size Measurement with a Four-Point Optical Fiber Probe, Part. Part. Syst. Charact. 20 (2003) 219–230.

[22] C. Sobrino, J.A. Almendros-Ibáñez, D. Santana, C. Vázquez, M. de Vega, Maximum entropy estimation of the bubble size distribution in fluidized beds, Chem. Eng. Sci. 64 (2009) 2307–2319.

[23] P.A. Olowson, A.E. Almstedt, Hydrodynamics of a bubbling fluidized bed: influence of pressure and fluidization velocity in terms of drag force, Chem. Eng. Sci. 47 (1992) 357–366.

[24] P.A. Olowson, A.E. Almstedt, Influence of pressure and fluidization velocity on the bubble behaviour and gas flow distribution in a fluidized bed, Chem. Eng. Sci. 45 (1990) 1733–1741.

[25] J. Schweinzer, O. Molerus, Bubble flow in pressurized gas/solid fluidized beds, Chem. Eng. Technol. - CET. 10 (1987) 368–375.

[26] J. Werther, O. Molerus, The local structure of gas fluidized beds —II. The spatial distribution of bubbles, Int. J. Multiph. Flow. 1 (1973) 123–138.

[27] T.M. Knowlton, High-pressure fluidization characteristics of several particulate solids, primarily coal and coal-derived materials, in: AIChE Symp. Ser, 1977: pp. 22–28.

[28] R.F. Mudde, H.B.M. Schulte, H.E.A. van den Akker, Analysis of a bubbling 2-D gas-fluidized bed using image processing, Powder Technol. 81 (1994) 149–159.

[29] B. Wu, G. Yu, C. Bellehumeur, A. Kantzas, Dynamic flow behavior measurements in gas–solid fluidized beds using different non-intrusive techniques and polyethylene powder, Process Tomogr. Flow Vis. 18 (2007) 197–203.

[30] J.S. Halow, G.E. Fasching, P. Nicoletti, J.L. Spenik, Observations of a fluidized bed using capacitance imaging, Chem. Eng. Sci. 48 (1993) 643–659.

[31] P.N. Rowe, P.U. Foscolo, A.C. Hoffmann, J.G. Yates, X-ray observation of gas fluidized beds under pressure, in: A.C. Kunnii, R. Toei (Eds.), Fluidization, Engineering Foundation, New York, 1983: pp. 53–60.

[32] A.W. Weimer, G.J. Quarderer, On dense phase voidage and bubble size in high pressure fluidized beds of fine powders, AIChE J. 31 (1985) 1019–1028.

[33] J. van der Schaaf, J.C. Schouten, F. Johnsson, C.M. van den Bleek, Non-intrusive determination of bubble and slug length scales in fluidized beds by decomposition of the power spectral density of pressure time series, Int. J. Multiph. Flow. 28 (2002) 865–880.

[34] G. Yasui, L.N. Johanson, Characteristics of gas pockets in fluidized beds, AIChE J. 4 (1958) 445–452.

[35] M. Rüdisüli, T.J. Schildhauer, S.M.A. Biollaz, J.R. van Ommen, Bubble characterization in a fluidized bed by means of optical probes, Int. J. Multiph. Flow. 41 (2012) 56–67.

[36] J.G. Yates, Effects of temperature and pressure in gas-solid fluidization, Chem. Eng. Sci. 51 (1996) 167–205.

[37] P.N. Rowe, The effect of pressure on minimum fluidisation velocity, Chem. Eng. Sci. 39 (1984) 173–174.

[38] S.C. Saxena, G.J. Vogel, Measurement of incipient fluidisation velocities in a bed of coarse dolomite at temperature and pressure, Trans Inst Chem Eng. 55 (1977) 184–189.

[39] D.F. King, D. Harrison, Dense phase of a fluidised bed at elevated pressures, Trans. Inst. Chem. Eng. 60 (1982) 26–30.

[40] L.E.L. Sobreiro, J.L.F. Monteiro, The effect of pressure on fluidized bed behaviour, Powder Technol. 33 (1982) 95–100.

[41] G.C. Brouwer, E.C. Wagner, J.R. van Ommen, R.F. Mudde, Effects of pressure and fines content on bubble diameter in a fluidized bed studied using fast X-ray tomography, Chem. Eng. J. 207–208 (2012) 711–717.

[42] A.C. Hoffmann, J.G. Yates, Experimental observations of fluidized beds at elevated pressures, Chem. Eng. Commun. 41 (1986) 133–149.

[43] D.C. Chitester, R.M. Kornosky, L.-S.-S. Fan, J.P. Danko, Characteristics of fluidization at high pressure, Chem. Eng. Sci. 39 (1984) 253–261.

[44] I.H. Chan, C. Sishtla, T.M. Knowlton, The effect of pressure on bubble parameters in gas-fluidized beds, Powder Technol. 53 (1987) 217–235.

[45] A. Orta, B. Wu, M. Ghods, A. Guerrero, C. Bellehumeur, A. Kantzas, Pressure effect on hydrodynamics of a high pressure X-ray transparent polyethylene fluidized bed, Int. J. Chem.

React. Eng. 9 (2011).

[46] J. Wiman, A.E. Almstedt, Influence of pressure, fluidization velocity and particle size on the hydrodynamics of a freely bubbling fluidized bed, Chem. Eng. Sci. 53 (1998) 2167–2176.

[47] R.F. Dye, Patent No. 3023203, 1962.

[48] F.J. Karol, I.J. Levine, Preparation of low and medium density ethylene polymer in fluid bed reactor, US 4011382 A, 1977.

[49] T. Xie, K.B. McAuley, J.C.C. Hsu, D.W. Bacon, Gas phase ethylene polymerization: Production processes, polymer properties, and reactor modeling, Ind. Eng. Chem. Res. 33 (1994) 449–479.

[50] N. Ellis, Hydrodynamics of gas-solid turbulent fluidized beds, The university of british columbia, 2003.

[51] J. Cross, Electrostatics: Principles, Problems and Applications, Adam Hilger, Bristol, U.K, 1987.

[52] P.E. Shaw, Experiments on Tribo-Electricity. I. The Tribo-Electric Series, Proc. R. Soc. A. 94 (1917) 16–33.

[53] M. Mardiguian, Electrostatic Discharge Phenomenon, in Electrostatic Discharge: Understand, Simulate, and Fix ESD Problems, John Wiley & Sons, Inc., Hoboken, NJ, USA, 2009.

[54] D.J. Montgomery, Static Electrification of Solids, Solid State Phys. - Adv. Res. Appl. 9 (1959) 139–197.

[55] J. Lowell, A. Rose-Innes, Contact electrification, Adv. Phys. 29 (1980) 947–1023.

[56] S. Matsusaka, H. Maruyama, T. Matsuyama, M. Ghadiri, Triboelectric charging of powders: A review, Chem. Eng. Sci. 65 (2010) 5781–5807.

[57] K. Tanoue, H. Masuda, Electrostatic Separation, in: H. Masuda, K. Higashitani, H. Yoshida (Eds.), Powder Technol. Handbook, CRC Press LLC, 2006: p. 656.

[58] G.S.P. Castle, Contact charging between insulators, Proc. 8th Int. Conf. Electrost. 40–41 (1997) 13–20.

[59] V. Rojo, J. Guardiola, A. Vian, A capacitor model to interpret the electric behaviour of fluidized beds. Influence of apparatus geometry, Chem. Eng. Sci. 41 (1986) 2171–2181.

[60] M.W. Williams, Triboelectric charging of insulating polymers-some new perspectives, AIP Adv. 2 (2012).

[61] D.J. Lacks, The unpredictability of electrostatic charging, Angew. Chemie - Int. Ed. 51

(2012) 6822–6823.

[62] W.R. Harper, Contact and Frictional Electrification, Oxford at the Clarendon Press (Oxford Univ. Press), London, 1967.

[63] H. Bauser, W. Klöpffer, H. Rabenhorst, On the charging mechanism of insulating solids, in: Adv. Static Electr., Auxilia S. A., Brussels, 1970: pp. 2–9.

[64] R.G.C. Arridge, The static electrification of nylon 66, Br. J. Appl. Phys. 18 (1967) 1311–1316.

[65] D.K. Davies, Charge generation on dielectric surfaces, J. Phys. D. Appl. Phys. 2 (1969) 1533–1537.

[66] I.I. Inculet, E.P. Wituschek, Static Electrification, in: Instutute Phys. Conf. Ser. No. 4, 1967: pp. 37–42.

[67] M.I. Kornfeld, Nature of frictional electrification, Sov. Phys. Solid State. 2 (1969) 1306–1310.

[68] M.I. Kornfeld, Frictional electrification, J. Phys. D. Appl. Phys. 9 (1976) 1183–1192.

[69] W.R. Harper, Adhesion and Charging of Quartz Surfaces, Proceddings R. Socity London Seaies A. 231 (1955) 388–403.

[70] P.E. Wagner, Electrostatic charge separation at metal-insulator contacts, J. Appl. Phys. 27 (1956) 1300–1310.

[71] W.R. Salaneck, A. Paton, D.T. Clark, Double mass transfer during polymer-polymer contacts, J. Appl. Phys. 47 (1976) 144–147.

[72] M.M. Apodaca, P.J. Wesson, K.J.M. Bishop, M.A. Ratner, B.A. Grzybowski, Contact electrification between identical materials, Angew. Chemie - Int. Ed. 49 (2010) 946–949.

[73] H.T. Baytekin, A.Z. Patashinski, M. Branicki, B. Baytekin, S. Soh, B.A. Grzybowski, The mosaic of surface charge in contact electrification, Science (80-.). 333 (2011) 308–312.

[74] D.J. Lacks, R. Mohan Sankaran, Contact electrification of insulating materials, J. Phys. D. Appl. Phys. 44 (2011) 453001.

[75] R. Pham, R.C. Virnelson, R.M. Sankaran, D.J. Lacks, Contact charging between surfaces of identical insulating materials in asymmetric geometries, J. Electrostat. 69 (2011) 456–460.

[76] M. Sow, R. Widenor, A. Kumar, S.W. Lee, D.J. Lacks, R.M. Sankaran, Strain-induced reversal of charge transfer in contact electrification, Angew. Chemie - Int. Ed. 51 (2012) 2695–2697.

[77] T.A.L. Burgo, T.R.D. Ducati, K.R. Francisco, K.J. Clinckspoor, F. Galembeck, S.E.

Galembeck, Triboelectricity: Macroscopic charge patterns formed by self-arraying ions on polymer surfaces, Langmuir. 28 (2012) 7407–7416.

[78] S. Matsusaka, M. Ghadiri, H. Masuda, Electrification of an elastic sphere by repeated impacts on a metal plate, J. Phys. D. Appl. Phys. 33 (2000) 2311–2319.

[79] T. Matsuyama, H. Yamamoto, Charge relaxation process dominates contact charging of a particle in atmospheric conditions, J. Phys. D. Appl. Phys. 28 (1995) 2419–2423.

[80] T. Matsuyama, H. Yamamoto, Characterizing the electrostatic charging of polymer particles by impact charging experiments, Adv. Powder Technol. 6 (1995) 211–220.

[81] P. Cartwright, S. Singh, A.G. Bailey, L.J. Rose, Electrostatic Charging Characteristics of Polyethylene Powder During Pneumatic Conveying, IEEE Trans. Ind. Appl. IA-21 (1985) 541–546.

[82] K.M. Forward, D.J. Lacks, R.M. Sankaran, Triboelectric charging of granular insulator mixtures due solely to particle - Particle interactions, Ind. Eng. Chem. Res. 48 (2009) 2309–2314.

[83] F. Sharmene Ali, M. Adnan Ali, R. Ayesha Ali, I.I. Inculet, Minority charge separation in falling particles with bipolar charge, J. Electrostat. 45 (1998) 139–155.

[84] H. Zhao, G.S.P. Castle, I.I. Inculet, A.G. Bailey, Bipolar charging of poly-disperse polymer powders in fluidized beds, IEEE Trans. Ind. Appl. 39 (2003) 612–618.

[85] A. Giffin, P. Mehrani, Comparison of influence of fluidization time on electrostatic charge build-up in the bubbling vs. slugging flow regimes in gas-solid fluidized beds, J. Electrostat. 68 (2010) 492–502.

[86] Z. Liu, X.T. Bi, J.R. Grace, Electrostatic charging behaviour of dielectric particles in a pressurized gas-solid fluidized bed, J. Electrostat. 68 (2010) 321–327.

[87] P. Mehrani, H.T. Bi, J.R. Grace, Electrostatic charge generation in gas-solid fluidized beds, J. Electrostat. 63 (2005) 165–173.

[88] A. Sowinski, L. Miller, P. Mehrani, Investigation of electrostatic charge distribution in gas-solid fluidized beds, Chem. Eng. Sci. 65 (2010) 2771–2781.

[89] A. Sowinski, A. Mayne, P. Mehrani, Effect of fluidizing particle size on electrostatic charge generation and reactor wall fouling in gas-solid fluidized beds, Chem. Eng. Sci. 71 (2012) 552–563.

[90] J. Lowell, W.S. Truscott, Triboelectrification of identical insulators : II. Theory and further experiments, J. Phys. D. Appl. Phys. 19 (1986) 1281–1298.

[91] T.B. Jones, Electrostatic and Dust Explosions in Powder Handling, in: W.C. Yang (Ed.),

Fluid. Solids Handl. Process. Ind. Appl., Noyes Publications, Park Ridge, NJ, 1998: pp. 817–871.

[92] M. Leva, Elutriation of fines from fluidized systems, Chem.Eng.Progress. 47 (1951) 39–45.

[93] C.O. Miller, A.K. Logwinuk, Fluidization Studies of Solid Particles., Ind. Eng. Chem. 43 (1951) 1220–1226.

[94] G.L. Osberg, D.H. Charlesworth, Elutriation in a fluidized bed, Chem.Eng.Prog. 47 (1951) 566–570.

[95] R.H. Wilhelm, M. Kwauk, Fluidization of solid particles, Chem.Eng.Prog. 44 (1948) 201–218.

[96] R. Hagerty, M. Muhle, A. Agapiou, C.-T. Kuo, M. Goode, F.D. Hussein, R. Pannel, J. Szul, Method for controlling sheeting in gas phase reactors, US20050148742 A1, 2005.

[97] M.G. Goode, D.M. Hasenberg, T.J. McNeil, T.E. Spriggs, Method for reducing sheeting during polymerization of alpha-olefins, US4803251 A, 1989.

[98] G.H. Song, A.S. Rhee, G.R. Lowder, Method for reducing sheeting and static charges during polymerization of ethylene polymers, US5391657 A, 1995.

[99] K. Kubo, M. Morikawa, Y. Sano, S. Suga, M. Watanabe, Y. Yamaguchi, Method for producing polyolefin, 1995.

[100] B. Fulks, S. Sawin, C. Aikman, J. Jenkins, Process for reducing sheeting during polymerization of alpha-olefins, US4532311, 1985.

[101] J. Guardiola, G. Ramos, A. Romero, Electrostatic behaviour in binary dielectric/conductor fluidized beds, Powder Technol. 73 (1992) 11–19.

[102] M.G. Goode, F.D. Hussein, K.H. Lee, T.J. McNeil, C.C. Williams, Static control in olefin polymerization, US6111034 A, 2000.

[103] L. Fasso, B.T. Chao, S.L. Soo, Measurement of electrostatic charges and concentration of particles in the freeboard of a fluidized bed, Powder Technol. 33 (1982) 211–221.

[104] J.R. Mountain, M.K. Mazumder, R.A. Sims, D.L. Wankum, T. Chasser, P.H. Pettit Jr., Triboelectric charging of polymer powders in fluidization and transport processes, IEEE Trans. Ind. Appl. 37 (2001) 778–784.

[105] W.O. Moughrabiah, J.R. Grace, X.T. Bi, Effects of pressure, temperature, and gas velocity on electrostatics in gas-solid fluidized beds, Ind. Eng. Chem. Res. 48 (2009) 320–325.

[106] G. Tardos, R. Pfeffer, A method to measure electrostatic charge on a granule in a fluidized bed, Chem. Eng. Commun. 4 (1980) 665–671.

[107] A. Sowinski, F. Salama, P. Mehrani, New technique for electrostatic charge measurement in gas-solid fluidized beds, J. Electrostat. 67 (2009) 568–573.

[108] M. Bafrnec, J. Bena, Quantitative data on the lowering of electrostatic charge in a fluidized bed, Chem. Eng. Sci. 27 (1972) 1177–1181.

[109] V.N. Kiselnikov, V. V Vyalkov, V.M. Filatov, On the problem of electrostatic phenomena in a fluidized bed, Int.Chem.Eng. 7 (1967) 428–431.

[110] R.W. Ham, P.A. Gauthier, M.A. Bergougnou, Electrostatic in an air/catalyst fluidized bed at ambient temperature and pressure, Fluid. Eng. Found. New York. (1992) 611–620.

[111] A. Gajewski, Investigation of the electrification of polypropylene particles during the fluidization process, J. Electrostat. 17 (1985) 289–298.

[112] J. Revel, C. Gatumel, J.A. Dodds, J. Taillet, Generation of static electricity during fluidisation of polyethylene and its elimination by air ionisation, Powder Technol. 135–136 (2003) 192–200.

[113] L. Yao, H.T. Bi, A.H. Park, Characterization of electrostatic charges in freely bubbling fluidized beds with dielectric particles, J. Electrostat. 56 (2002) 183–197.

[114] M. Murtomaa, E. Räsänen, J. Rantanen, A. Bailey, E. Laine, J.P. Mannermaa, J. Yliruusi, Electrostatic measurements on a miniaturized fluidized bed, J. Electrostat. 57 (2003) 91–106.

[115] T.A. Alsmari, J.R. Grace, X.T. Bi, Effects of superficial gas velocity and temperature on entrainment and electrostatics in gas-solid fluidized beds, Chem. Eng. Sci. 123 (2015) 49–56.

[116] J. Guardiola, V. Rojo, G. Ramos, Influence of particle size, fluidization velocity and relative humidity on fluidized bed electrostatics, J. Electrostat. 37 (1996) 1–20.

Chapter 2
Implementation of Faraday Cup Electrostatic Charge Measurement Technique in High-Pressure Gas-Solid Fluidized Beds at Pilot-Scale

Di Song, Fawzi Salama, Johnny Matta, Poupak Mehrani*

Chemical and Biological Engineering Department, University of Ottawa
161 Louis Pasteur, Ottawa, ON, Canada, K1N 6N5
* poupak.mehrani@uottawa.ca, Tel: 1 (613) 562-5800 Ext. 6098, Fax: 1 (613) 562-5172

The current chapter is a manuscript published in the journal of Powder Technology "Powder Technology, 290, 21–26, 2016"

Abstract

Elevation of operating pressure in gas-solid fluidized beds affects the bed hydrodynamics, which in turn could affect the extent of bed electrification and reactor wall coating due to electrostatic charge generation. In this work, a pilot plant high-pressure gas-solid fluidization system housing the Faraday cup electrostatic charge measurement technique is introduced in order to study the underlying mechanism of electrostatic charge generation causing fluidized bed wall fouling at pressures up to 2600 kPa. A previously developed online electrostatic charge measurement technique containing two Faraday cups was successfully implemented in the high-pressure system. The effect of operating pressure on gas-solid fluidized bed electrification was examined under operating pressures of 101 and 2600 kPa (abs) by fluidizing polyethylene resin directly received from a commercial reactor. Experimental results showed that the magnitude of reactor wall coating increased with the increase of operating pressure. The wall coating contained positively as well as negatively charged particles indicating the occurrence of bipolar charging within the fluidized bed. Finally, based on the experimental results obtained in this work the mechanism of fluidized bed column wall coating formation was discussed.

Keywords: Gas-Solid Fluidization, Electrostatics, Particle Wall Coating, Electrostatic Charge Distribution, Electrostatic Charge Measurement

2.1 Introduction

Electrostatic charge generation in gas-solid fluidized beds due to the continuous contacts amongst particles and the particles and the column wall may give rise to major nuisances in some processes. The generated charges might cause particle agglomeration causing deviation from the desired particle properties, large electrostatic discharge endangering operators and equipment, and the adhesion of particles to the reactor wall and other surfaces necessitating regular shutdown for clean-up. An example of a commercial process that has faced critical operational challenges by electrostatic charge generation is the gas-phase ethylene polymerization to produce polyethylene. In this process, charged fluidizing particles (catalyst and polyethylene resin) adhere to, or coat, the walls and dome of the fluidized bed reactor, causing a problem known as "sheeting" [1-4].

Commercial gas-solid fluidized bed reactors for polyethylene production are operated in turbulent flow regime at pressures of 2500-3000 kPa and temperatures of 80-110°C [5]. It has been known that increasing the fluidization operating pressure affects the fluidization hydrodynamics where smoother fluidization, reduction of the gas bubbles size and elevation of their rise velocity have been reported [6-12]. As a result, the increase of operating pressure affects particles movement and mixing within the fluidized bed; and in turn could affect the degree of electrostatic charge generation within the bed. In addition, for each flow regime beyond minimum fluidization, different flow regimes result in different particle movement patterns and thus, affect contact charging between particles, and particle and column wall [13]. Therefore, it is beneficial to conduct studies in relation to polyethylene reactor electrifications under industrially-relevant operating conditions.

Although there has been some progress in the understanding of electrostatic charging in fluidized beds and several proposed solutions, the problem persists. The fundamental mechanisms of charge generation and dissipation in gas-solid fluidized beds are poorly understood, particularly when the fluidized particles are insulating such as polyethylene. This is partly due to the complex nature of the fluidization process and the fundamental processes underlying electrostatic charging in insulators. The majority of works studying the underlying mechanism of electrostatic charge generation in gas-solid fluidized beds, except for very few [14-15], investigated the phenomenon under atmospheric conditions in bubbling or slugging flow regime at room

temperature [16]. Moughrabiah *et al.* [14] and Liu *et al.* [15] used the same experimental apparatus and determined the local particles charge during fluidization at pressures up to 724 kPa using electrostatic probes installed at various heights within the fluidized bed. Moughrabiah *et al.* [14] measured electrostatic charge generated on the probes during fluidization for 500 seconds and reported as a measure of bed electrification. Utilizing glass beads as the fluidized particles, they concluded that increasing operating pressure from 379 to 724 kPa increased bed electrification. Liu *et al.* [15], utilizing the same apparatus studied the effect of operating pressure on the fluidization of various polyethylene resins with pressures from 138 to 621 kPa. The authors concluded that it was difficult to predict the effect of operating pressure on electrostatics. This could have been due to measurement technique used in their study which only enables very local charge measurements that could be significantly influenced by the changes in the bed hydrodynamics and particles bipolar charging.

Therefore, there is a need to investigate the effects of fluidization pressure on the degree of fluidizing particles electrostatic charging, and most importantly, to examine the extent of the wall coating generated due to the bed electrification. This is a parameter that to the authors' knowledge has not been evaluated and reported in literature under pressure. Since commercial reactors, at least those of gas-phase polyethylene production which are affected the most by electrostatic phenomenon, are operated at pressures of 2500-3000 kPa, it is essential to extend the investigation to such elevated pressures.

In this work a pilot plant high-pressure gas-solid fluidization system was built in order to study the underlying mechanism of electrostatic charge generation as well as bed hydrodynamics in gas-solid fluidized beds at elevated pressures. The system was designed to operate with pressures up to 2600 kPa, temperatures up to 100°C, and fluidizing gas velocities up to 1 m/s. A successfully applied online electrostatic charge measurement technique that was previously developed by our research group [13, 16-17] was implemented into the new system. The technique contained two removable Faraday cups in which allowed the simultaneous measurement of particles specific charge, mass and size distribution in three different regions of the fluidized bed: particles in bulk, those adhered to the column wall, and those entrained. The method also enabled the qualitative examination of particle wall coating. The present work introduces the newly custom-built pilot plant high-pressure system and compares the results

obtained for the degrees of wall coating for two operating conditions of atmospheric and 2600 kPa (abs).

2.2 Methods and Material

The schematic diagram of the high-pressure gas-solid fluidization system is shown in Figure 2.1 (images of the system are shown in Appendix C). The system was designed to be operated at pressures up to 2600 kPa (abs), temperatures up to 100°C, and fluidizing gas velocities up to 1 m/s. The system consisted of a 3-D stainless steel fluidization column with a total height of 4.5 m (Appendix C, Figure C.2). The column contained a fluidization section with a height of 2.5 m and diameter of 0.154 m, and two expanded sections, 0.34 m in diameter each, located at the top and the bottom of the column. The fluidization column was equipped with two ABB pressure transducers, one to measure the differential pressure across the bed and another to detect the system operating gauge pressure.

The electrostatic charge measurements were achieved by two copper Faraday cups located within the top and bottom expanded sections of the column, which also acted as the outer Faraday cups. The two copper cups were electrically isolated from the body of the column, which was grounded. At the top, the exit of the column was fitted with a filter bag, also located inside the top Faraday cup to enable the capture of entrained fines and thus their cumulative net charge measurements during fluidization. Both Faraday cups were connected to Keithley digital electrometers model 6514. Similar to the system of Sowinski *et al.* [13,17], the distributor plate was a modified 0.15 m in diameter pneumatic knife gate valve (Appendix C, Figure C.3). As a result, the distributor plate could be opened and closed easily, allowing the bed particles to discharge into the bottom Faraday cup for their net charge measurement. The blade of the knife gate valve consisted of two porous stainless steel 316 plates and a metal screen sandwiched between them. Since it was desired to operate the system at high pressure but still conveniently access the inner Faraday cups, two manways (GD Engineering, UK) were used to enclose the top and bottom (Appendix C, Figure C 4).

The flowrate of the gas entering the fluidization column is measured by using a Rosemount orifice plate meter. The fluidizing gas is supplied by two sources depending on the system operating pressure: (a) compressed building air (23°C and 3% RH) for atmospheric operations;

and (b) from a gas cylinder for non-atmospheric operations. More information about the fluidizing gas is shown in Appendix D.1. In the case of atmospheric operations, fluidizing gas entering the system is vented at the top of the column. For non-atmospheric operations (pressures up to 2600 kPa), any type of fluidizing gas (e.g., nitrogen) supplied from a gas cylinder can be used. In this case, while the vent line is closed, the system is first filled with the supply gas to the desired pressure. A variable speed centrifugal compressor (FIMA, Germany) then enables the recirculation of fluidization gas in the system and the control of the gas flowrate. A plate heat exchanger (GEA, Canada) cools the gas upon compression. All measurement devices are connected to a PC, and all data is collected and recorded using the LabView software.

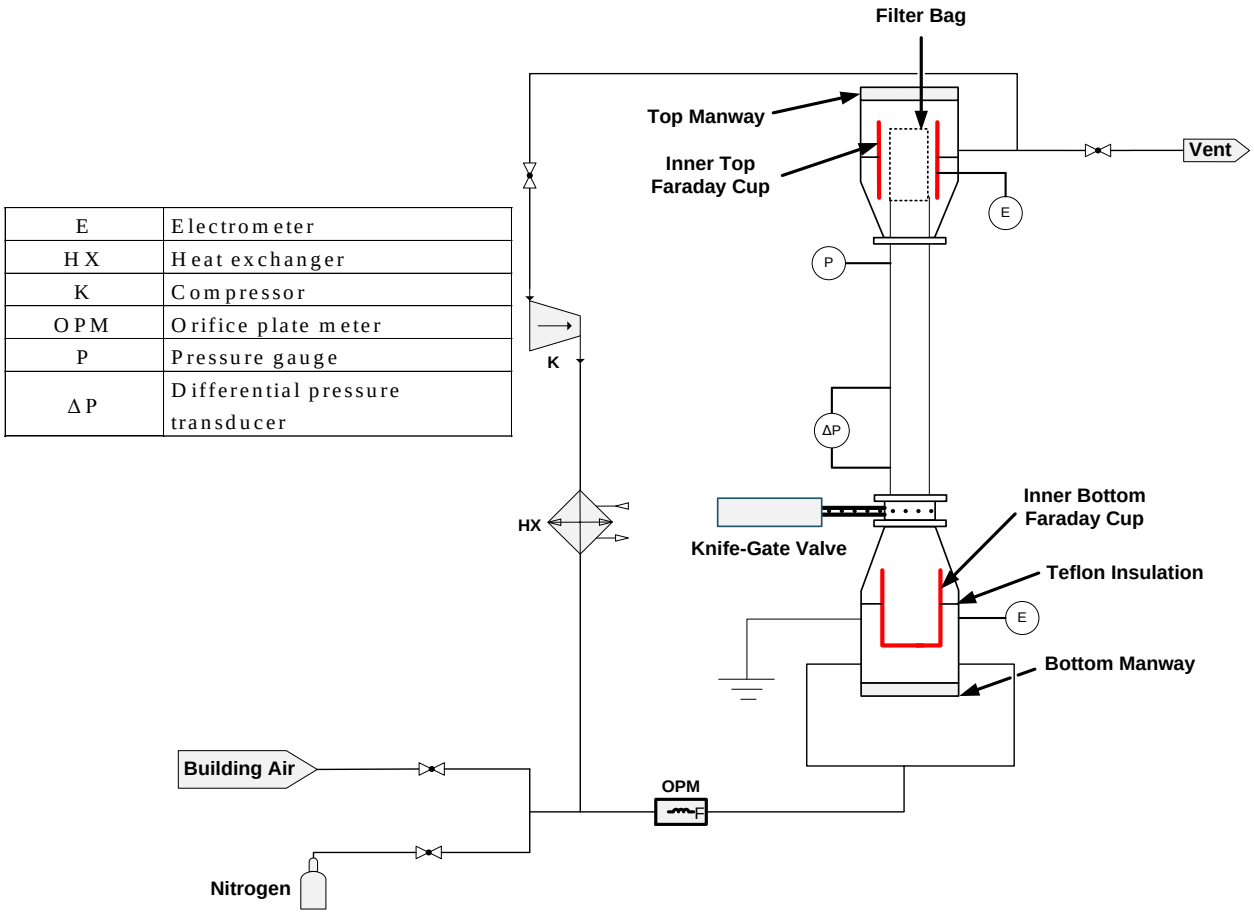

Figure 2.1: Schematic diagram of the pilot plant high-pressure fluidization system.

Experiments were conducted by fluidization of a metallocene-based resin of linear low-density polyethylene (LLDPE) directly received from commercial reactors (referred to as PE_A in Appendix D.2.1). The resin was Geldart group B with a particle density of 918 kg/m^3 and a wide

size distribution of 20-2000 micron with an average particle size of approximately 710 µm. Experiments were conducted at two operating pressures of atmospheric and 2600 kPa (abs). Nitrogen from a gas cylinder was used as the fluidizing gas for runs at elevated pressure. All trials were conducted in bubbling flow regime with a fluidizing gas velocity of 1.25 times the minimum fluidization velocity and lasted for one hour. Experiments were repeated three times to confirm reproducibility.

At the beginning of all experiments, an external Faraday cup was used to measure the net charge of the particles before putting them into the fluidization column from the top and mounting the filter bag and the top Faraday cup. Upon the completion of fluidization period, the top manway was opened (after the system was depressurized for the non-atmospheric operations) and the filter bag was removed for measuring the mass of entrained particles (referred to as "fines" or "fine particles"). The distributor plate was then opened allowing the particles in the bulk (referred to as "bulk" or "bulk particles") to drop into the bottom Faraday cup to measure their net charge. The bottom manway was then opened and the bottom Faraday cup was removed to measure the mass of the bulk particles. At this point, the column inner wall was inspected for any particle wall coating and a photographic image of the layer (referred to as "wall" or "wall particles") was taken. The bottom Faraday cup was then cleaned and returned to the column for collecting and measuring the net charge of wall particles. In order to dislodge the wall particles from the column wall into the bottom Faraday cup, a tube was inserted into the column from the top which had compressed building air passing through (Appendix C, Figure C.5). For all trials, samples of bulk, wall and fines were analyzed for their particles size distribution by a Malvern Mastersizer 2000 particle size analyzer.

2.3 Results and Discussion

The pilot plant high-pressure facility equipped with a fluidization column able to handle elevated pressures and housing the charge measurement method developed earlier by Sowinski *et al.* [13,17] was effectively operated at two conditions of atmospheric and 2600 kPa. This confirmed the application of the developed online Faraday cup technique for high pressure facilities at pilot scale. Thus, investigation of the effect of any operating parameters, including pressure, on the extent of the fluidizing particles electrostatic charging and especially the magnitude of the

particles coating the reactor wall was permitted by this system under the industrially relevant operating conditions.

For all experimental trials, several properties of the fluidizing particles were determined prior to their fluidization including particles mass (m), net charge (q) and mean particles diameter. The initial net specific charge (q/m) of particles was found to be relatively small at -0.01 ± 0.03 μC/kg, indicating that all trials were initiated with very small q/m values.

For all trials, particles charge, mass and mean particle diameter was found in three regions of the fluidized bed, namely the bulk, wall and the fines. The amount of fine particles was found to be negligible and thus no results about these particles are discussed here. From all experimental runs, it was found that 95-97% of the mass of particles initially placed in the column prior to fluidization remained in the bulk after fluidization, while wall particles only occupied 2-4% of the initial mass. It can be seen in Figure 2.2 that the total mass of wall particles increased by almost a factor of two when the operating pressure was elevated from 101 to 2600 kPa.

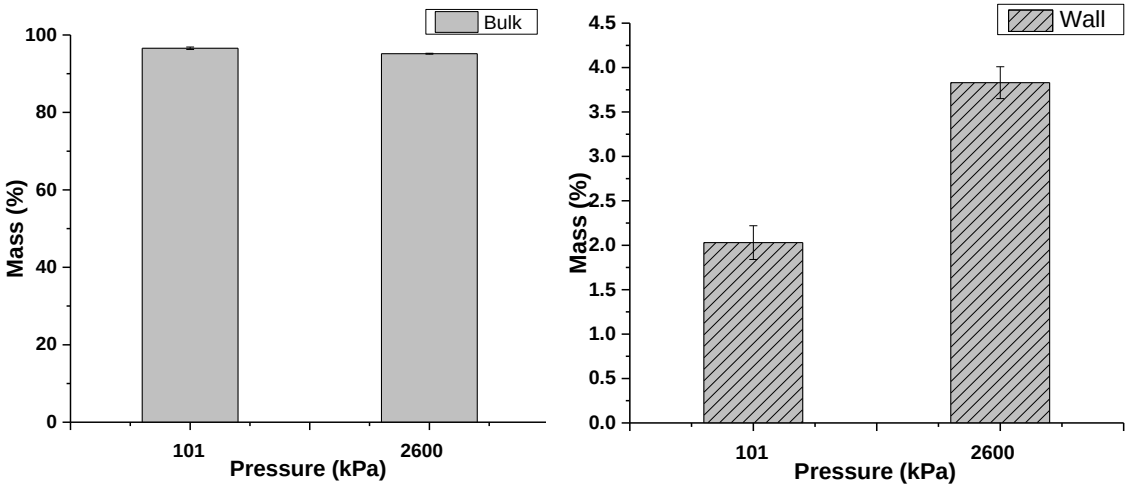

(a) (b)

Figure 2.2: Mass percentage of particles collected from (a) the bulk and (b) the wall regions of the fluidized bed at atmospheric and 2600 kPa.

While collecting the wall particles it was observed that as the particle removal progressed towards the layers closer to the column wall, the polarity of particles changed from positive to negative. An example of such a measurement is illustrated in Figure 2.3. These two oppositely charged layers were then referred to as "outer layer" and "inner layer", respectively. After completing the collection of the outer layer, the bottom Faraday cup was removed for measuring

the mass of these particles and samples were taken for particle size distribution analysis. Then the bottom Faraday cup was returned to the column to collect and measure the charge and the mass of particles in the inner layer.

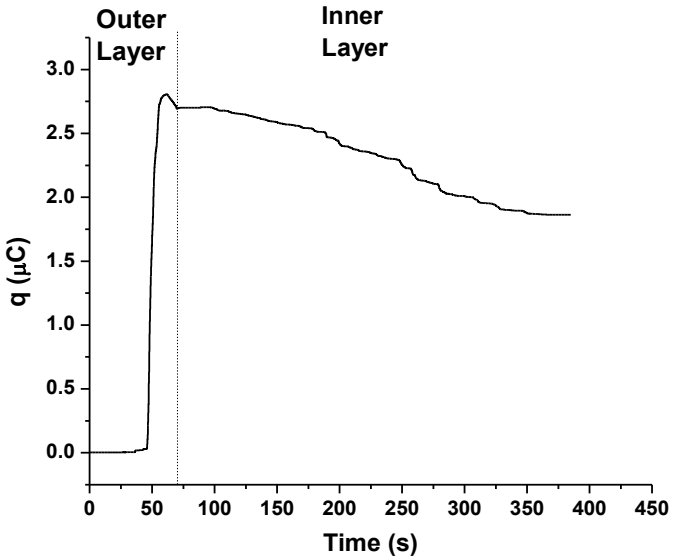

Figure 2.3: An example of particles charge measured as the wall coating was collected.

In gas-solid fluidized beds, electrostatic charges are generated due to triboelectrification between the fluidizing particles, and the particles and the column wall. In this work, because of negligible entrainment, the net specific charge observed within the bed (i.e., with the bulk and wall particles) can only be a result of particle-wall contacts. The net charge due to particle-particle contacts would be zero. In this work, due to the different work funcitons between the polyethylene particles and the stainless steel fluidization column wall, polyethylene particles were negatively charged. In addition, because the fluidization column is made of a conductive material, the image forces between the fluidization column wall and the particles in bed caused some of the negatively charged particles to be attracted and adher to the inner column wall. This mechanism forms the inner wall layer observed in this work. In addition, the image force attracting particles to the wall decays, according to Coulomb's law, with the increasing of the distance between the particles and the wall and the increase in the dielectric constant due to the presence of a layer of particles between the particle and the wall. Hence, at some distance away, negatively charged particles will not be attracted to the column wall. On the other hand, the inner negatively charged layer on the column wall will attract the positively charged particles, forming the outer layer observed in this work. Figure 2.4 illustrates the above-mentioned wall coating

formation mechanism. This confirms the hypothesis presented by Sowinski *et al.* [16] whereby particles form succeeding layers of opposing charge on the fluidization column wall.

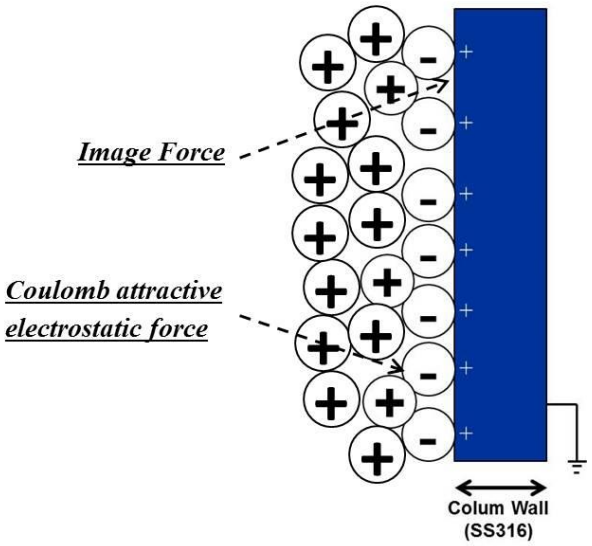

Figure 2.4: Fluidized bed wall coating formation mechanism.

Figure 2.5 presents the magnitude of reactor outer and inner wall coating at the operating pressures of 101 and 2600 kPa. The mass percentage of both outer and inner layers at 2600 kPa was higher than those at atmospheric condition, with almost a factor of two.

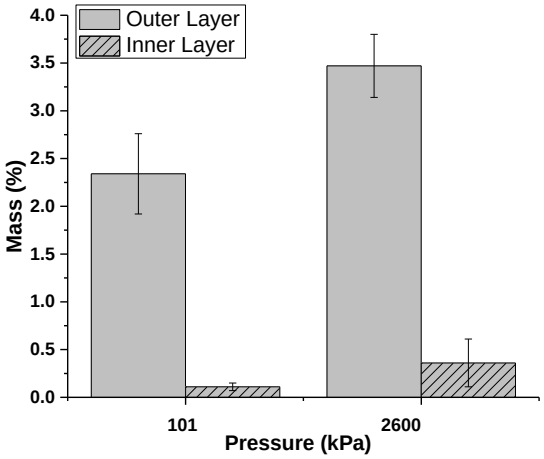

Figure 2.5: Mass percentage of particles collected off of the column wall forming the inner and outer wall layers at atmospheric and 2600 kPa.

The degree of column wall coating was also visually examined by taking photos of the inner column wall upon the removal of the bulk particles. Figure 2.6 shows an example of images taken from the inside of column prior to the removal of wall particles, after removing the outer layer and the inner layer. Similar images were obtained in all of trials. After removal of outer layer, only a thin layer of particles was left on the vessel wall, meaning most of wall particles were in outer layer.

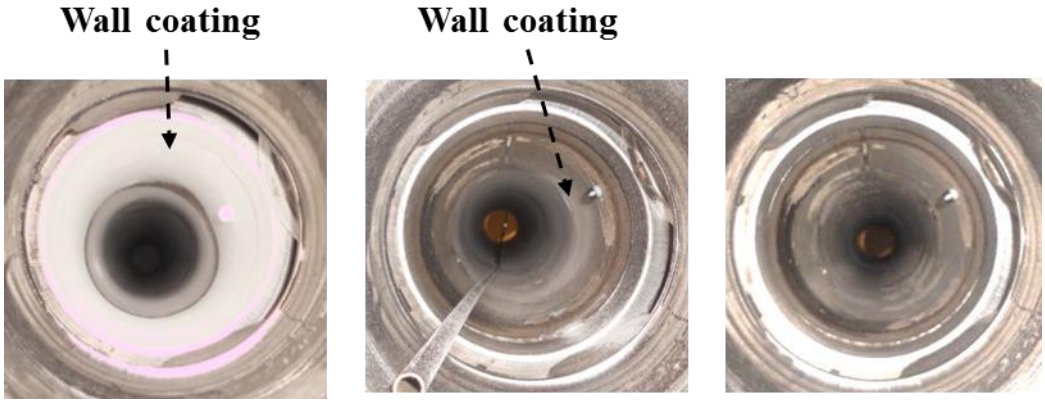

Figure 2.6: An example of images of wall coating taken for a run at 2600 kPa. (a) After the removal of the bulk particles; (b) After removing the outer layer; and (c) After removing the inner layer.

As can be seen in Figure 2.7, the net specific charge of particles in the wall outer layer at atmospheric condition was almost three times higher than that at 2600 kPa while the results were comparable for the inner layers. Considering the aforementioned results where the mass percentage of particles in the inner layer were almost doubled by elevating the pressure, the results of the net specific charge suggest that particles net charge must have also increased by a factor of two to keep the *q/m* relatively constant. Those particles are considered to be closer to the column wall and had relatively more contact with it. However similar analysis for particles in the outer wall layer implies that the net charge of particles kept similar with the increase of pressure. Comparing the particles absolute net specific charge implies that at atmospheric condition, results were comparable for the outer and inner layers, however at 2600 kPa, the inner layer had a significantly larger absolute *q*/*m*, almost four times higher than that of outer layer.

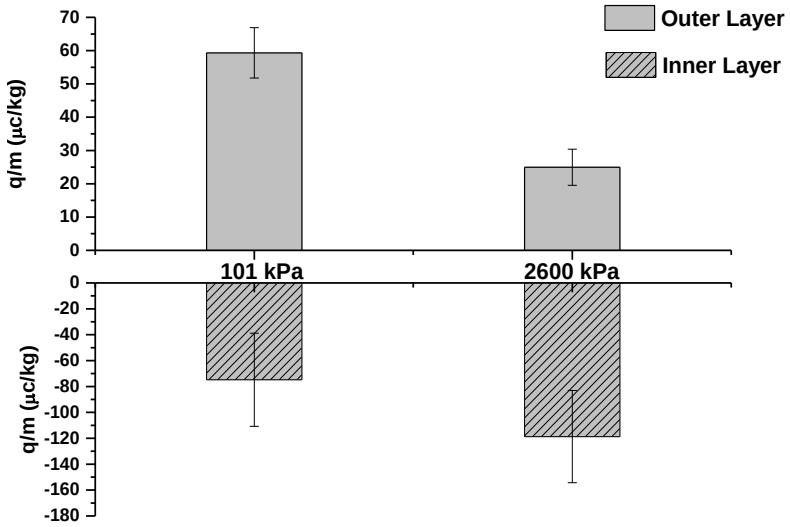

Figure 2.7: Net specific charge of particles in the outer and inner layers of coating on the column wall at atmospheric and 2600 kPa.

Samples taken from bulk particles and the wall inner and outer layers were analyzed for their particle size distribution. As presented in Figure 2.8, for both of the operating conditions, particles adhered to the column were comparable in size and smaller than those in bulk of the bed. Particles forming the inner and outer layers of the wall coating at both operating pressures were found to be of similar size.

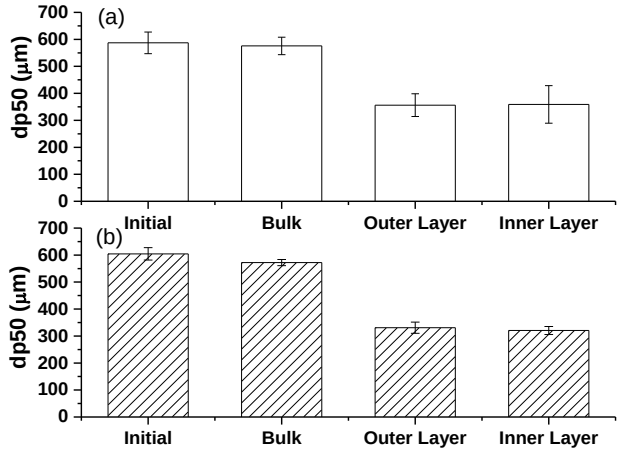

Figure 2.8: Mean diameter of particles found in different regions of the fluidized bed. (a) Atmospheric; and (b) 2600 kPa.

Elevating operating pressure in gas-solid fluidization results in an increase in the inertia of the gas and leading to a higher drag force; and thus, affecting the fluidization behaviour. From the studies reported in literature it is found that with fluidization of Geldart group B particles, increasing operating pressure decreases bubble size [18, 19] as well as slightly increasing bubble rise velocity [12]. Higher bubble rise velocities enhance the movement and mixing of particles within the bed, and thus increase particle contacts with other particles and with the column wall. More contacts mean higher degree of electrostatic charge generation on the particles and the column wall, resulting in higher degree of net charge in the bulk of the bed rendering a higher degree of image force between the bulk of particles and the column wall. Godlieb *et al.* [20] also determined the granular temperature of a bed of polyethylene particles modeled using discrete particle model (DPM) and reported that the granular temperature increases with increasing pressures up to 64 bar. They attributed the increase in granular temperature to the increase of the bed porosity, meaning that elevating pressure allows particles to have more movement; and thus, increases contacts within the bed. These findings support the results obtained in this study in which as the operating pressure increased from 101 to 2600 kPa, higher net charges and mass were found for particles forming the inner wall layer coating.

The higher absolute net specific charge of inner layer at 2600 kPa might be the reason of the elevation of the outer layer wall particle magnitude from atmospheric to 2600 kPa. The existence of the higher negative charge of inner layer gave rise to a stronger attraction to the positively charged particles in bulk, giving them a higher driving force to adhere to the column wall.

2.4 Conclusions

A pilot plant high-pressure gas-solid fluidization system was designed and built for the purpose of investigating electrostatic charge generation in gas-solid fluidized beds as well as fluidized bed hydrodynamics at high pressure (up to 2600 kPa) and temperatures (up to 100°C). The new system successfully implemented an existing online electrostatic charge measurement technique consisting of two online Faraday cups that allowed the particles mass, net charge and size distribution measurements in various regions of the fluidization system, especially those of the wall coating, and visual examination of the column wall coating under high pressure conditions. Elevating the system pressure from atmospheric condition to 2600 kPa gave rise to higher degree of fluidized bed wall coating. This finding was suggested to be as a result of changes in the bed hydrodynamics (i.e., more particles movements and contacts) at elevated pressures. Further research is required in this area to investigate the effect of operating pressure by specific evaluation of the bubble dynamics.

Results also illustrated that the wall layer consisted of positively as well as a smaller amount of negatively charged particles, implying the occurrence of bipolar charging within the bulk of the bed. Due to negligible entrainment, it was concluded that net specific charge of the bed was mainly due to particles contacting the fluidization column wall. In addition, this net specific charge resulted in image forces between the negatively charged particles and the metallic column wall and found to be the underlying mechanism of the inner wall layer formation. The formation of the outer wall layer was suggested to be due to the attractive electrostatic forces between the negatively charged inner layer and the positively charged particles within the bulk of the bed.

Acknowledgements

Financial support by Natural Sciences and Engineering Research Council (NSERC) of Canada, Canada Foundation for Innovation (CFI), and financial assistance and input from Univation Technologies, LLC (USA) are acknowledged with gratitude.

References

[1] M.G. Goode, F.D. Hussein, K.H. Lee, T.J. McNeil, C.C. Williams, Static control in olefin polymerization, US 6111034 A (2000).

[2] R.O. Hagerty, M.E. Muhle, A.K. Agapiou, C. Kuo, M.G. Goode, F.D. Hussein, R.B. Pannell, J.F. Szul, Method for controlling sheeting in gas phase reactors, US 7985811 B2 (2011).

[3] M.G. Goode, D.M. Hasenberg, T.J. McNeil, T.E. Spriggs, Neutralization of electrostatic charges, US 4803251 A (1989).

[4] G.H. Song, A.S. Rhee, G.R. Lowder, Monitoring electrostatic levels, adding positive or negative charge generating inorganic chemical additive to maintain neutral static charges in reactor, US 5391657 A (1995).

[5] S. Beret, J.M. Jenkins, T.M. Jones, R.L. Jones, Method for fluidized bed polymerization, US 4588790 A (1986).

[6] G. Barreto, J. Yates, P. Rowe, The effect of pressure on the flow of gas in fluidized beds of fine particles, Chem. Eng. Sci. 38 (1983) 1935-1945.

[7] J.S. Botterill, M. Desai, Limited factors in gas-fluidized bed heat transfer, Powder Technol. 6 (1972) 231-238.

[8] J. Chen, D. Keairns, Particle segregation in a fluidized bed, Can. J. Chem. Eng. 53 (1975) 395-402.

[9] D.C. Chitester, R.M. Kornosky, L. Fan, J.P. Danko, Characteristics of fluidization at high pressure, Chem. Eng. Sci. 39 (1984) 253-261.

[10] J.G. Yates, Effects of temperature and pressure in gas-solid fluidization, Chem. Eng. Sci. 51 (1996) 167-205.

[11] P.A. Olowson, A.E. Almstedt, Hydrodynamics of a bubbling fluidized bed: influence of pressure and fluidization velocity in terms of drag force, Chem. Eng. Sci. 47 (1992) 357-366.

[12] P.A. Olowson, A.E. Almstedt, Influence of pressure and fluidization velocity on the bubble behaviour and gas flow distribution in a fluidized bed, Chem. Eng. Sci. 45 (1990) 1733-1741.

[13] A. Sowinski, L. Miller, P. Mehrani, Investigation of electrostatic charge distribution in gas-solid fluidized beds, Chem. Eng. Sci. 65 (2010) 2771-2781.

[14] W.O. Moughrabiah, J.R. Grace, X.T. Bi, Effects of pressure, temperature, and gas velocity on electrostatics in gas-solid fluidized beds, Ind. Eng. Chem. Res. 48 (2009) 320-325.

[15] Z. Liu, X.T. Bi, J.R. Grace, Electrostatic charging behaviour of dielectric particles in a pressurized gas-solid fluidized bed, J. Electrostat. 68 (2010) 321-327.

[16] A. Sowinski, A. Mayne, P. Mehrani, Effect of fluidizing particle size on electrostatic charge generation and reactor wall fouling in gas-solid fluidized beds, Chem. Eng. Sci. 71 (2012) 552-563.

[17] A. Sowinski, F. Salama, P. Mehrani, New technique for electrostatic charge measurement in

gas-solid fluidized beds, J. Electrostat. 67 (2009) 568-573.

[18] A.C. Hoffman, J.G. Yates, Experimental observations of fluidized beds at elevated pressures. Chem. Eng. Commun. 41 (1986) 133-149.

[19] A. Orta, B. Wu, M. Ghods, A. Guerrero, C. Bellehumeur, A. Kantzas, Pressure effect on hydrodynamics of a high pressure X-ray transparent polyethylene fluidized bed, Int. J. Chem. React. Eng. 9 (2011) 1542-6580.

[20] W. Goldlieb, N. Deen, J. Kuipers, On the relationship between operating pressure and granular temperature: A discrete particle simulation study, Powder Technol. 182 (2008) 250-256.

Chapter 3
Bubble Characteristics Evaluation in a Pilot Plant Pressurized Gas-Solid Fluidized Bed Using an Optical Fiber Probe and Differential Pressure Signal Analysis

D. Song, V.N. Ellapani, M.O. Sharif, P. Mehrani*

Chemical and Biological Engineering Department, University of Ottawa
161 Louis Pasteur, Ottawa, ON, Canada, K1N 6N5
* poupak.mehrani@uottawa.ca, Tel: 1 (613) 562-5800 Ext. 6098, Fax: 1 (613) 562-5172

The current chapter is a manuscript to be submitted for journal publication

Abstract
In this work, effect of operating pressure on bubble dynamics including bubble size, rise velocity, and frequency was investigated in a pilot plant pressurized gas-solid fluidized bed. Experiments were conducted with glass beads and linear low-density polyethylene resin at various pressures ranging from atmospheric to 2600 kPa (abs). The local gas bubble properties were examined by using an optical fiber probe placed at one axial and two radial locations (column center as well as close to the column wall) within the fluidized bed. The average gas bubble sizes measured by the optical probe were compared to those obtained from differential pressure signal analysis at the same axial location. Results of the optical fiber probe showed that for both types of particles and at both radial locations average bubble size decreased with the increase in operating pressure. This trend was supported by bubble size distribution that showed a decline in the frequency of larger bubbles as the operating pressure was elevated. The average rise velocity of bubbles at the column center was found to be slightly higher than those near the column wall. Overall, results obtained with polyethylene particles were suspected to have been influenced by the generation of electrostatic charges. Average gas bubble sizes found by the optical fiber probe and differential pressure fluctuation signal analysis were found to be in reasonable agreement with those predicted by the model proposed by Cai *et al.* [1] and Chan *et al.* [2].

Keywords: Gas-Solid Fluidization, Fluidized Bed Hydrodynamics, Bubble Size, Optical Probe

3.1 Introduction

Gas-solid fluidization technology is widely employed in many chemical industries such as petrochemical, oil and gas, food, to name just a few, due to excellent characteristics of providing high degree of heat and mass transfer, as well as mixing. It has been long recognized that fluidized bed hydrodynamics including transition velocities between fluidization regimes, gas bubble size and rise velocity, and terminal velocity of particles are influenced by the physical properties of fluidizing gas such as density and viscosity, which are in turn affected by fluidization operating pressure [3-7]. Among the aforementioned parameters, the rising gas bubbles create particles motion within the fluidized bed and in turn create the solids mixing, which is a factor essential for the bed mass and heat exchange performance. In contrast, the solid mixing influences the degree of contacts between the fluidizing particles, and the particles and the fluidization vessel wall which result in generation of electrostatic charges [8-11]. One operational challenge resulting from bed electrification that has been observed in commercial processes such as gas-phase ethylene polymerization to produce polyethylene is known as "sheeting" which leads to frequent reactor shutdown for clean-up [11-14]. Such process is typically carried out in a catalytic gas-solid fluidized bed reactor operated at elevated pressures up to 3,000 kPa [15-17]. Thus, understanding the bubble dynamics in gas-solid fluidized beds is not only vital in improving process efficiency but also is important in shedding light on the mechanisms of particles charging in such reactors. Since commercial processes such as those of polyethylene production are operated at elevated pressures, the evaluation of gas bubble dynamics necessitates the assessment of the influence of operating pressure on bubble characteristics.

At the point of fluidization, voids act as a bypass for the fluidizing gas. In bubbling flow regime, gas bubbles are generated at the distributor plate, rise upwards, and burst at the bed surface. As bubbles rise, their sizes increase due to bubble coalescence [18,19]. Hoffmann and Yates [7] experimentally observed that both bubble coalescence and splitting increased with the increase in fluidization pressure. They suggested that bubbles are almost evenly distributed across the bed at atmospheric condition, while at higher pressures the bubble flow tends to concentrate around the vertical axis of the bed and form a 0.05-0.1 m central channel in which the resistance to gas flow would be lower. This then results in an increase in bubble coalescence, which is exhibited as an

increase in bubble size. At the same time, with the rise of pressure, bubbles tended to split due to the decrease of stability [7, 20]. Moreover, the tendency of non-uniform distribution of bubbles over the bed cross section with increasing pressure has indicated the necessity of studying the local bubble properties at different radical positions [7, 20].

Although the effects of pressure on bubble dynamics, such as bubble size, rise velocity, and bubble frequency have been investigated experimentally and reported in literature, but no conclusive point has been made due to variation in results reported. With Group B particles Hoffmann and Yates [7] found that the gas bubbles diameter slightly increases when pressure is increased from 101 to 1100 kPa and then decreases thereafter up to 6100 kPa. Similar results for the effect of pressure on bubble size have been observed by others [20-23]. However, in experiments conducted by few other researchers [2,24-26] bubble size was found to continuously decline with the increase of pressures ranging from 100 to 3200 kPa, and thus the initial increase in bubble size at lower pressures reported by Hoffmann and Yates [7] was not noticed. Moreover, King and Harrison [27] did not find an influence from operating pressures on bubble size while fluidizing Geldart group B particles for pressures up to 2500 kPa. As for bubble rise velocity, Hoffmann and Yates [7] developed a relation between bubble size and rise velocity for Geldart Group A and B particles suggesting that bubble rise velocity is not proportional to its size. The experimental results reported by Chan *et al.* [2], supported this statement, whereas other researchers [21,22,28] concluded the opposite. In relation to bubble frequency, a few works have reported that the bubble frequency increases with elevation in pressure from 100 to 3200 kPa [2,21,22]. One the other hand Chitester and Kornosky [23] reported a decline in frequency at pressures of 3242 to 6485 kPa. They observed the trend in the experiments fluidizing coal and char in a 0.16 × 0.19 m two-dimension Plexiglas column with nitrogen gas at pressures up to 6485 kPa. The coal and char particles had wide size distributions, and had average sizes of 195 and 203 μm, respectively.

Techniques employed for bubble dynamic measurements can be divided into two categories: intrusive methods including fiber optic [29-34] and capacitance [20,22,24,35] probes; and non-intrusive techniques including visual observation [36,37], pressure signal analysis [32,38,39] and X-ray and capacitance tomography [21,38,40]. Visual observation can only be used in gas-liquid bed or 2-D gas-solid beds with transparent column walls. X-ray photography can be applied in 3-

D gas-solid beds but the fluidization column has to have a relatively thin or transparent column wall in order to detect the bubble movement inside, and thus cannot be applied in large industrial units [32].

Differential pressure fluctuation analysis is a method utilized for estimating bubble size in fluidized beds [32,39,41]. Average bubble size can be estimated based on the standard deviation of the differential pressure (DP) signal measured at any axial position of a fluidized bed [32]. Pressure fluctuation signal analysis is a non-intrusive method that can be applied in both laboratory and commercial-scale fluidization units. However, it can only provide the global average bubble size at the axial location where the measurement is conducted.

Optical fiber probes have been widely used to detect rising bubbles in atmospheric fluidized beds since 1950s [42,43]. In comparison to other measurement technics, optical fiber probes have advantages of being less expensive and applicable in large fluidized beds, especially in cold and non-reactive systems [43]. Additionally, optical fiber probes can measure properties of both bubble and dense phase locally, allowing the investigation of local bubble properties at different radial and axial positions. Moreover, unlike analyzing pressure signals which is only able to give an average bubble size, optical fiber probes provide the entire distribution of bubble properties at the measurement location [32,43].

To the knowledge of the authors all works found in literature employing optical fiber probes in gas-solid fluidized beds have reported experiments limited to atmospheric condition [29-34]. In addition, although the most popular intrusive and non-intrusive technics, optical fiber probe and pressure fluctuation signal analysis, have already drawn extensive attention, no works, except for one [32], has been found in literature comparing the results from the two technics. Therefore, the aim of this work is to investigate the effect of operating pressure on bubble characteristics including bubble size, rise velocity, and frequency using both aforementioned measurement techniques. In addition, the average bubble sizes obtained by the two technics are compared with the predictions made by existing models by Cai *et al.* [1] and Chan *et al.* [2].

3.2 Method and Material

A pilot-scale pressurized gas-solid fluidization system previously designed by the same research group was used in this work [44,45] (Chapter 2, Figure 2.1). The stainless steel fluidization

column had an inner diameter of 0.15 m and a fluidization section height of 2.5 m. Experiments were carried out at room temperature, and pressures ranging from atmospheric to 2600 kPa (abs) with incremental changes of 500 kPa. Compressed building air was used as the fluidizing gas for the atmospheric operation while nitrogen from a gas cylinder was used for high-pressure experiments. For above atmospheric pressures, the system was operated in a closed loop mode where a centrifugal compressor with a variable speed drive was used to circulate the gas within the system at the desired velocity. In this case, a plate heat exchanger was used to maintain the fluidizing gas temperature at ambient condition. Pressure inside the fluidization system was monitored by a gauge pressure transducer. The flowrate of gas entering the fluidization column for all experiments was measured by an orifice plate meter.

The gas bubbles characteristics were investigated by using an optical fiber probe as well as differential pressure fluctuation measurements. An optical fiber probe provided by Particulate Solid Research, Inc. (Chicago, USA), built for high-pressure applications, was employed. The one-inch probe contained two vertically arranged tips with center-to-center distance of 0.013 m. Each tip contained a bundle of optical fibers, one bundle emitting light into bed and one bundle receiving light reflected by particles. The reflected light collected by the fibers was converted to a voltage signal and recorded by the LabView program. The probe was installed at 0.4 m above the distributor plate and its radial position was varied from the column center to near the column wall. Differential pressure measurements were conducted by an ABB differential pressure transducer with its inlet and outlet located 0.075 m (3 inches) above and below the optical fiber probe.

Two types of particles were used in this work. Glass beads with a narrow particle size distribution of 430-600 μm and a particle density of 2500 kg/m^3 were used (more information is shown in Appendix A.2.2). In addition, linear low-density polyethylene (LLDPE) directly received from commercial reactors (supplied by Univation Technologies, LLC) were used since their electrostatic charging behavior was also of interest (referred to as PE_A in Appendix D.2.1). These particles had a density of 915 kg/m^3 and a wide size distribution of 20 – 1500 μm with a Sauter mean diameter of 560 μm. The static bed height was maintained at 0.45 m in all trials. Minimum fluidization velocities at various pressures were found experimentally from bed pressure drop measurements at various superficial gas velocities. As the fluidization pressure

varied from atmospheric pressure to 2600 kPa, minimum fluidization velocity ranged from 0.17 to 0.083 m/s for glass beads and 0.13 to 0.075 m/s for polyethylene particles. Experiments were conducted in bubbling flow regime for all trials at a gas velocity of $1.75U_{mf}$ for glass beads and 1.5 U_{mf} for polyethylene particles. Differential pressure and optical probe signals were recorded for a period of 2 min after fluidization for 10 min at each desired operating pressure. The data collection was limited to the beginning of each run because especially with the polyethylene resin, due to generation of electrostatic charges, particles would adhere to any surface within the bed including the tip of the optical probe. Data measured by optical fiber probe and differential pressure transducer was collected and recorded with a sampling frequency of 2000 Hz while those obtained from other instruments were recorded at 100 Hz. All experiments were repeated at least twice to confirm reproducibility.

3.2.1 Optical fiber probe signal analysis

In order to detect gas bubbles from the voltage signals obtained from the optical fiber probe and to determine the bubbles size distribution and rise velocity, an in-house code was developed in LabView program based on the method proposed by Liu *et al.* [32] and the algorithm reported by Ruedisueli *et al.* [43]. The average bubble size and bubble rise velocity was obtained by analyzing the probe dual signal, while the number of bubbles per minute was determined by only analyzing the signal from the bottom tip of the probe. The later was done for the purpose of detecting all bubbles including those that may not have travelled vertically and thus failed to be identified by the top tip of the probe. Results presented in this work were limited to the bubbles with size range of 0.1-0.15 m. More information about the signal analysis is presented in Appendix A.

3.2.2 Differential pressure fluctuations signals analysis

van der Schaaf *et al.* [46] related the bed pressure fluctuations to gas bubble diameter using the absolute pressure measured at certain heights of the fluidized bed. It was proposed that the powder spectral density of absolute pressure signals can be separated into two parts, a coherent component (COP) and incoherent component (IOP) [32,46]. The incoherent component was considered to be related to the gas bubble diameter (d_b):

$$d_{b,IOP} \propto \frac{\sigma_{xy,i}}{\rho_P g(1-\varepsilon_{mf})} \quad [3.1]$$

where $\sigma_{xy,i}$ is the standard deviation of IOP, ρ_P is the particle density, and ε_{mf} is the bed voidage at minimum fluidization velocity. This relation was then modified by Liu *et al.* [32] to employ differential pressure signals instead of absolute pressure signals. Based on this method, the gas bubble diameter was estimated by

$$d_{b,DP} \propto \frac{\sigma_{DP}}{\rho_P g(1-\varepsilon_{mf})} \quad [3.2]$$

where σ_{DP} is the standard deviation of the differential pressure signal. A proportionality constant of one is typically applied in using this equation. In this work, the approach by Liu *et al.* [32] was adopted to determine the average bubble size.

3.3 Results and Discussion

Figures 3.1 and 3.2 show the gas bubbles size distribution obtained by fluidization of glass beads and polyethylene resin, respectively, as a function of pressure. Results were obtained by the optical fiber probe at the center and near the wall of the fluidization column for glass beads, while only the column center location was used with polyethylene particles. For both type of particles, at atmospheric and 600 kPa the bubble size distributions did not vary with pressure as well as the bubbles radial location. However, as the pressure was further elevated the frequency of smaller bubbles increased while the reverse was observed for the frequency of large bubbles. At pressures higher than 600 kPa, the radial location of the bubbles did not affect the frequency of the smaller bubbles but less number of large bubbles was detected near the column wall. It has been reported that with the rise of pressure up to 1600 kPa, the tendency of both bubble coalescence and splitting increases [7,20]. In this work, the combination of bubbles coalescence and splitting could have been the reason for the bubble size not to change significantly when pressure was increased from atmospheric to 600 kPa. However, the decline of the frequency of larger bubbles at higher pressure is an indication of bubble splitting. Results presented in Figures 3.1 and 3.2 clearly imply that as operating pressure was increased, the gas bubble distribution

shifted towards the smaller bubbles for both locations of the column center and closer to the column wall.

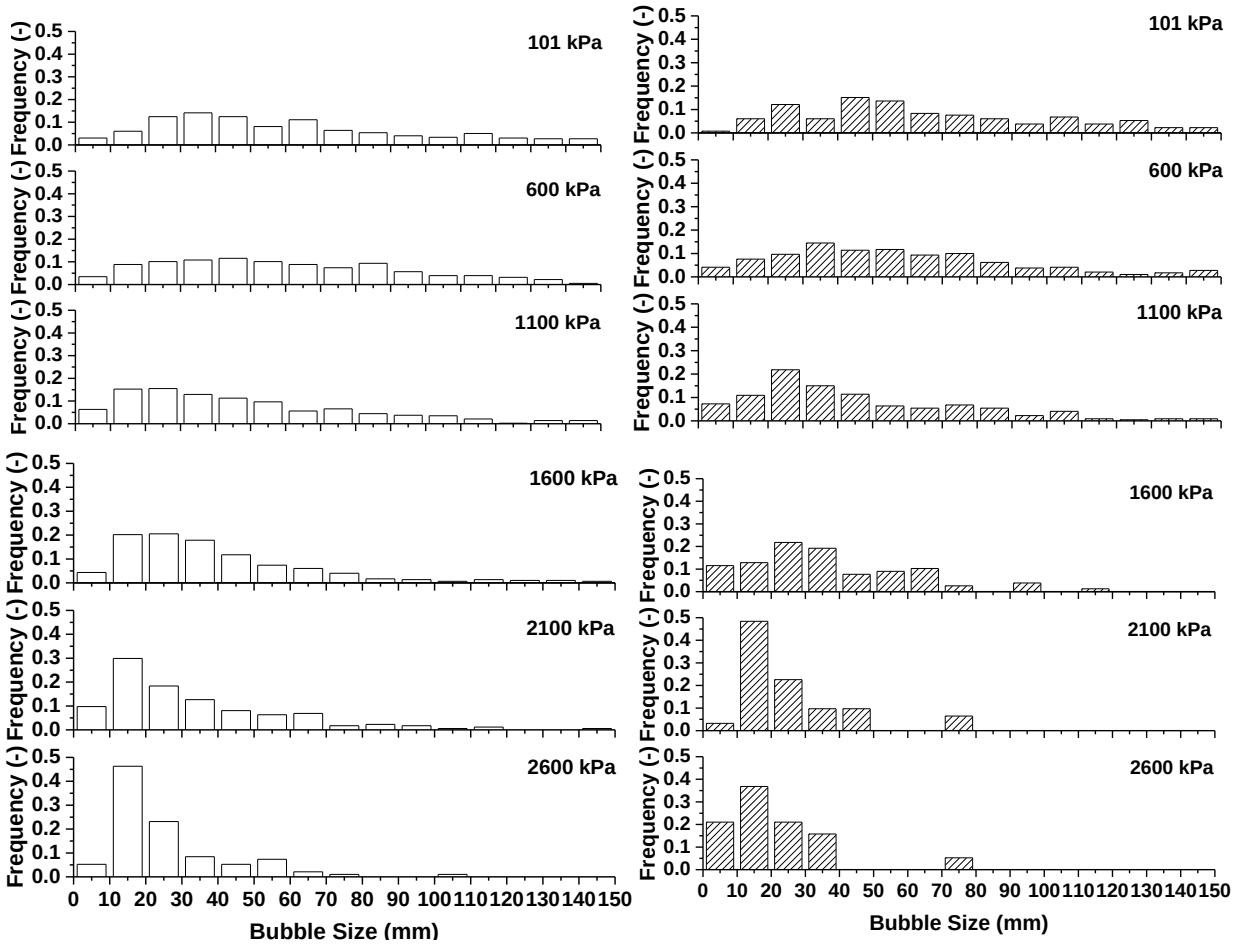

Figure 3.1: Bubble size distribution: (a) at the center; and (b) near the wall of the fluidization column detected by the optical fiber probe while fluidizing glass beads under various operating pressures.

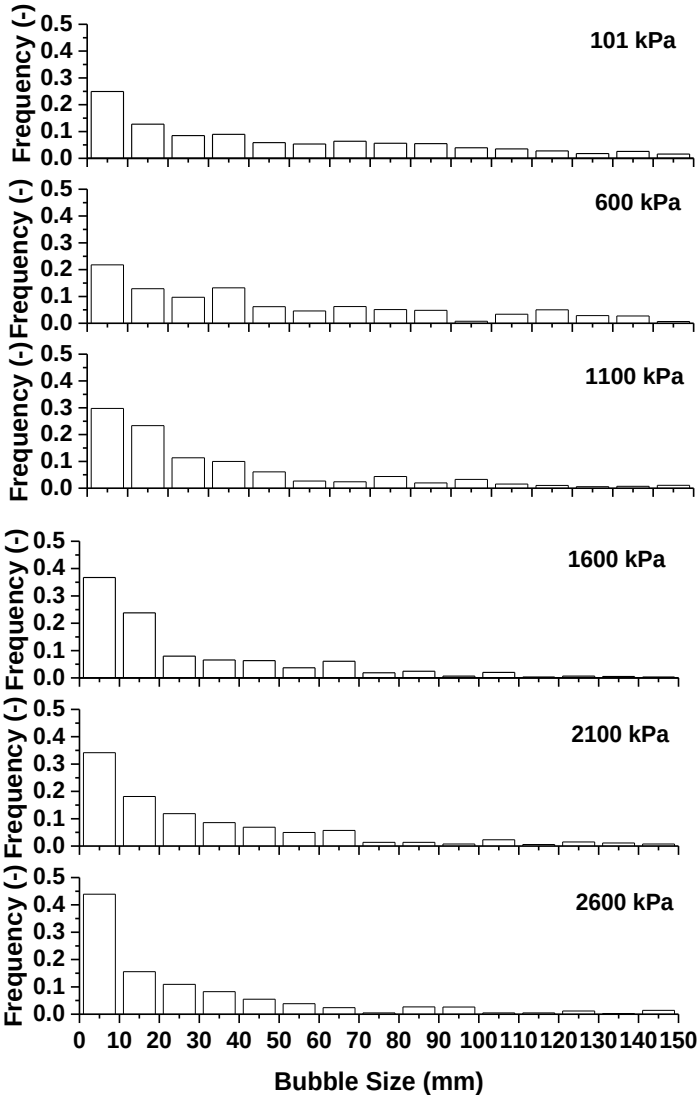

Figure 3.2: Bubble size distribution at the center of the fluidization column detected by the optical fiber probe while fluidizing polyethylene resin under various operating pressures.

The abovementioned findings are also visible from the average gas bubble size results presented in Figure 3.3 where the mean gas bubble size declined with the elevation of operating pressure for both types of particles. Unlike those of glass beads, the average bubble sizes obtained from polyethylene bed (Figure 3.3b) kept similar at ambient pressure and 600 kPa, followed by a decline up to 1100 kPa and then kept similar thereafter. It is predicted that while fluidizing polyethylene resin the generation of electrostatic charges could have influenced the measurement. Polyethylene particles could have adhered to the column wall as a result of electrostatic charge generation. Experiments carried out previously with the same system and polyethylene resin [44,45] indicate that charged particles begin coating the fluidized bed wall as

early as the first 15 minutes of the fluidization [47], and the magnitude of the wall accumulation is affected by the operating pressure. Our previous works also indicate that most of the particles that coat the column wall are 400 μm and smaller [44]. As a result, in this work the particle size distribution of the bulk of bed could have slightly changed throughout the run; thus, influencing the gas bubble characteristics.

Figure 3.3 also illustrates the average bubble size estimated by differential pressure (DP) signal analysis under various operating pressures. As can be seen in Figure 3.3a, the DP signal analysis slightly underestimated the mean bubble sizes than those detected by the optical fiber probe. However, the trends of results were similar from both measurement techniques. These results are similar to those reported by Liu *et al.* [32] who measured and compared bubble sizes obtained from optical probe and differential pressure signal analysis at atmospheric condition. They attributed the underestimated values to the fact that very small bubbles tend to bypass the tips of the probe instead of passing through them.

The mean bubble sizes found by the DP signal analysis for polyethylene experiments (Figure 3.3b) were small, comparing to probe results and did not show a trend with elevation in pressure. This was predicated to be due to the electrostatic charge generation resulting in polyethylene particles coating the column wall and thus dampening the measured DP signal fluctuations. Overall, results found in this work suggest that for polyethylene fluidized beds, where electrostatic charging effects are significant, the usage of optical probes and DP signal analysis for bubble characteristic investigation should be considered with care.

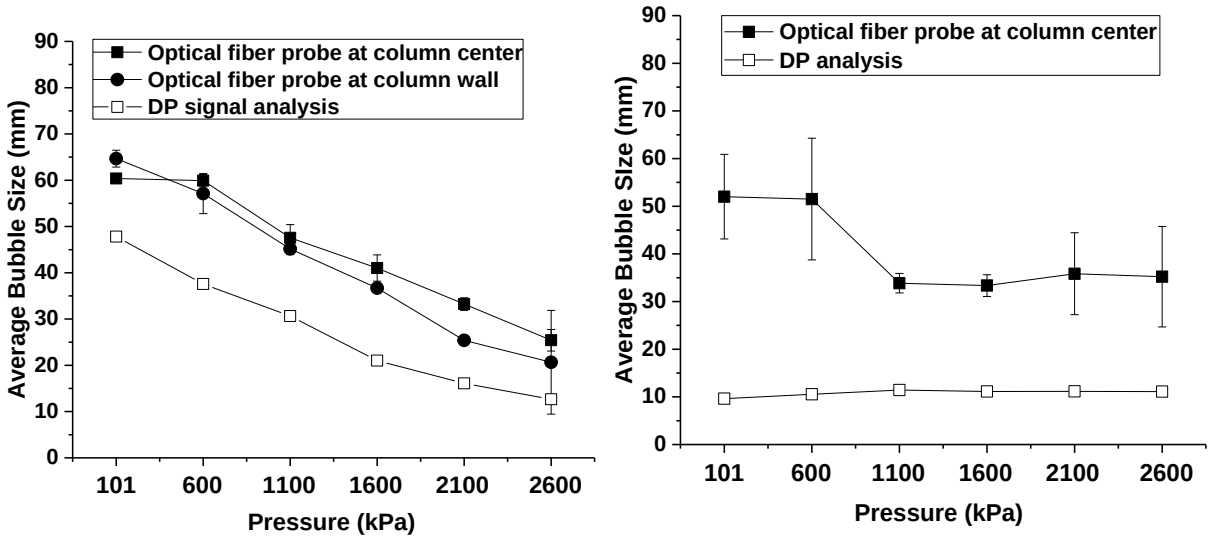

(a) (b)

Figure 3.3: Mean gas bubble size detected by the optical fiber probe and the differential pressure (DP) signal analysis at the center and near the wall of the fluidization column at various operating pressures by fluidization of (a) glass beads and (b) polyethylene resin.

As shown in Figure 3.4, mean gas bubble rise velocity in glass beads experiments at both radial locations remained the same for pressures up to 1100 kPa but begun to decline thereafter. The overall declining trend of bubble rise velocity under elevated pressures agrees with works by Hoffman and Yates [7] and Chan *et al.* [2] but is opposite to the observations of Oloswon *et al.* [22], Rowl *et al.* [21], and Wiman *et al.* [28]. Hoffman and Yates experimentally determined the velocity coefficient, *K*, from Davies-Taylor equation [48] for gas-solid fluidized beds and found that *K* factor first decreases and then increases with operating pressure [7]. This indicates that bubble rise velocity is not proportional to bubble size (Chapter 1, Figure 1.7). The disagreement between different works could be attributed to the differences in measurement positions and techniques employed. The results from the latter works presented the bubble rise velocities at the mid-height of the bed, while those presented by Hoffman and Yates and Chan *et al.* [2,7] as well as in this work were measured at the upper part of the bed. Figure 3.4 also illustrates that the average rise velocity of bubbles at column center was slightly higher than those found near the column wall.

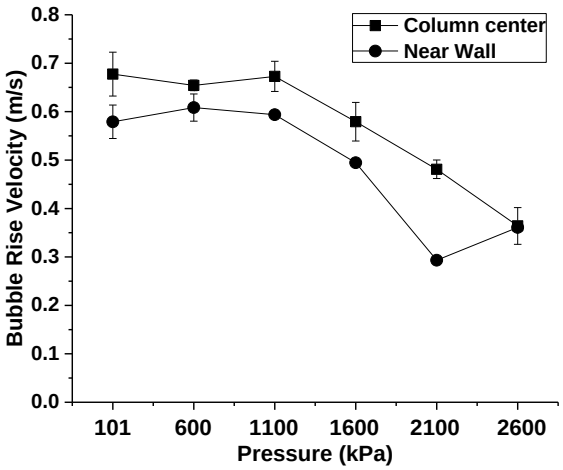

Figure 3.4: Average bubble rise velocity obtained from the optical fiber probe in glass beads experiments at two radial locations of the column center and near the column wall.

Figure 3.5 presents the number of bubbles per minute detected by the optical fiber probe located at the column center and near the column wall when fluidizing glass beads. The number of bubbles per minute detected in this work was at similar magnitude to those detected by Olowson *et al.* [22] and Chan *et al.* [2], but lower than Rowe *et al.*'s [21] results. Olowson *et al.* [22] fluidized silica sand (at the boundary of Geldart group B and D) in a 0.2 × 0.3 m Plexiglas column with excess gas velocities of 0.1 m/s, and measured the bubble frequency with a capacitance probe at the center of the column at pressures from atmospheric condition to 1600 kPa. Chan *et al*. [2] fluidized lignite char with average particle size of 400 μm in a 0.25 m (15 inch) I.D. carbon steel column with excess gas velocity of 0.09 m/s. They detected the bubbles at the center of the column with pressure probes. Rowe *et al*. [21] fluidized alumina powders with average particle size of 450 μm in a 0.175 × 0.125 m aluminum vessel with excess gas velocity of 0.01 m/s, and observed the bubble behavior in bed with an X-ray equipment. The bubble frequencies detected by Olowson *et al.* [22] and Chan *et al*. [2] at all operating pressures were less than 100 per minute, which is at similar magnitude as the observation in this work, while those detected by Rowe *et al*. [21] were higher than 600 per minute. Such variations are due to the measurement techniques utilized by various researchers. In works by Olowson *et al.* and Chan *et al.*, as well as in this work, the number of bubbles was detected locally by various types of probes. However, in the work presented by Rowe *et al.*, X-ray cine-photographs of bubbles were used to detect all bubbles at a certain height of the bed.

Hoffmann and Yates [7] found higher numbers of gas bubbles at the center of the column than near the column wall at elevated pressure, while at atmospheric condition, bubbles were almost evenly distributed across bed. However, in this work, less number of bubbles was detected near the column wall than at the column center at all pressures, although the difference of the bubbles numbers at the two radical positions slightly increased with the increase of pressure.

At both radial locations, number of bubbles detected first increased and then decreased with elevation in pressure. At the column center, the number of bubbles peaked close to 1600 kPa, while at the column wall area, it was the highest at approximately 600 kPa. This result agrees with the work by Olowson *et al.* [22] who reported an increasing trend of the number of bubbles as the pressure increased up to 1600 kPa. Chan *et al.* [2] also reported that the bubble frequency increased with the increase of pressure, up to 2100 kPa. Although their result did not show a decline of bubble frequency after 1600 kPa, it is in basic agree with the results in this work. At high pressures, similar to the results in this work, Chitester and Kornosky [23] concluded a decline trend of bubble frequency at high pressures (3242 and 6485 kPa) when fluidizing Geldart group B particles, and observed gas bubbles using a high-speed camera. They attributed the phenomenon to their observation that the movement in bed was more turbulent when bubbles move beyond middle-bed. This could also be the reason of the decline trend observed in this work at high pressure, since the measurement height in this work is close to the static bed height. However, the trends of bubble frequency at elevated pressures obtained in this work were opposite to that reported by Rowe *et al.* [21].

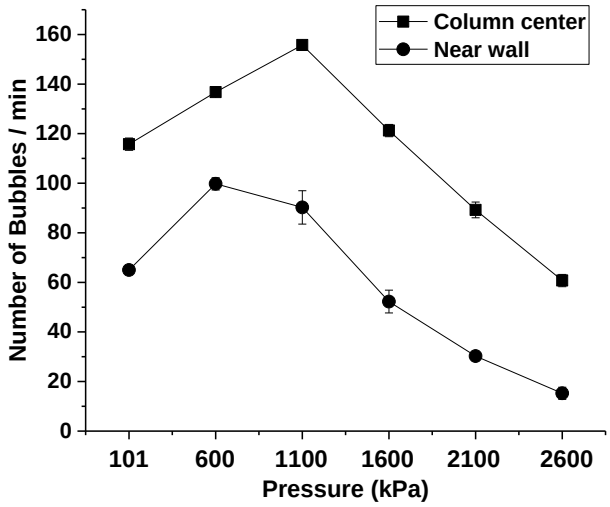

Figure 3.5: Number of bubbles per minute obtained from the optical fiber probe in glass beads experiments at two radial locations of the column center and near the wall.

3.3.1 Model comparisons

Several empirical models are found in literature predicting bubble diameter in gas-solid fluidized beds. However, majority of these works are based on experimental data obtained at atmospheric pressure, and thus may not be applicable to high-pressure operations. Cai *et al.* [1] developed a model based on experimental data found in literature obtained at high pressures. Their model was developed for Geldart group B particles in bubbling and turbulent flow regimes under pressures from atmospheric to 7000 kPa, and from room temperature to the typical operating temperatures of pressurized fluidized bed combustors [1]. Chan *et al.* [2] fluidized Geldart group B particles with average particle sizes from 100 – 400 μm in a 0.38 m diameter fluidization column and investigated bubble characteristics including bubble pierced length, rise velocity, and frequency by installing pressure probes at different vertical positions of the column under pressures of 135 – 3200 kPa. They developed a relationship between bubble size and velocity under different pressures based on their experimental data. This correlation can be applied to fluidized beds with expanded bed heights of 0.45 – 1.55 m, particle diameter of 100 – 400 μm, excess fluidization velocity of 0.02 – 0.12 m/s, particle density of 1250 – 2560 kg/m^3, and fluidizing gas density of 1.28 – 40 kg/m^3 [2].

Results obtained in present work were compared against predictions of these two existing models. Figure 3.6 compares the predicted bubble diameters from Cai *et al.* [1] and Chan. *et al.*

[2] models with those found experimentally in this work by differential pressure (DP) signal analysis and the optical fiber probe. Although Cai *et al.* model overestimated and Chan *et al.* model underestimated the average bubble size, overall the measured results were in good agreement with predictions of both models and showed similar trends as a function of operating pressure. Chan *et al.* model provided predictions in closer agreement with the experimental results than the Cai *et al.* model.

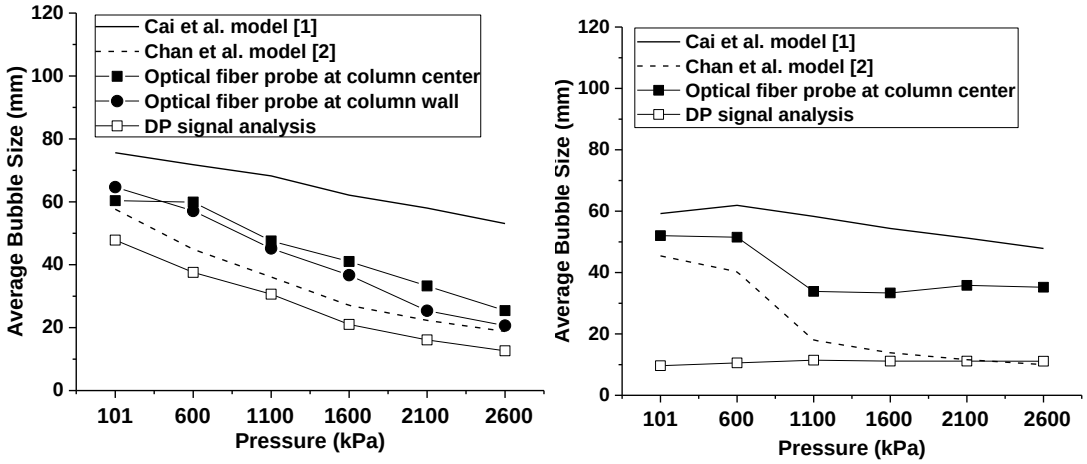

Figure 3.6: Comparison of average gas bubble sizes determined by the optical fiber probe and DP signal analysis with Cai *et al.* [1] and Chan *et al.* [2] model predictions for (a) glass beads and (b) polyethylene experiments.

3.4 Conclusions

Effects of operating pressure on bubble hydrodynamics including bubble size, rise velocity, and frequency were investigated by fluidizing glass beads and polyethylene resin in a pilot-plant system under pressures ranging from atmospheric condition to 2600 kPa. Bubble dynamics were determined by using an optical fiber probe as well as analyzing differential pressure fluctuation signals. The local bubble properties at the column center and close to the column wall were investigated by the optical fiber probe for glass beads, and at column center for polyethylene resin. An algorithm was developed based on the methods reported by Liu *et al.* [32] and Ruedisueli *et al.* [43] to analyze data obtained by the optical fiber probe. Pressure fluctuation signals were analyzed with the method introduced by Liu *et al.* [32].

In fluidization of both types of particles, the gas bubble distribution shifted towards the smaller bubbles for both locations of the column center and closer to the column wall as the operating pressure was elevated. In the case of glass beads, average bubble size decreased approximately linearly with the increase in the operating pressure. However, in the case of polyethylene resin although the overall trend of average bubble size was found to decline with increase in pressure, but the results implied that the bubble characteristics could have been slightly influenced by particle wall coating due to electrostatic charge generation. The wall coating not only affected the differential pressure signal but also could have altered the bed particles size distribution as fluidization progressed since the coating on the column wall would have consisted of particles of 400 micron and smaller. While fluidizing glass beads, the trends of average bubble size with respect of operating pressure were similar for both measurement techniques. The mean gas bubble sizes found by the DP signal analysis in the polyethylene bed were quite small compared to the optical probe results due to the electrostatic charge generation.

Mean gas bubble rise velocity at both radial locations while fluidizing glass beads did not change from atmospheric condition to 1100 kPa but then decreased thereafter. The average rise velocity of bubbles at column center was found to be slightly higher than those near the column wall. Less number of bubbles was detected near the column wall than at the column center when fluidizing glass beads and the number of bubbles detected first increased and then decreased with the increase of pressure. Bubble sizes predicted by models presented by Cai *et al.* and Chan *et al.* [1,2] were in reasonable agreement with those obtained by the optical fiber probe and differential pressure fluctuation analysis.

Acknowledgements

Authors wish to thank Particulate Solid Research, Inc (PSRI) for providing the optical fiber probe. Financial support by Natural Sciences and Engineering Research Council (NSERC) of Canada, and Canada Foundation for Innovation (CFI) are acknowledged with gratitude.

Nomenclature

Symbol	Meaning	Units
$d_{b,DP}$	Bubble diameter estimated by differential pressure analysis	m
$d_{b,IOP}$	Bubble diameter estimated by incoherent part of absolute pressure fluctuations analysis	m
g	Gravitational constant	m/s^2
K	Bubble velocity coefficient	–
ε_{mf}	Voidage at minimum fluidization	–
ρ_P	Particle density	kg/m^3
σ_{DP}	Standard deviation of differential pressure fluctuations	Pa
$\sigma_{xy,i}$	Standard deviation of incoherent part of absolute pressure fluctuations	Pa

References

[1] P. Cai, M. Schiavetti, G. De Michele, G.C. Grazzini, M. Miccio, Quantitative estimation of bubble size in PFBC, Powder Technol. 80 (1994) 99-109.

[2] I. Chan, C. Sishtla, T. Knowlton, The effect of pressure on bubble parameters in gas-fluidized beds, Powder Technol. 53 (1987) 217-235.

[3] H.T. Bi, N. Ellis, I.A. Abba, J.R. Grace, A state-of-the-art review of gas-solid turbulent fluidization, Chem. Eng. Sci. 55 (2000) 4789-4825.

[4] J. Yerushalmi, N.T. Cankurt, Further studies of the regimes of fluidization, Powder Technol. 24 (1979) 187-205.

[5] J.G. Yates, Effects of temperature and pressure in gas-solid fluidization, Chem. Eng. Sci. 51 (1996) 167-205.

[6] C.Y. Wen, Y.H. Yu, A generalized method for predicting the minimum fluidization velocity, AICHE J. 12 (1966) 610-612.

[7] A.C. Hoffmann, J.G. Yates, Experimental observations of fluidized beds at elevated pressures, Chem. Engng. Commun. 41 (1986) 133-149.

[8] A. Sowinski, L. Miller, P. Mehrani, Investigation of electrostatic charge distribution in gas-

solid fluidized beds, Chem. Eng. Sci. 65 (2010) 2771-2781.

[9] F. Salama, A. Sowinski, K. Atieh, P. Mehrani, Investigation of electrostatic charge distribution within the reactor wall fouling and bulk regions of a gas-solid fluidized bed, J. Electrostat. 71 (2013) 21-27.

[10] Y. Tian, P. Mehrani, Effect of particle size in fluidization of polyethylene particle mixtures on the extent of bed electrification and wall coating, J. Electrostat. 76 (2015) 138-144.

[11] M.G. Goode, D.M. Hasenberg, T.J. McNeil, T.E. Spriggs, Method for reducing sheeting during polymerization of alpha-olefins, US4803251 A (1989).

[12] M.G. Goode, F.D. Hussein, K.H. Lee, T.J. McNeil, C.C. Williams, Static control in olefin polymerization, US 6111034 A (2000).

[13] R.O. Hagerty, M.E. Muhle, A.K. Agapiou, C. Kuo, M.G. Goode, F.D. Hussein, R.B. Pannell, J.F. Szul, Method for controlling sheeting in gas phase reactors, US 7985811 B2 (2011).

[14] G.H. Song, A.S. Rhee, G.R. Lowder, Method for reducing sheeting and static charges during polymerization of ethylene polymers, US 5391657 A (1995).

[15] F.J. Karol, I.J. Levine, Preparation of low and medium density ethylene polymer in fluid bed reactor, US 4011382 A (1977).

[16] T. Xie, K.B. McAuley, J.C.C. Hsu, D.W. Bacon, Gas phase ethylene polymerization: Production processes, polymer properties, and reactor modeling, Ind Eng Chem Res. 33 (1994) 449-479.

[17] S. Beret, J.M. Jenkins, T.M. Jones, R.L. Jones, Method for fluidized bed polymerization, US 4588790 A (1986).

[18] J.F. Davidson, Symposium on fluidization: discussion, Trans. Inst. Chem. Eng. 39 (1961) 230.

[19] G.B. Wallis, One-dimensional waves in two-component flow (with particular reference to the stability of fluidized beds). AEEW-R162 (1962).

[20] P.A. Olowson, A.E. Almstedt, Hydrodynamics of a bubbling fluidized bed: influence of pressure and fluidization velocity in terms of drag force, Chemical Engineering Science. 47 (1992) 357-366.

[21] P.N. Rowe, P.U. Foscolo, A.C. Hoffmann, J.G. Yates, X-ray observation of gas fluidized beds under pressure, in: A.C. Kunnii, R. Toei (Eds.), Fluidization, Engineering Foundation, New York, 1984, pp. 53.

[22] P.A. Olowson, A.E. Almstedt, Influence of pressure and fluidization velocity on the bubble behaviour and gas flow distribution in a fluidized bed, Chemical Engineering Science. 45 (1990)

1733-1741.

[23] D.C. Chitester, R.M. Kornosky, L.-. Fan, J.P. Danko, Characteristics of fluidization at high pressure, Chem. Eng. Sci. 39 (1984) 253-261.

[24] J. Schweinzer, O. Molerus, Bubble flow in pressurized gas/solid fluidized beds, Chem. Eng. Technol. 10 (1987) 368-375.

[25] A. Orta, B. Wu, M. Ghods, A. Guerrero, C. Bellehumeur, A. Kantzas, Pressure effect on hydrodynamics of a high pressure X-ray transparent polyethylene fluidized bed, Int. J. Chem. React. Eng. 9 (2011).

[26] G.C. Brouwer, E.C. Wagner, J.R. van Ommen, R.F. Mudde, Effects of pressure and fines content on bubble diameter in a fluidized bed studied using fast X-ray tomography, Chem. Eng. J. 207-208 (2012) 711-717.

[27] D.F. King, D. Harrison, Dense phase of a fluidised bed at elevated pressures, Trans. Inst. Chem. Eng. 60 (1982) 26-30.

[28] J. Wiman, A.E. Almstedt, Influence of pressure, fluidization velocity and particle size on the hydrodynamics of a freely bubbling fluidized bed, Chem. Eng. Sci. 53 (1998) 2167-2176.

[29] B. Bai, S. Gheorghiu, J.R. van Ommen, J. Nijenhuis, M.-. Coppens, Characterization of the void size distribution in fluidized beds using statistics of pressure fluctuations, Powder Technol. 160 (2005) 81-92.

[30] L.R. Glicksman, W.K. Lord, M. Sakagami, Bubble properties in large-particle fluidized beds, Chem. Eng. Sci. 42 (1987) 479-491.

[31] R. Andreux, J. Chaouki, Behaviors of the bubble, cloud, and emulsion phases in a fluidized bed, AIChE J. 54 (2008) 406-414.

[32] M. Liu, Y. Zhang, H. Bi, J.R. Grace, Y. Zhu, Non-intrusive determination of bubble size in a gas–solid fluidized bed: An evaluation, Chem. Eng. Sci. 65 (2010) 3485-3493.

[33] S. Guet, R.V. Fortunati, R.F. Mudde, G. Ooms, Bubble Velocity and Size Measurement with a Four-Point Optical Fiber Probe, Part. Part. Syst. Charact. 20 (2003) 219-230.

[34] C. Sobrino, J.A. Almendros-Ibáñez, D. Santana, C. Vázquez, M. de Vega, Maximum entropy estimation of the bubble size distribution in fluidized beds, Chem. Eng. Sci. 64 (2009) 2307-2319.

[35] J. Werther, O. Molerus, The local structure of gas fluidized beds —II. The spatial distribution of bubbles, Int. J. Multiph. Flow 1 (1973) 123-138.

[36] T. Knowlton, High-pressure fluidization characteristics of several particulate solids, primarily coal and coal-derived materials, AIChE Symp. Ser. 73 (1977) 22-28.

[37] R.F. Mudde, H.B.M. Schulte, H.E.A. van den Akker, Analysis of a bubbling 2-D gas-fluidized bed using image processing, Powder Technol. 81 (1994) 149-159.

[38] B. Wu, G. Yu, C. Bellehumeur, A. Kantzas, Dynamic flow behavior measurements in gas–solid fluidized beds using different non-intrusive techniques and polyethylene powder, Flow Meas. Instrum. 18 (2007) 197-203.

[39] P. Cai, S.P. Chen, Y. Jin, Z.Q. Yu, Z.W. Wang, Effect of operating temperature and pressure on the transition from bubbling to turbulent fluidization, AIChE Symp. Ser. 85 (1989) 37-43.

[40] J.S. Halow, G.E. Fasching, P. Nicoletti, J.L. Spenik, Observations of a fluidized bed using capacitance imaging, Chem. Eng. Sci. 48 (1993) 643-659.

[41] A. Weimer, G. Quarderer, On dense phase voidage and bubble size in high pressure fluidized beds of fine powders, AIChE J. 31 (1985) 1019-1028.

[42] Yasui. G, L. N. Johanson, Characteristics of gas pockets in fluidized beds, AIChE J. 4 (1958) 445-452.

[43] M. Rüdisüli, T.J. Schildhauer, S.M. Biollaz, J.R. van Ommen, Bubble characterization in a fluidized bed by means of optical probes, Int. J. Multiph. Flow. 41 (2012) 56-67.

[44] D. Song, F. Salama, J. Matta, P. Mehrani, Implementation of Faraday Cup Electrostatic Charge Measurement Technique in High-Pressure Gas-Solid Fluidized Beds at Pilot-Scale, Powder Technol. 290 (2015) 21-26.

[45] F. Salama, D. Song, P. Mehrani, Characterizing Electrostatic Charges in High-Pressure Gas-Solid Fluidized Beds: Experimental Design and Preliminary Results, Proceedings of the Fluidization XIV-From Fundamentals to Products. (2013).

[46] J. van der Schaaf, J.C. Schouten, F. Johnsson, C.M. van den Bleek, Non-intrusive determination of bubble and slug length scales in fluidized beds by decomposition of the power spectral density of pressure time series, Int. J. Multiph. Flow. 28 (2002) 865-880.

[47] Y. Tian, Study of the Effect of Polyethylene Resin Particle Size on the Degree of Fluidized Bed Reactor Electrification and Wall Fouling, University of Ottawa. (2011) 71-72.

[48] R.M. Davies, G. Taylor, The mechanics of large bubbles rising through extended liquids and through liquids in tubes, Proceedings of the Royal Society A. 200 (1950) 375.

Chapter 4
Effect of Pressure on Electrostatic Charge Generation in a Pilot Scale Gas-solid Fluidized Bed of Polyethylene Particles

Di Song, Poupak Mehrani*

Chemical and Biological Engineering Department, University of Ottawa
161 Louis Pasteur, Ottawa, ON, Canada, K1N 6N5
* poupak.mehrani@uottawa.ca, Tel: 1 (613) 562-5800 Ext. 6098, Fax: 1 (613) 562-5172

The current chapter is a manuscript submitted to the journal of Chemical Engineering Science "Publication under review, Manuscript No.: CES-D-16-02164"

Abstract

Electrostatic charge generation in gas-solid fluidized beds results in operational challenges in some industrial processes such as polyethylene production. Such reactors operate at elevated pressures and thus the aim of this work was to investigate fluidized bed electrification at pressurized conditions. The degree of particle charging and wall coating in a pressurized pilot-scale gas-solid fluidized bed of polyethylene resin was studied from atmospheric pressure to 2600 kPa (abs), while the gas bubble dynamics were concurrently measured by an optical fiber probe. The average gas bubble size was found to be larger at atmospheric condition along with the frequency of large bubbles, resulting in a larger degree of particle-wall contacts. The degree of fluidized bed wall coating increased with the increase of pressure. This finding was related to the decline in the gas bubble size and the increase in frequency of small bubbles found at elevated pressures, promoting particle-particle contacts and thus bipolar charging. Bipolar charging was detected with particles that fouled on the column wall with small particles being negatively charged.

Keywords: Gas-Solid Fluidization, Electrostatics, Particle Wall Coating, Fluidized Bed Hydrodynamic

4.1 Introduction

Electrostatic charge generation in gas-solid fluidized beds results from continuous contacts between particles and between particles and the column wall. This charge generation gives rise to multiple operational challenges, including particle agglomeration and adhesion to the fluidization column. Gas-phase ethylene polymerization to produce polyethylene is an example of an industrial process that is suffering from the negative effects of electrostatic charge generation in gas-solid fluidized bed reactors. In this process, charged particles, including catalyst and polyethylene resin, adhere to the reactor wall and dome, and form a sheet of fused particles, causing a problem known as "sheeting" [1]. Sheeting then necessitates frequent reactor shutdown for clean-up and in turn causes significant economic loss. Although few works have been reported in literature on detecting the occurrence of electrostatic charge build up within such reactors and reducing its magnitude, the problem still persists [1–5]. This is due to the complex nature of the gas-solid fluidization process, and more importantly, the lack of comprehensive understanding of the underlying mechanism of electrostatic charge generation and dissipation in such processes; particularly when the fluidizing particles are insulators such as polyethylene.

To understand particles charging in industrial reactors, including the commercial polyethylene reactors, it is essential to investigate electrostatic charge generation in gas-solid fluidized beds under industrially relevant operating conditions. For example, commercial polyethylene reactors are operated at high pressures close to 3,000 kPa [6]. However, the majority of works studying electrostatic charge generation in gas-solid fluidized beds have been conducted under atmospheric conditions, with very few exceptions [7–10]. Moughrabiah *et al.* [8] and Liu *et al.* [7] studied the local electrostatic charge generation using electrostatic probes under pressures up to 724 kPa by fluidizing glass beads and polyethylene particles. In both works, particles were fluidized in the bubbling flow regime and maintained constant excess gas velocities [7,8]. Although both works used the same experimental apparatus, their findings varied. Moughrabiah *et al.* [8] concluded that bed electrification increased with an increase in pressure, while Liu *et al.* [7] concluded that the effect of operating pressure on the degree of electrostatic charge generation was difficult to predict. Their inconclusive results could have been a result of the use of collision type electrostatic probes that only provide a local measurement of the degree of bed

charging during a very short period of 500 s and may suffer from additional charge generation due to the collision of particles with the probe. In addition, such measurement technique does not provide any information regarding the reactor fouling due to electrostatic charging of particles. Moughrabiah *et al.* [8] related the increase in bed electrification to the influence of operating pressure on the gas bubble dynamics, which in turn would affect the particle mixing behavior within the fluidized bed. However, they did not make a measurement of gas bubble dynamics.

It has long been reported that operating pressure influences gas bubble dynamics, such as bubble size and rise velocity in gas-solid fluidized beds. Hoffman and Yates [11] fluidized 184 μm and 450 μm particles (Geldart group B) under pressures of 101 – 8000 kPa and monitored the gas bubbles size and movement in the bed by X-ray tomography in the bubbling flow regime with excess gas velocities of 0.028 and 0.039 m/s. They found that the diameter of gas bubbles slightly increased when pressure was increased from 1,000 kPa; the bubble diameter decreased thereafter. Similar results were reported by other authors [12,13]. Orta *et al*. [14] examined the effect of bed hydrodynamic by X-ray fluoroscopy technology under pressures of 200 – 2900 kPa by fluidizing polyethylene particles at 1.5 times minimum fluidization velocity (bubbling flow regime). They found that the average bubble diameter decreased with the increase of pressure. Brouwer *et al*. [15] fluidized polystyrene particles (Geldart group B) under pressures of 101 – 500 kPa at superficial gas velocities of 0.1 – 0.3 m/s. They obtained similar results as Orta *et al.* [14] using the same measurement technique.

Olowson and Almstedt [12] measured the effect of pressure on bubble rise velocity with silica sand (Geldart group B) for a pressure range of 101 – 1600 kPa and excess gas velocities from 0.1 to 0.6 m/s. A capacitance probe was used in their work and they found that bubble rise velocity increased with the increase in pressure, although the influence of pressure was smaller at elevated pressures. However, Orta *et al*. [14], who used polyethylene particles, concluded that the operating pressure did not influence bubble rise velocity.

The aforementioned studies all confirm that increasing the operating pressure in gas-solid fluidized beds affects the bubble dynamics. Since bubble characteristics will affect the particles' movement within the bed, it is evident that gas bubble behavior could in turn influence the degree of electrostatic charge generation in such systems. Majority of works reported in literature have either studied bubble dynamics or electrostatic charge generation in gas-solid fluidized

beds. To the authors' knowledge, there is no work reported in open literature that investigated gas bubble dynamics and bed electrification simultaneously, and more specifically the effect of operating pressure on reactor wall fouling. The aim of this work was to concurrently investigate the effect of operating pressure on electrostatic charge generation and gas bubble dynamicsin a pilot-scale gas-solid fluidized bed.

4.2 Experimental setup and method

A pilot plant pressurized gas-solid fluidization system detailed elsewhere was used in this work [9,10]. As illustrated in Figure 4.1, the system contained of a stainless steel fluidization column, 0.15 m in diameter. The particle charge measurement was achieved by two Faraday cups, housed in the top and bottom expanded sections and connected to digital electrometers (Keithley model 6514). The whole fluidization column was grounded and thus the two expanded sections at the top and the bottom of the fluidization column acted as the outer Faraday cups. The two copper inner Faraday cups were electrically isolated from the outer cups by Teflon pieces. A filter bag was placed in the top Faraday cup to capture the entrained fines to allow the measurement of their cumulative charge during the fluidization. The perforated distributor plate was a modified knife-gate valve, which enabled the discharge of the fluidizing particles into the bottom Faraday cup without any particle handling.

Experiments were conducted in bubbling flow regime and at various pressures ranging from atmospheric to 2600 kPa (abs) (increments of 500 kPa). The static bed height was 0.45 m for all experiments. The minimum fluidization velocity was measured at each operating pressure and the fluidizing gas velocity was set at 1.5 times the minimum fluidization velocity, for all operating pressures. Compressed building air and nitrogen gas from a gas cylinder were used as sources of fluidizing gas at atmospheric and pressurized experiments, respectively. For experiments conducted at pressures higher than atmospheric, the system was first pressurized to the desired pressure by using nitrogen gas and then a centrifugal compressor with a variable speed drive was used to circulate the gas within the system at the desired gas velocity.

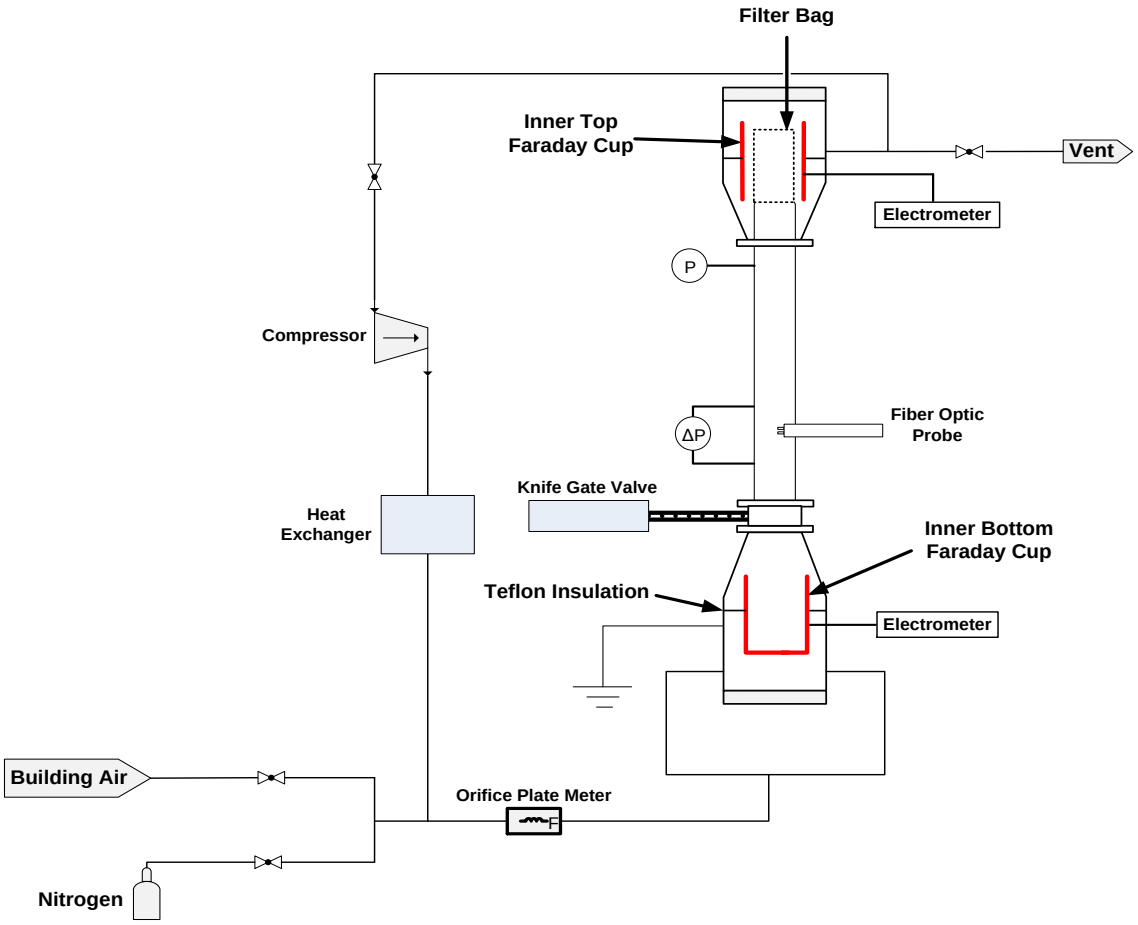

Figure 4.1: Schematic of pilot plant pressurized gas-solid fluidization system.

Linear low-density polyethylene (LLDPE) resin directly received from a commercial reactor (referred to as PE_A in Appendix D.2.1) was fluidized in this work. The resin was of Geldart group B with a particle density of 918 kg/m^3. The resin had a wide size distribution of 20 – 1500 µm, with an average particle size of 560 µm (Table 4.1). A fresh batch of particles was uesd in each run and fluidization was carried out for 60 min. Minimum fluidization velocities, obtained by the bed pressure drop measurements at various superficial gas velocities, are summarized in Table 4.2.

Table 4.1: Particles size distribution of the polyethylene particles utilized in this work.

Particle Size Range (μm)	wt.%
< 500	26.44
500 – 700	28.54
> 710	45.02

Table 4.2: Minimum fluidization velocity (U_{mf}) of polyethylene particles at various operating pressures.

Pressure (kPa)	U_{mf} (m/s)
101	0.13
600	0.12
1100	0.1
1600	0.092
2100	0.084
2600	0.075

An optical fiber probe with a dual tip supplied by Particulate Solid Research, Inc., Chicago, USA, was used to detect gas bubbles in the fluidized bed and obtain bubble properties. The probe was installed 0.4 m above the distributor plate and at the center of the column. Measurements were taken at a sampling frequency of 2000 Hz for 2 min. A LabView based program was developed in-house based on the algorithm introduced by Ruedisueli *et al.* [16] to analyze the data obtained from the optical probe. In this work, the average bubble size and frequencies were limited to bubbles with sizes up to 0.15 m. More information of the signal analysis method is presented in Appendix A.

In all experiments, as-received particles (referred to as "initial" or "initial particles") were placed in the fluidization column after measuring their mass and net charge. During fluidization, the entrained particles were captured by the filter bag and their cumulative charge was measured by the top Faraday cup. Since charged polyethylene particles have a tendency to adhere to any surface within the bed including the tip of the optical probe, the gas bubble measurements were limited to the beginning of each run. Upon completion of a 60 min fluidization, the system was depressurized and the top of the column was opened so that the filter bag could be removed to measure the mass of entrained particles (referred to as "fines" or "fine particles"). The distributor plate was then opened, allowing particles remaining in the bulk of the bed (referred to as "bulk" or "bulk particles") to drop into the bottom Faraday cup to measure their net charge. The bottom

Faraday cup was then removed to measure the mass of the bulk particles. After visually examining the inner column wall for any particle fouling, the cleaned bottom Faraday cup was put back to collect and measure the net charge of these particles (referred to as "wall" or "wall particles"). Compressed building air was passed through a long tube inserted from the top of the column in order to dislodge the wall particles from the column wall into the bottom Faraday cup to measure their net charge and mass. For all experiments, samples of initial, bulk, wall, and fines were collected and analyzed for particle size distribution by a Malvern Mastersizer 2000 particle size analyzer. All experiments were conducted at least two times to ensure the reproducibility of the results.

4.3 Results and discussion

4.3.1 Effect of pressure on bubble dynamics

Since the electrostatic charge generation in gas-solid fluidized beds is due to continuous contacts between the particles, as well as contacts between particles and the column wall, understanding the factors that influence the degree of particle mixing is essential. Hence, in this work it was important to determine the effect of fluidization pressure on bed hydrodynamics, namely gas bubble size and frequency which in turn would affect the degree of particle-particle and particle-wall contacts in bed. Figures 4.2 and 4.3 present the gas bubble properties obtained by an optical fiber probe at various operating pressures. The average gas bubble size was larger at atmospheric conditions and 600 kPa and decreased by further increasing the fluidizing pressure. Although the average bubble size did not vary between atmospheric and 600 kPa experiments, the frequency of small bubbles (< 0.05 m) increased, while that of large bubbles (0.05 – 0.1 m) declined. Overall, the frequency of bubbles with size range of 0.1 – 0.15 m was quite low (approximately 10%) and declined with the increase in pressure. The aforementioned results agree well with those reported in literature [11,14].

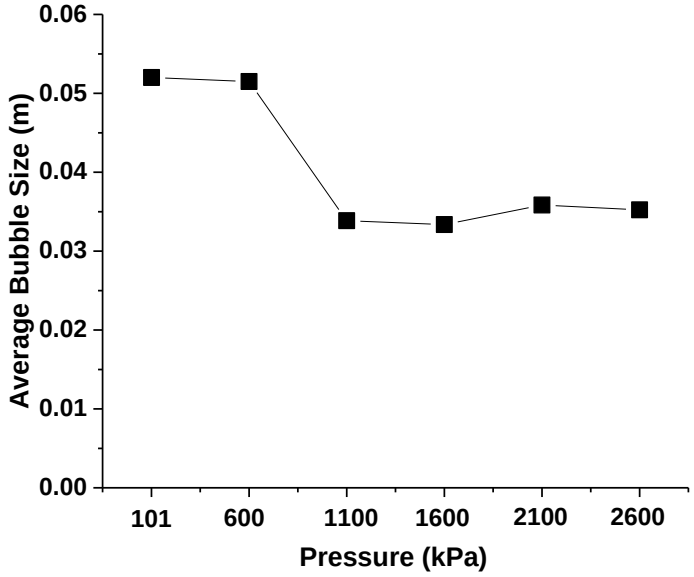

Figure 4.2: Average gas bubble size found by optical probe at various fluidization pressures.

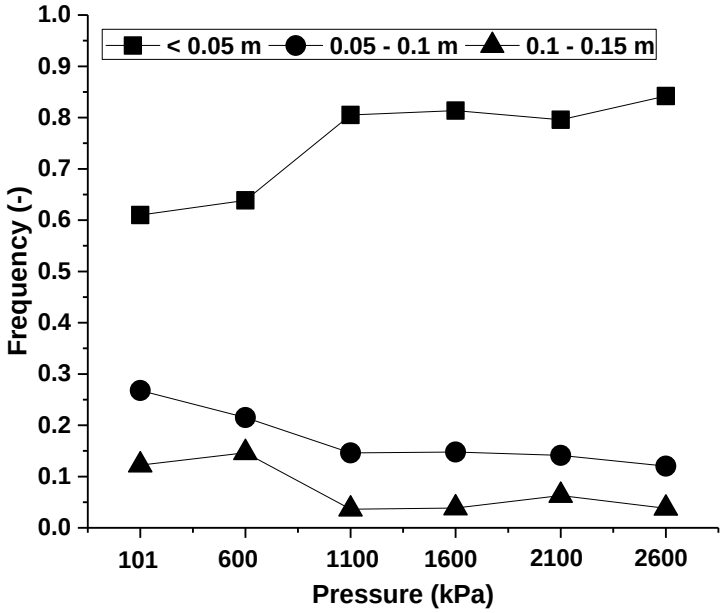

Figure 4.3: Frequency of < 0.05, 0.05 – 0.1, 0.1 – 0.15 m gas bubbles within all bubbles detected at various fluidization pressures.

4.3.2 Effect of pressure on electrostatic charge generation

The mass (m), net charge (q), and size distribution (PSD) of particles initially placed into the fluidization column (referred to as "initial particles") were determined prior to each experiment. Results indicated that for all trials, these particles had a relatively small q/m (0.04 ± 0.02 μC/kg) and a similar particle size distribution.

4.3.2.1 Visual examination of wall coating

For all trials, upon the completion of the fluidization period, the degree of the column coating was visually examined by taking photos of the inner column wall after the removal of the bulk particles. Figure 4.4a is an example of an inner wall coating image. As can be seen in this Figure particle coating covers the whole column wall, from the distributor plate to the outlet of the column. This figure also illustrates that the coating consisted of two layers, one thicker layer at the bottom of the column extending to the expanded bed height, and a second thinner layer at the top (Figure 4.4b). Particles that coated the top and bottom areas of the column were referred to as "top layer" and "bottom layer", respectively.

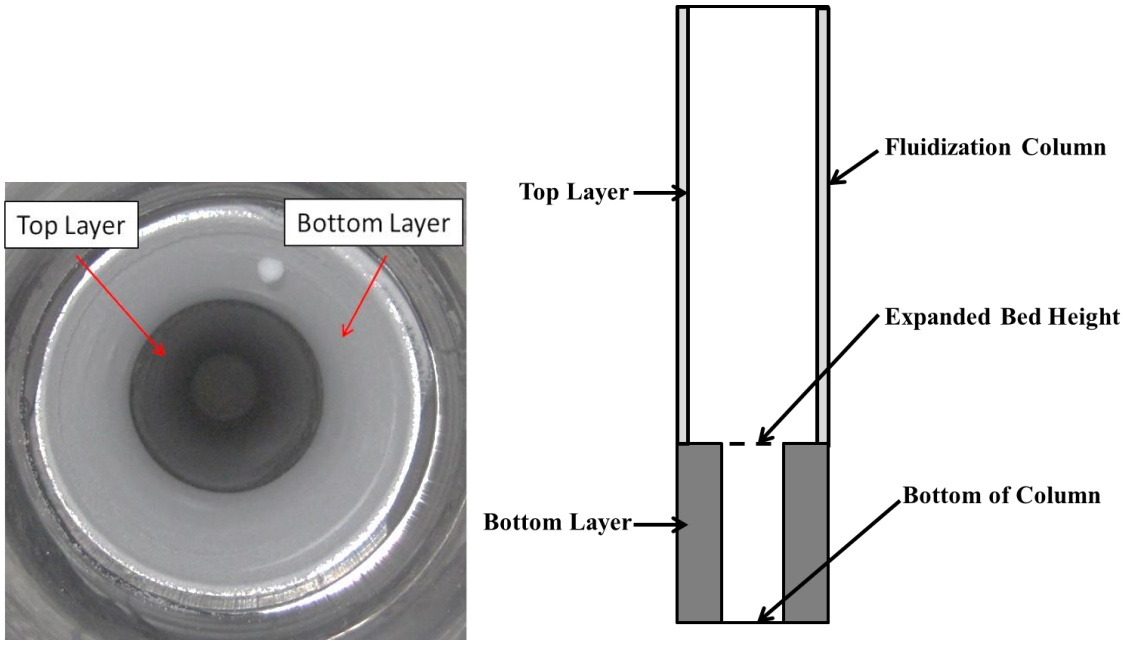

(a) (b)

Figure 4.4: (a) An example of wall coating image illustrating the top and bottom coating layers; (b) Schematic of the wall coating.

4.3.2.2 Particles mass

Mass percentage of particles collected from the bulk and wall regions of the fluidization column at various operating pressures are presented in Figure 4.5. For all trials, in average 92 – 97% of the initial particles mass remained in the bulk of the bed after fluidization, while the mass of particles adhered to the column wall only occupied 2 – 6% of the initial mass. The fluidization operating pressure influenced the degree of column wall fouling where double the amount of

particles coated the column wall at elevated pressures, in comparison to atmospheric operation. However, assessing the results at elevated pressures from 600 to 2600 kPa showed that, on average, the extent of wall fouling slightly increased by increasing the operating pressure. Since the top wall layer coating was extended to the column outlet, the particles in this layer must have been those that were able to entrain from the bed but due to being highly charged, they adhered to the wall. This is evident since almost no fine particles were collected in all the experiments, and thus no results about these particles are discussed here.

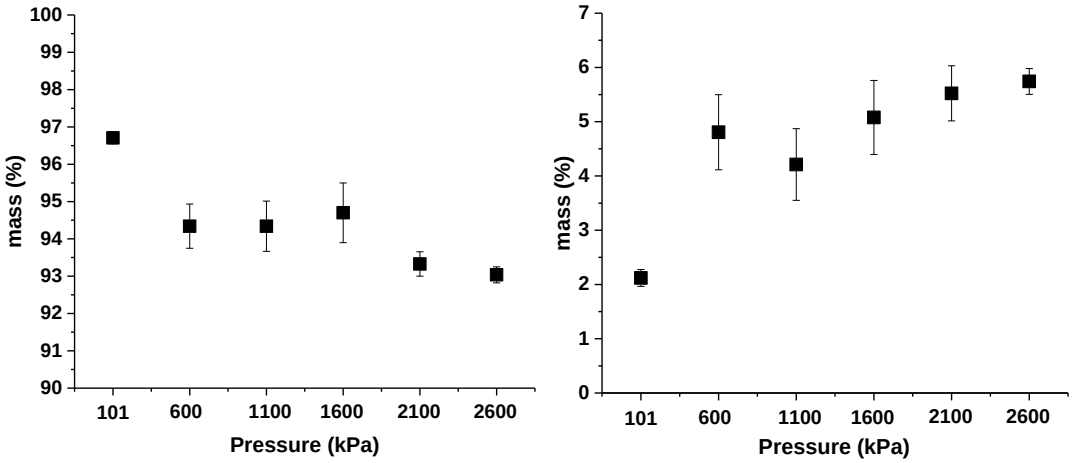

Figure 4.5: Mass percentage of particles collected from (a) bulk and (b) wall region (top and bottom layer) of the fluidization column at different fluidization pressures.

As can be seen in Figure 4.6, the amount of wall particles in bottom layers was 2 – 6% of that of initial particles, while only 0.2 – 0.5% of initial particles formed the top layer. This implies that the majority of particles that adhered to the column wall were located in the region where the fluidization was taking place. For the bottom layer, the particles mass percentages increased by a factor of 3 when the fluidization pressure increased from atmospheric to 600 kPa, and remained constant when the system was further pressurized. For top layer particles, the mass percentages did not vary significantly with the change of operating pressure.

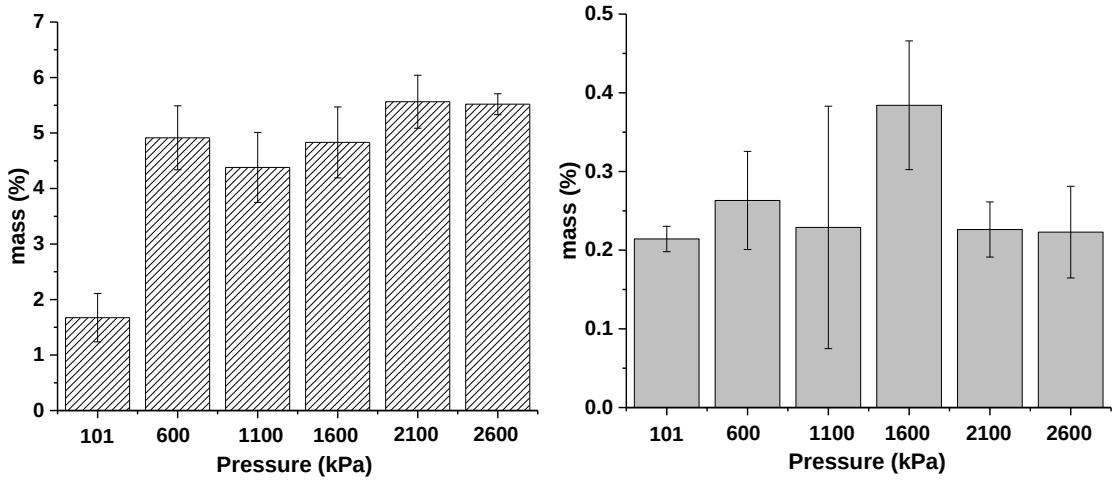

Figure 4.6: Mass percentage of particles adhered to the fluidization column wall at various fluidization pressures for the (a) bottom layer and (b) top layer.

4.3.2.3 Particles size distribution

Among all experiments, the average particle sizes of bulk particles were in a range of 650 – 700 µm, similar with those of initial particles. Therefore, as can be seen in Figure 4.7, the particles that formed the bottom wall layers at all operating conditions were on average smaller than those in the bulk of the bed. The results also showed that, on average, bottom wall particles were smaller at atmospheric conditions than those found at higher pressures. Because mass of the top wall layer particles was not sufficient for particle size measurements, no results for these particles are discussed here. However, it should be noted that the particles forming the top wall layer are those entrained from the bed; and thus, they must have been smaller than those remained within the bed

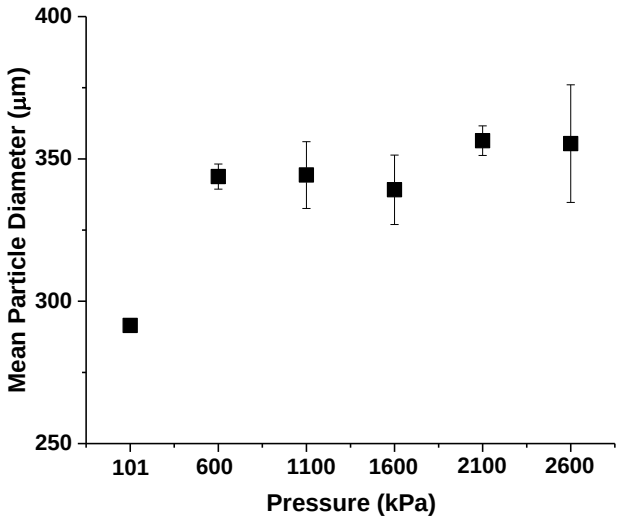

Figure 4.7: Mean particle diameter of bottom wall layer particles at various fluidization pressures.

4.3.2.4 Particles charge density

The net specific charges of the bulk particles ranged from 0.13 to 0.18 μC/kg, and did not vary with the operating pressure. The net specific charge of particles that occupied the bottom and top coating layers are presented in Figure 4.8. At atmospheric condition, both layers had a net negative charge, whereas at higher pressures, the bottom and top layers were oppositely charged. Overall results indicate the occurrence of bipolar charging for all operating conditions tested, which has been reported to be related to particle size [18–21]. Elevating the fluidizing pressure from atmospheric to 2600 kPa did not significantly affect the net specific charge of particles in the top wall layer. Since the mass of this layer was also relatively constant with the increase in pressure, the net charge of particles must have remained the same to keep the q/m relatively constant.

Comparing the absolute values of the net specific charge of top layer particles with that of the bottom layer at elevated pressures indicates that the particles net specific charge in the top wall layer was significantly (by a factor of 3) larger than in the bottom wall layer. Considering that the mass percentage of particles in the top layer was more than 10 times smaller than that in the bottom layer, the particles net charge in the top layer must have been 10 - 20 times larger.

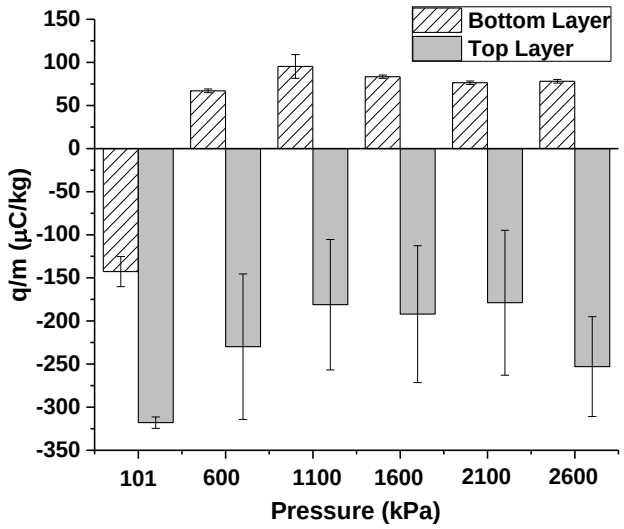

Figure 4.8: Net specific charge (*q/m*) of wall bottom and top particle layers.

To further investigate the charging behavior of particles that adhered to the column wall, the bottom layer particle charge distribution was measured by using a charge particle separator (CPS) unit. The details of the CPS unit is presented elsewhere [17]. The unit consisted of two slanted copper plates located above four Faraday cups (FC1 to FC4) with FC1 located closer to the positively charged plate and FC4 being furthest away. Therefore, Faraday cups FC1 and FC4 collected the highly negatively and positively charged particles, respectively. The positive plate was connected to a high voltage power supply set at 36 kV. Experiments were only conducted for the two fluidization pressures of 1600 and 2600 kPa where the bottom Faraday cup was replaced with the CPS unit prior to the removal of the bottom wall layer. More information about the charged particle separator is presenetd in Appendix C.2.

As can be seen in Figure 4.9, although the majority of particles within the bottom wall layer were positively charged, this layer also contained a small amount of negatively charged particles which were also slightly smaller than the positively charged particles. These results again confirm the presence of bipolar charging

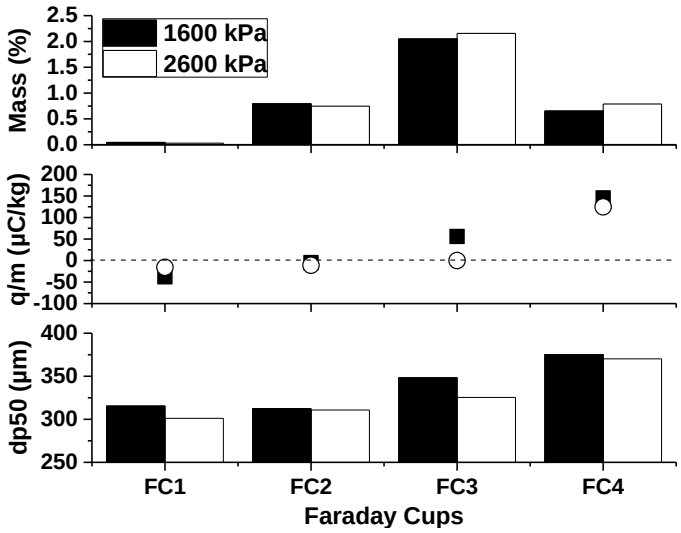

Figure 4.9: Bottom wall layer particles charge distribution measured using the CPS unit at pressures of 1600 and 2600 kPa.

For the pressurized experiments, the fluidization system was depressurized after the 60 min fluidization period so that a small tube could be inserted into the fluidization column from the top to enable the removal of the wall particles. In order to determine the influence of system depressurization on particles charge, a new test was conducted at 2600 kPa. When the 60 min fluidization period was completed, the distributor plate was opened prior to the system depressurization, allowing the collection and charge measurement of bulk particles. After the bulk particles dropped into the bottom Faraday cup, the system was slowly depressurized while the charge of bulk particles was still being recorded. The result of this test is shown in Figure 4.10. The net charge of bulk particles did not vary during depressurization. This means that the net charge of particles was not affected by depressurizing the system prior to making any particle charge measurement.

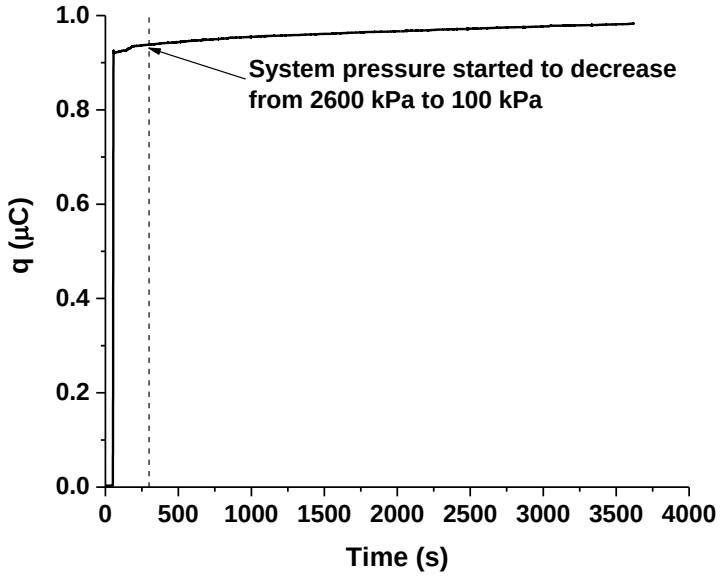

Figure 4.10: The net charge of bulk particles monitored over time while the fluidized bed depressurized from 2600 kPa to atmospheric.

4.3.3 Relation between particles charging and bubble dynamics

As discussed in a previous work from the same group [10] (Chpater 2), in fluidization systems with negligible entrainment, the net specific charge within the bed (i.e., with the bulk and wall particles) is primarily the result of the particle-wall contacts. During the fluidization process, polyethylene particles close to the stainless steel column wall contact the wall, and as a result of the difference in the work functions of the two materials, the fluidizing particles gain a negative net charge. This in turn results in an equal amount of positive charge to be accumulated on the inner column wall, resulting in the creation of image force between the negatively charged particles and the fluidization column wall. This mechanism forms the first negatively charged wall layer. On the other hand, the attractive Coulomb force results in the negatively charged layer to attract the positively charged particles from the bulk of the bed. In addition, the positively charged particles in the bulk repel each other, leading to the migration of the positive particles towards the column wall. These mechanisms forms a positively charged second layer.

In gas-solid fluidized beds, the extent of the charged particle adherence to the column wall is influenced by the balance between the gravitational, drag, image and Coulomb forces. With the increase in operating pressure, the inertial of the fluidizing gas increases, in turn leading to a higher drag force; and thus, influencing the fluidization behaviour. In bubbling flow regime,

particles are picked up in gas bubble wakes from close to the distributor plate and move up to the bed surface. The particles then move downwards within the bubble-free region of the bed, thus inducing the mixing of particles within the bed [22]. It is reported that the amount of particles carried upwards by gas bubbles is about 0.5–0.8 times of the bubble volume [22–25]. This suggests that the increase in gas bubble size gives rise to a larger amount of particles carried upwards from the bottom of the bed, thus improving the degree of contacts between particles in bed and the fluidization column wall. Therefore, in this work where at atmospheric condition the frequency of larger bubbles was higher, higher degree of particles-wall contacts were expected, in turn leading to a higher degree of image force. Therefore, more negatively charged particles were attracted to the column wall (Figure 4.11a). In pressurized experiments, however, lower average bubble sizes and higher frequency of small bubbles were observed that would give rise to higher degrees of particle-particle contacts and formation of more positively charged particles. This will then lead to a higher degree of attractive Coulomb force between the wall layer and positively charged particles within the bed. Thus, the second wall layers were found to be positively charged in pressurized conditions (Figure 4.11b).Although in pressurized experiments the particles net charge in the bottom wall layers were positive, the results of CPS tests (Figure 4.9) confirmed the existence of negatively charged particles. The higher degrees of particle-particle contacts in pressurized experiments also resulted in a greater degree of bipolar charging. Consequently, particles that coated the wall had higher absolute net charges, as well as higher mass fraction, in these experiments.

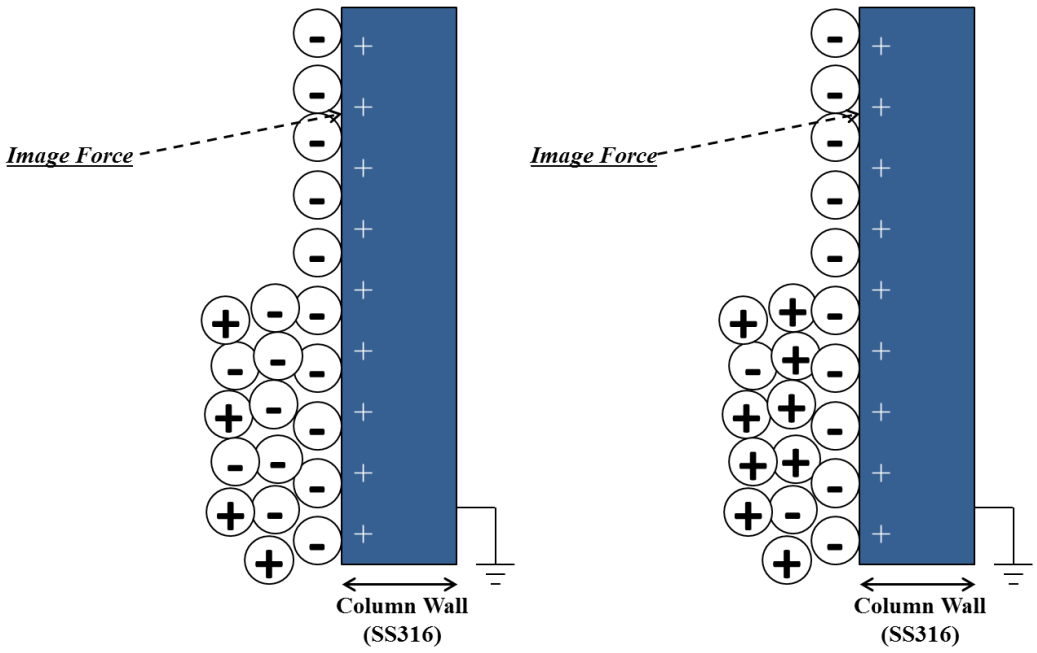

Figure 4.11: Fluidized bed wall coating formation mechanism at (a) atmospheric conditions, and (b) under higher pressures.

4.4 Conclusion

The effect of operating pressure on electrostatic charge generation as well as gas bubble dynamics were investigated in a gas-solid fluidized bed of polyethylene resin. Experiments were conducted under pressures ranging from atmospheric to 2600 kPa (similar to commercial polyethylene reactors). Elevating the system pressure from atmospheric condition to 600 kPa doubled the fluidized bed wall coating. However, further increasing the pressure had no additional effect. The wall coating consisted of two layers: one thicker layer at the bottom of the column extended to the expanded bed height and a thinner layer up to the column exit.. At atmospheric conditions, the net charges of particles in both layers were negative. However, at higher pressures, the bottom layer was positively charged, while the top layer was negatively charged.

The polarity of the bottom wall layer was suggested to be as a result of the image force between the metallic column wall and the particles, as well as the attractive Coulomb force between the wall layer and oppositely charge particles in the bulk of the bed. At atmospheric condition, larger

gas bubbles gave rise to more contacts between the particles and the column wall. As a result, due to image forces, particles that coated the wall were mainly negatively charged. As the system was pressurized, formation of smaller gas bubbles enhanced the particle-particle contacts. Thus, the attractive Coulomb forces between the negatively charged wall layer and positively charged particles in the bulk of the bed gave rise to net positive bottom wall layers.

Acknowledgements

Authors wish to thank Particulate Solid Research, Inc., PSRI) for providing the optical fiber probe. Financial support by Natural Sciences and Engineering Research Council (NSERC) of Canada, Canada Foundation for Innovation (CFI), and financial assistance and input from Univation Technologies, LLC (USA) are acknowledged with gratitude.

References

[1] G. Hendrickson, Electrostatics and gas phase fluidized bed polymerization reactor wall sheeting, Chem. Eng. Sci. 61 (2006) 1041–1064.

[2] M.G. Goode, F.D. Hussein, K.H. Lee, T.J. McNeil, C.C. Williams, Static control in olefin polymerization, US6111034 A, 2000.

[3] M.G. Goode, D.M. Hasenberg, T.J. McNeil, T.E. Spriggs, Method for reducing sheeting during polymerization of alpha-olefins, US4803251 A, 1989.

[4] R.O. Hagerty, M.E. Muhle, A.K. Agapiou, C. Kuo, M.G. Goode, F.D. Hussein, R.B. Pannell, J.F. Szul, Method for controlling sheeting in gas phase reactors, US7985811 B2, 2011.

[5] G.H. Song, A.S. Rhee, G.R. Lowder, Method for reducing sheeting and static charges during polymerization of ethylene polymers, US5391657 A, 1995.

[6] S. Beret, J.M. Jenkins, T.M. Jones, R.L. Jones, Method for fluidized bed polymerization, US4588790 A, 1986.

[7] Z. Liu, X.T. Bi, J.R. Grace, Electrostatic charging behaviour of dielectric particles in a pressurized gas-solid fluidized bed, J. Electrostat. 68 (2010) 321–327.

[8] W.O. Moughrabiah, J.R. Grace, X.T. Bi, Effects of pressure, temperature, and gas velocity on electrostatics in gas-solid fluidized beds, Ind. Eng. Chem. Res. 48 (2009) 320–325.

[9] F. Salama, D. Song, P. Mehrani, Characterizing Electrostatic Charges in High-Pressure Gas-Solid Fluidized Beds: Experimental Design and Preliminary Results, in: 14th Int. Conf. Fluid. – From Fundam. to Prod., Netherland, 2013.

[10] D. Song, F. Salama, J. Matta, P. Mehrani, Implementation of Faraday Cup Electrostatic Charge Measurement Technique in High-Pressure Gas-Solid Fluidized Beds at Pilot-Scale, Powder Technol. 290 (2016) 21–26.

[11] A.C. Hoffmann, J.G. Yates, Experimental observations of fluidized beds at elevated pressures, Chem. Eng. Commun. 41 (1986) 133–149.

[12] P.A. Olowson, A.E. Almstedt, Influence of pressure and fluidization velocity on the bubble behaviour and gas flow distribution in a fluidized bed, Chem. Eng. Sci. 45 (1990) 1733–1741.

[13] P.A. Olowson, A.E. Almstedt, Hydrodynamics of a bubbling fluidized bed: influence of pressure and fluidization velocity in terms of drag force, Chem. Eng. Sci. 47 (1992) 357–366.

[14] A. Orta, B. Wu, M. Ghods, A. Guerrero, C. Bellehumeur, A. Kantzas, Pressure effect on hydrodynamics of a high pressure X-ray transparent polyethylene fluidized bed, Int. J. Chem. React. Eng. 9 (2011).

[15] G.C. Brouwer, E.C. Wagner, J.R. van Ommen, R.F. Mudde, Effects of pressure and fines content on bubble diameter in a fluidized bed studied using fast X-ray tomography, Chem. Eng. J. 207–208 (2012) 711–717.

[16] M. Rüdisüli, T.J. Schildhauer, S.M.A. Biollaz, J.R. van Ommen, Bubble characterization in a fluidized bed by means of optical probes, Int. J. Multiph. Flow. 41 (2012) 56–67.

[17] F. Salama, A. Sowinski, K. Atieh, P. Mehrani, Investigation of electrostatic charge distribution within the reactor wall fouling and bulk regions of a gas-solid fluidized bed, J. Electrostat. 71 (2013) 21–27.

[18] P. Cartwright, S. Singh, A.G. Bailey, L.J. Rose, Electrostatic Charging Characteristics of Polyethylene Powder During Pneumatic Conveying, IEEE Trans. Ind. Appl. IA-21 (1985) 541–546.

[19] K.M. Forward, D.J. Lacks, R.M. Sankaran, Triboelectric charging of granular insulator mixtures due solely to particle - Particle interactions, Ind. Eng. Chem. Res. 48 (2009) 2309–2314.

[20] F. Sharmene Ali, M. Adnan Ali, R. Ayesha Ali, I.I. Inculet, Minority charge separation in falling particles with bipolar charge, J. Electrostat. 45 (1998) 139–155.

[21] H. Zhao, G.S.P. Castle, I.I. Inculet, A.G. Bailey, Bipolar charging of poly-disperse polymer powders in fluidized beds, IEEE Trans. Ind. Appl. 39 (2003) 612–618.

[22] W.C. Yang, Bubbling Fluidized Beds, in: W.C. Yang (Ed.), Handb. Fluid. Fluid-Particle Syst., CRC Press, 2003: p. 99.

[23] A.G. Fane, N.P. Nghiem, Bubble Including Mixing and Segregation in a Gas-Fluidized

Bed., J. Chinese Inst. Chem. Eng. 14 (1983) 215–224.

[24] P.N. Rowe, Experimental properties of bubbles, in: Fluidization, Academic Press London, 1971: pp. 121–191.

[25] P.N. Rowe, B.A. Partridge, An X-ray study of bubbles in fluidized beds, Trans. Inst. Chem. Engrs. 43 (1965) 157–175.

Chapter 5
Comparison of Electrostatic Charge Generation in Gas-solid Fluidized Beds in Turbulent versus Pre-Turbulent Flow Regime

Di Song, Poupak Mehrani*

Chemical and Biological Engineering Department, University of Ottawa
161 Louis Pasteur, Ottawa, ON, Canada, K1N 6N5
* poupak.mehrani@uottawa.ca, Tel: 1 (613) 562-5800 Ext. 6098, Fax: 1 (613) 562-5172

The current chapter is a manuscript to be submitted for publication in a refereed journal

Abstract

In this work, the effect of gas velocity on the electrostatic charge generation in gas-solid fluidized beds was studied with a specific focus on the transition to turbulent flow regime. Experiments were conducted at a pressure of 2600 kPa (abs) with fluidizing gas velocities of 1.5, 3, and 5 times of U_{mf} (pre-turbulent regimes) and 7.5 times of U_{mf} (turbulent regime). Increasing the gas velocity and transitioning to the turbulent flow regime improved particle-wall contacts; and thus, augmented the extent of wall fouling, which indicates the increase in bed electrostatic charge generation. The amount of fouling was approximately five times larger in turbulent flow regime (7.5 U_{mf}) in comparison to that for the lowest gas velocity examined in bubbling flow regime (1.5 U_{mf}). The particles coating on the column wall consisted of a thick bottom layer which extended to a height of approximately 1 m above the distributor plate, and a thin top layer which extended to the top of the column near the outlet. The bottom and top layers had a net positive and a negative charge, respectively. While the bottom layer was found to contain both positively and negatively charged particles, a distinct negatively charged particle layer was detected in the turbulent regime experiments (7.5 U_{mf}). The particles net specific charge in the top and bottom layers did not vary with the increase in gas velocity. However, the net charge of these particles increased. The fine particles entrained from the bed had a net negative charge resulting in a net positive charge to be left behind in the bed contributing to the increase in the magnitude of wall fouling at higher gas velocities, especially in turbulent flow regime.

Keywords: Gas-solid fluidization, Electrostatics, Particle wall coating, Turbulent

5.1 Introduction

Gas-solid fluidized beds have been widely employed in industries such as petrochemical, oil and gas and food due to their excellent characteristics of providing a high degree of heat and mass transfer as well as mixing. In some of the gas-solid fluidization processes, such as the gas-phase polymerization of ethylene to produce polyethylene, the generation of electrostatic charge is present and results from the continuous contacts between fluidizing particles and the particles and the fluidization column wall. This leads to significant operational challenges including: particle agglomeration and particle adherence to the reactor wall and dome, resulting in a problem known as "sheeting" [1]. As the sheets grow thicker, they may dislodge from the reactor wall and fall to potentially block the fluidized bed distributor plate which necessitates reactor shutdown for clean-up and in turn imposes significant economic losses. Although attempts have been made in finding means of reducing sheeting in commercial reactors, the problem still remains [1–5]. This is due to the complexity of electrostatic charging in relation to gas-solid fluidization, and more importantly, the lack of a comprehensive understanding of the underlying mechanisms of charge generation.

One area of research that has received minimal attention is the understanding of fluid bed electrification in various fluidization flow regimes, especially those related to the commercial operations. For instance, commercial polyethylene reactors are typically operated under a wide range of gas velocities, 1.5 – 10 times the minimum fluidization velocity (U_{mf}) [6–10]. As the gas velocity increases beyond minimum fluidization, various fluidization flow regimes are achieved. Excess gas beyond the minimum fluidization velocity forms bubbles at the distributor plate which grow, rise to the bed surface and burst. As gas velocity is raised even higher, the bubbles grow larger to a point where they nearly take up the entirety of the column diameter and the slugging regime is reached [11]. When the fluidization gas velocity is large enough that the top surface of the bed becomes difficult to detect and the entrainment becomes significant, turbulent fluidization is reached [12]. Due to its high gas-solids contact efficiency, the turbulent flow regime is more suitable than other flow regimes for processes that require high productivity, limited axial mixing of gas, and high heat transfer efficiency [13–15].

A few works have studied electrostatic charge generation in bubbling [16–24] and slugging [25–28] gas-solid fluidized beds. Ciborowki and Wlodarski [16] fluidized multiple types of particles

with size range of 300 – 500 μm in a 0.049 m diameter glass column at superficial gas velocities of 0.08 – 0.5 m/s. The authors measured the potential of the bed with an electrode and showed that the electrode potential increased with the increase of fluidizing gas velocity. Gajewski [25] glued copper rings connected to a microammeter on the inner surface of a 0.25 m in diameter glass column to measure the electrical current inside the bed. Polypropylene particles with diameter of 2000 μm were fluidized under gas velocities of 0.1 – 0.5 m/s while air at 40°C and relative humidity of 35% was used as the fluidizing gas. Their results showed that the electrostatic potential above the static bed height increased with the increase of fluidizing gas velocity. The electrostatic potential reached a peak at a gas velocity of 0.35 m/s, and then started to decrease. Revel *et al.* [19] fluidized polyethylene particles with an average size of 3000 μm in a 0.1 m in diameter acrylic column at gas velocities of 1.7 to 2.5 times U_{mf}. Air at room temperature with a relative humidity of less than 5 % was used as the fluidizing gas. They showed that the net specific charge (q/m) of particles sampled at 0.035 m above the distributor plate increased with the increase of fluidizing gas velocity. Liu *et al.* [21] studied the effect of fluidizing gas velocity on the degree of electrostatic charge generation in a 0.15 m in diameter carbon-steel gas-solid fluidization column. Polyethylene particles with an average size of 646 μm were fluidized at 138 kPa and at excess gas velocities of 0.05, 0.10, 0.15, 0.20 m/s. Air at room temperature with a relative humidity of 8 – 11% was used as the fluidizing gas. The measurements from three current collision probes located at different radial and axial positions in the column showed that the electrostatic charge increased with the increase of fluidizing gas velocity. Alsmari *et al.* [24] used the same apparatus as Liu *et al.* [21], and conducted free-bubbling experiments. They fluidized a binary mixture of large glass beads (425 – 600 μm) and 5 wt% fine glass beads (25 – 50 μm) at 207 kPa and a range of gas velocities of 0.2 – 0.6 m/s (1 – 3 times minimum fluidization velocity). Air at 20°C with a relative humidity of 12% was used as the fluidizing gas. The particles charge densities were determined by current collision probes. The results showed that as the superficial gas velocity increased, the degree of electrostatic charge measured locally at the probe tip increased.

As mentioned previously, many industrial fluidized beds including that of polyethylene reactors are operated in turbulent flow regime. However, to the authors' knowledge, no work has been carried out to investigate the electrostatic charge generation and wall fouling in turbulent flow and its comparison with pre-turbulent flow regime. Moreover, industrial gas-solid fluidized bed

polyethylene reactors are operated at high pressures close to 3000 kPa [29]. Therefore, the goal of this work was to investigate and compare the degree of electrostatic charge generation in pre-turbulent and turbulent fluidization flow regimes at pressurized conditions, similar to that of commercial polyethylene reactors.

5.2 Experimental setup and method

Experiments were conducted in a pilot-scale pressurized gas-solid fluidization system, detailed previously [30,31]. The system contained a 0.15 m in diameter stainless steel fluidization column. Two copper inner Faraday cups were placed in the bottom and top expanded sections of the column. The two inner cups were electrically isolated from the expanded sections. The top and bottom expanded sections of the column acted as the outer Faraday cups. The Faraday cups were connected to digital electrometers for measuring the net electrostatic charge of fluidizing particles. The distributor plate was a modified knife-gate valve which allowed the in-bed particles to dislodge into the bottom Faraday cup without any particle handling. A filter bag was placed inside the top Faraday cup to capture the entrained particles and to help measure their cumulative charge during fluidization. In all experiments, the fluidization system was pressurized to the desired operating pressure with nitrogen gas from a gas cylinder. The gas was circulated at the desired fluidizing gas velocity with a centrifugal compressor having a variable speed drive. A plate type heat exchanger was used to maintain the temperature of the gas at room temperature. Linear low-density polyethylene (LLDPE) resin directly received from a commercial reactor (referred to as PE_A in Appendix D.2.1) was fluidized in this work with properties summarized in Table 5.1.

Table 5.1: Particles properties.

Particle Type	Geldart Group	Particle Density (kg/m^3)	Particle Size Distribution (μm)	Particle Mean Diameter (μm)
LLDPE	B	918	20 – 1500	560

The experimental conditions in this work are summarized in Table 5.2. Experiments were conducted with various gas velocities at factors of minimum fluidization velocity and at an elevated pressure, similar to the operating pressures of typical commercial polyethylene reactors. Experiments at 1.5 – 5 U_{mf} represented pre-turbulent flow, while those at 7.5 U_{mf} were at the

turbulent flow regime. Since significant mass of particle entrained from the bed in 5 and 7.5 U_{mf} experiments, the fluidization period was limited to 15 minutes for all trials in this work.

Table 5.2: Experimental Conditions.

Gas Velocities	1.5, 3, 5 U_{mf} (Pre-turbulent); 7.5 U_{mf} (Turbulent)
Fluidization Period	15 min
Operating Pressure	2600 kPa (abs)

5.2.1 Detection of minimum fluidization velocity and turbulent flow transition velocity

First the minimum fluidization velocity and the transition gas velocity to turbulent flow regime were established at the operating pressure of 2600 kPa. The minimum fluidization velocity, found by measuring the pressure drop across the bed at various superficial gas velocities, was 0.08 m/s.

The transition velocity to turbulent flow regime was found by monitoring the standard deviation of differential pressure signal across the bed at various superficial gas velocities. As the fluidizing gas velocity is increased, the resulting pressure fluctuations amplitude increases. However, beyond a certain superficial gas velocity, known as turbulent flow transition velocity (U_c), the amplitude of pressure fluctuations begins to decline and the large voids in the bed begin to disappear [14,32]. To find the turbulent flow transition velocity, in this work, the fluidizing gas velocity was elevated in increment of one U_{mf}, up to 8 U_{mf} which was at the limit of the compressor power. A fresh batch of polyethylene resin was used for each fluidizing gas velocity and the fluidization was carried out for 15 minutes, similar to the electrostatic trials. Since a significant amount of particles entrained from the bed when the fluidizing gas velocity was raised to 5 U_{mf} and higher, the bed particle size distribution and the turbulent transition velocity were influenced. Therefore, to determine any deviations in the U_c measurement, the differential pressure signal was measured for various fluidization periods including: 2, 6, and 12 minutes. The signal was recorded for 30 seconds for each time period, except for the 12 minutes run where the signal was recorded for 3 minutes giving a total run time of 15 min. The results presented in Figure 5.1 indicate that the turbulent transition gas velocity was between 6 and 7 times of U_{mf}. Thus, it was established that the system was operating in the turbulent flow regime at a fluidization velocity of 7.5 U_{mf}.

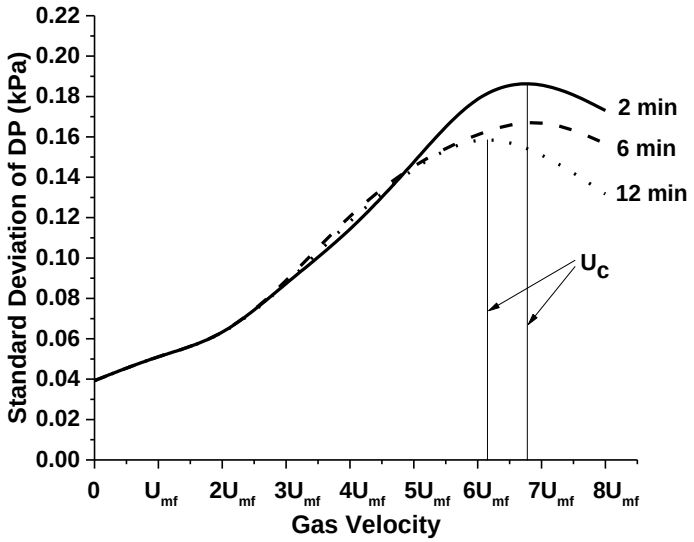

Figure 5.1: Turbulent transition velocity (U_c) measured for various fluidization periods of 2, 6, and 12 minutes at 2600 kPa.

5.2.2 Experimental procedure

In all trials, as received particles (referred to as "initial" or "initial particles") were poured into the fluidization column after taking their initial net charge. The desired fluidizing gas velocity was then reached by adjusting the speed of the centrifugal compressor after pressurizing the fluidization system to the desired operating pressure. During fluidization, the cumulative charges of entrained fine particles were measured by the top Faraday cup, containing a filter bag (referred to as "fines" or "fine particles"). After 15 minutes of fluidization, the compressor was gradually stopped and the system was depressurized. Then, the top manway of the column was opened to remove the filter bag and to measure the mass of the fine particles. The distributor plate was opened, allowing the particles remaining in bed to drop into the bottom Faraday cup to measure their net charge (referred to as "bulk" or "bulk particles"). After removing the bottom Faraday cup for measuring the mass of bulk particles, the inner column wall was visually examined from the bottom for any particle fouling (referred to as "wall" or "wall particles). Compressed building air was passed through a long tube inserted from the top of the column to dislodge the wall particles. These particles were collected in the cleaned bottom Faraday cup and their mass and net charge was measured. For all experiments, a sample of the initial, bulk, wall, and fine particles were collected and analyzed for particle size distribution by a Malvern Mastersizer

2000 particle size analyzer. Additionally, all the experiments were repeated at least twice to ensure the reproducibility of the results.

5.3 Results and discussion

The mass (m), net charge (q), and size distribution (PSD) of initial particles were determined prior to each experiment. Results indicated that, for all trials, these particles initially had relatively small net specific charges (q/m) of 0.06 ± 0.02 μC/kg, and similar particle size distributions.

5.3.1 Wall coating

Once the experiments were completed and the bulk particles were removed, the inside of the fluidization column was visually examined and pictures of the inner column wall were taken from the bottom. In all runs, particles were found to foul onto the entire length of the column (Figure 5.2). The wall coating consisted of two layers, a thicker bottom layer which extended to a height of approximately 1 m above the distributor plate, and a thin top layer which extended to the top of the column near the outlet.

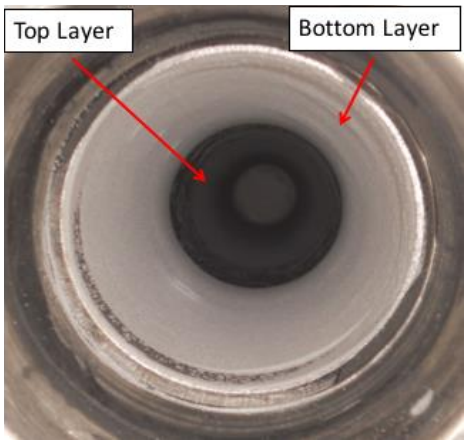

Figure 5.2: A typical picture of polyethylene particles wall fouling after 15 minutes fluidization, illustrating top and bottom wall layers.

When collecting the bottom wall particles in turbulent experiments (7.5 U_{mf}), it was observed that as the particle removal process progressed towards the layers closer to the column wall, the particle charge polarity changed from positive to negative. An example of such a measurement is illustrated in Figure 5.3a. These two oppositely charged layers were referred to as "bottom outer layer" and "bottom inner layer" (Figure 5.3b). After collecting the particles from the bottom

outer layer, the bottom Faraday cup was removed to measure the mass of the particles and take samples for a particle size distribution analysis. The bottom Faraday cup was then returned to the column to collect and measure the charge and the mass of particles in the bottom inner layer.

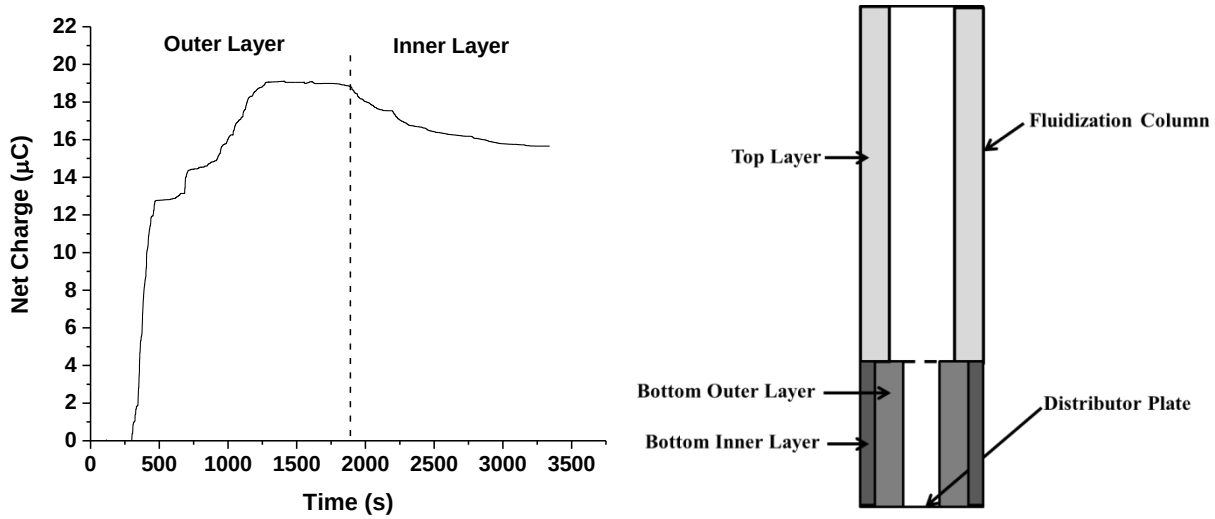

(a) (b)

Figure 5.3: (a) An example of particles charge measured during the collection of the wall coating in turbulent (7.5 U_{mf}) experiments. (b) Schematic of particle wall fouling layers.

5.3.2 Masses of particles settled in various regions of the column

Figure 5.4 presents the effect of fluidizing gas velocity on the mass percentages of bulk, wall, and fine particles. In all cases, over 80% of initial particles remained in the bulk of the bed after 15 min of fluidization. The mass percentages of bulk particles did not vary significantly when the gas velocity was raised from 1.5 to 3 U_{mf}, but declined as the gas velocity further increased. The mass percentage of the bulk particles in the turbulent flow (7.5 U_{mf}) was approximately 10% lower than those obtained in experiments at lower gas velocities. The mass percentage of wall particles increased with the increase of fluidizing gas velocity.

Almost no fine particles were captured at 1.5 U_{mf} and thus, the results of fine particles at this condition will not be discussed. As expected, the mass of entrainment significantly increased when the gas velocity rose from 5 U_{mf} to 7.5 U_{mf} and as the bed transitioned to turbulent flow regime. The results clearly indicate that the fluidizing gas velocity influenced the degree of column wall fouling, as well as the extent of particles entrainment.

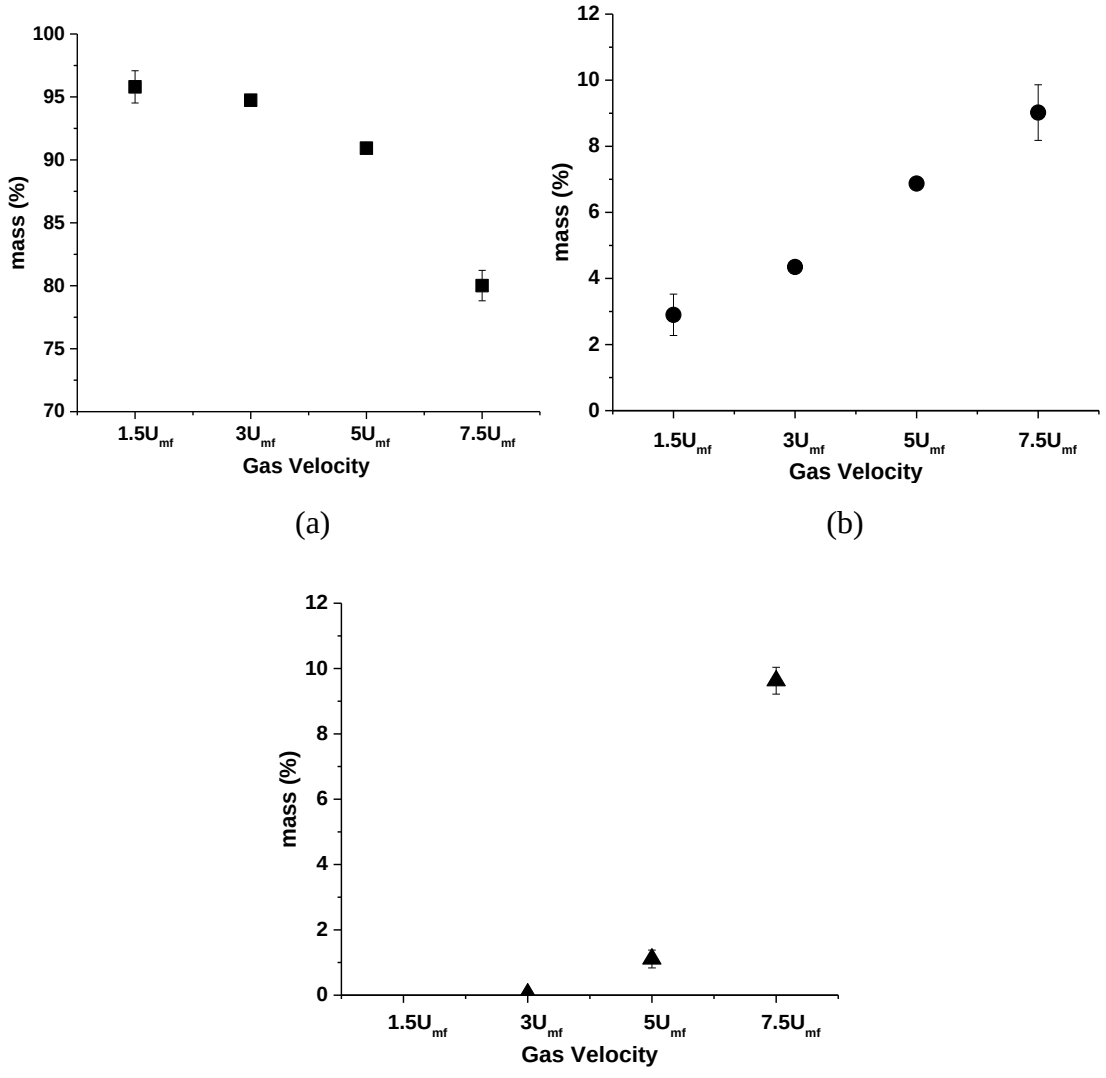

Figure 5.4: Mass percentages of (a) bulk, (b) wall, and (c) fine particles at various fluidizing gas velocities.

Figure 5.5 illustrates the mass percentages of particles in bottom and top wall layers at various fluidizing gas velocities. The bottom layer consisted of 2 – 7% of the mass of the initial particles while 0.5 – 3% of the initial mass was found in the top layer. The mass percentage of bottom wall layer increased almost linearly with gas velocity (Figure 5.5a). As indicated earlier, in turbulent flow regime (7.5 U_{mf}), a bottom inner layer which its polarity was opposite to that of the outer layer was found. This layer only occupied 0.5% of the initial mass of particles.

As for the top wall layers, the amount of particles collected increased considerably when the gas velocity reached the transition to turbulent flow (Figure 5.5b). This finding is partially attributed

to the significant increase in gas velocity which enabled more particles to reach the top of the column and, if highly charged, to adhere to the wall. Overall results demonstrate that the increase in fluidizing gas velocity and the transition of fluidization flow regimes augmented the magnitude of charged particles wall fouling.

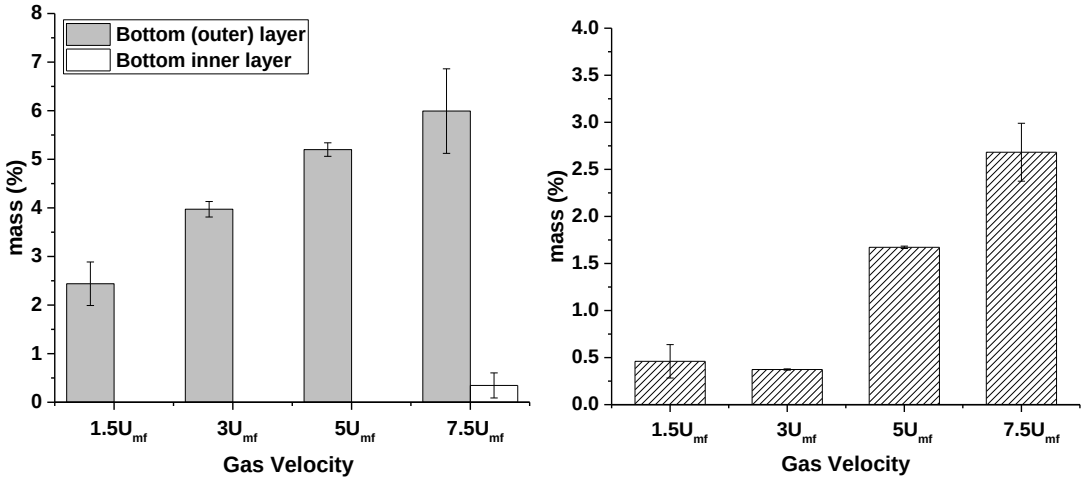

Figure 5.5: Mass percentages of particles in (a) bottom and (b) top wall layers at various fluidizing gas velocities.

5.3.3 Average particle size in various regions of the column

The average particle size of bulk particles was similar to those of the initial particles for all trials and thus not shown here. As can be seen in Figure 5.6a, the mean particle size of the bottom (outer) wall particles fell in a range of 300 – 500 µm, and slightly increased with the rise of the gas velocity. The particles mean size in the bottom inner wall layer in 7.5 U_{mf} experiments were approximately 350 µm, which was smaller than particles in the bottom outer layer and larger than those in the top layer. The adhesion of particles to the column wall is a result of a balance between the force of gravity and the drag, as well as the electrostatic and the image forces [33]. Thus, results imply that the attractive forces between the particles and the column wall (i.e., electrostatic and images forces) became larger with the rise of fluidizing gas velocity.

As expected, the mean particle diameter of fines increased almost linearly with the gas velocities of 3 to 7.5 U_{mf} (Figure 5.6b). However, the difference in particle mean size in the top wall layer was negligible between the 5 and 7.5 U_{mf} conditions. This result signifies that the maximum

particle size for the highly charged entrainable particles to adhere to the column wall was approximately 300 µm.

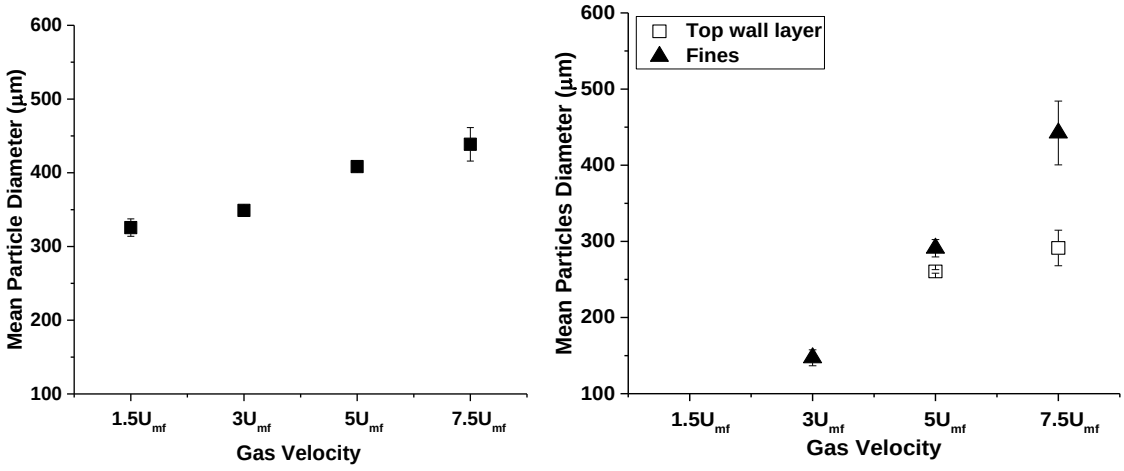

(a) (b)

Figure 5.6: Mean particle diameter of (a) bottom (outer) wall particles, and (b) top wall particles and fines.

5.3.4 Net charge density of bulk, wall and fine particles

After 15 minutes of fluidization, the net specific charge of particles that remained in the bulk of the bed was in the range of 0.08 - 0.19 µC/kg, and did not vary significantly with the elevation of the gas velocity. As can been seen in Figure 5.7a, in turbulent experiments (7.5 U_{mf}), the bottom wall layer consisted of two oppositely charged layers, while at the lower gas velocities only one layer of positively charged particles was detected. The top wall layers all had a net negative charge (Figure 5.7b). For both layers, the net *q/m* did not vary significantly with the change in the gas velocity. Considering that the mass of particles collected in both layers increased almost lineally with the increase of gas velocity (Figure 5.5), the net charge (*q*) of the particles of the two layers must have increased with the rise of the gas velocity. This denotes that the elevation of gas velocity increased the degree of particle charging within the fluidized bed.

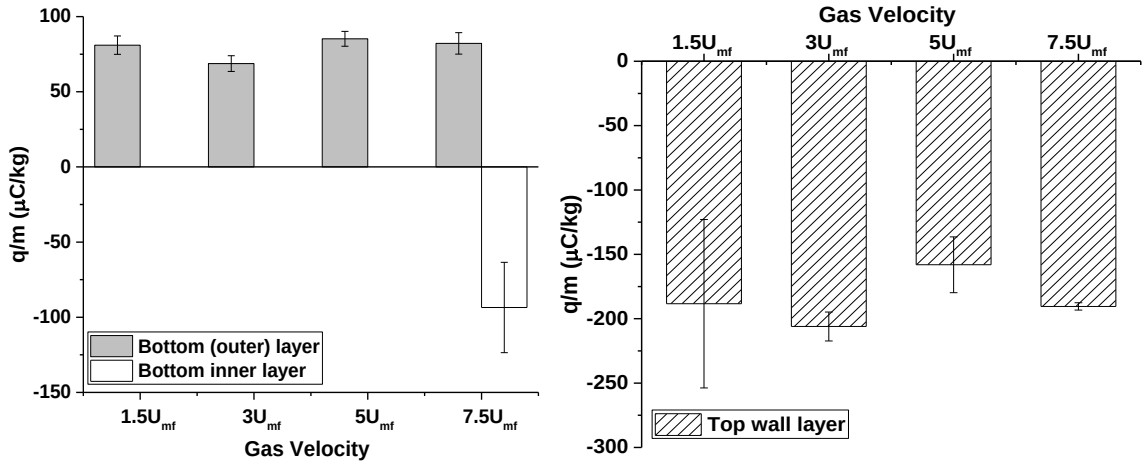

(a) (b)

Figure 5.7: Net specific charge of (a) bottom and (b) top wall layers.

As can be seen in Figure 5.8 the net specific charge of fine particles declined with the increase of fluidizing gas velocity. This was attributed to the significant rise of the fine particles' mass when the fluidizing gas velocity was increased. On the hand, the comparison of particle charge polarity in different regions of the fluidized bed confirms the existence of bipolar charging phenomenon in this work; where the larger bulk and outer wall layers were mainly positively charged while the smaller particles in the fines and the wall top layer were negatively charged. It is important to highlight that the fine particles collected in 3 U_{mf} experiments were much smaller than those at 5 and 7.5 U_{mf} (approximately 150 µm versus 300 to 450 µm) (Figure 5.5b). Therefore, higher fluidizing gas velocity would have allowed the entrainment of larger particles, which were likely less negatively charged. This is another factor resulting in the decline of the net specific charge of fine particles when the gas velocity increased above 3 U_{mf}.

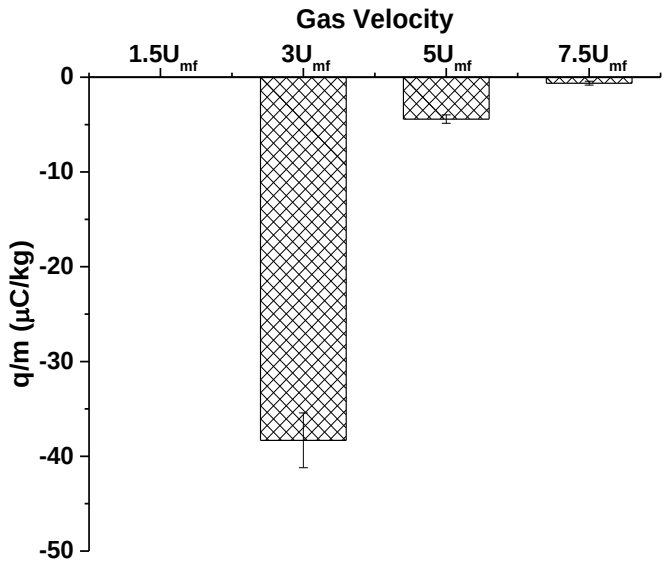

Figure 5.8: Net specific charge (*q/m*) of fines.

In order to investigate the electrostatic charge distribution of particles that coated the column wall during fluidization, a charged particle separator (CPS) apparatus, with details presented elsewhere [34], was used in some of the experiments. The unit consisted of four Faraday cups (FC1 to FC4) and two slanted copper plates placed between the particles drop point and the Faraday cups. One plate was connected to a high-voltage power supply (36 kV) and was positively charged, while the other plate was grounded and acted as the negative plate. FC1 was located close to the positive plate, and FC4 was close to the negative plate. The CPS unit was placed directly under the fluidization column, replacing the bottom Faraday cup and allowing the bottom (outer) wall layer particles to dislodge into the unit and between the two plates. The negatively charged particles were attracted by the positive plate and dropped into FC1 and FC2, while the positively charged particles were collected in FC3 and FC4.

Figure 5.9 illustrates that in both the pre-turbulent (1.5 U_{mf}) and turbulent (7.5 U_{mf}) flow regime experiments, the particles fouled at the bottom of the column wall contained both positively (larger) and negatively charged (smaller) particles. However, the majority of particles within the tested area were positively charged. The results again confirmed the existence of bipolar charging phenomenon which has been reported to be related to particle size.

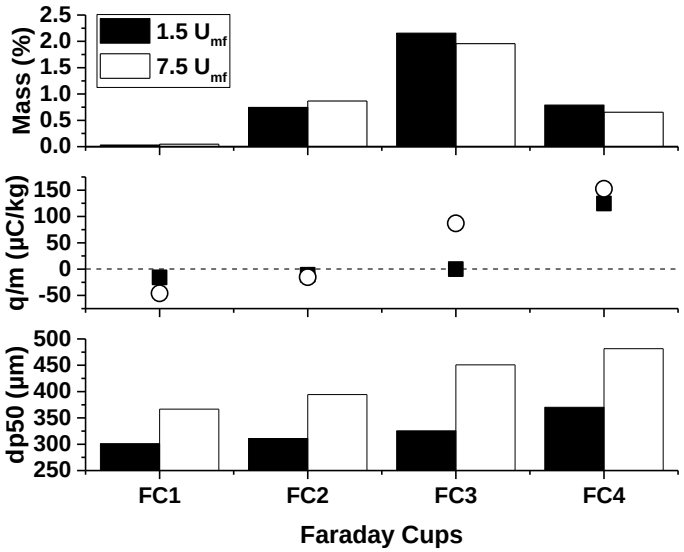

Figure 5.9: The charged particles distribution of the bottom (outer) wall layer particles measured using the CPS unit at 1.5 U_{mf} and 7.5 U_{mf} gas velocities.

5.3.5 Wall fouling formation

At low fluidizing velocities with negligible entrainment (1.5 U_{mf} operating condition), the net specific charge within the bed is primarily the result of the contacts between the fluidizing particles and the column wall. When significant entrainment is present (3 – 7.5 U_{mf} operating conditions), both particle-wall and particle-particle contacts can contribute to the net charge of the bed since particles leave a net opposite charge in the bed when they are entrained. The extent of the charged particle adherence to the column wall is influenced by the balance between the gravitational, drag, image and Coulomb forces. The image force is formed between the charged particles and the conductive fluidization column wall, while the attractive Coulomb force is created between the oppositely charged particles accumulated on the column wall and within the bulk of the bed [33].

In this work, a polyethylene resin was fluidized in a stainless-steel fluidization column. Due to the different work functions of the two materials, particle-wall contacts would have resulted in negatively charged particles and a positively charged column wall. In addition, bipolar charging was detected indicating that particle-particle contacts were also involved in particle charging. Finally, as mentioned above, the net negatively charged entrained fine particles also contributed to the net charge of the bed.

With the rise of fluidizing gas velocity in pre-turbulent flow regimes, the gas bubble size increases, improving the particle-wall contacts while reducing the contacts between particles. In the turbulent flow regime, the widely dispersed solid particles move through the column in a zigzag manner [12] which increases particle-wall contact and decreases particle-particle contact. Therefore, the rise of fluidizing gas velocity yields in-bed particles with a larger negative net charge. Conversely, the experimental results showed that the magnitude of the net negative charge of fine particles increased with the increase of gas velocity which in turn would have left a larger positive net charge in the bed (i.e. making the bulk of the bed space charge to become less negative). Overall, the change in the degree of the image force between the fluidizing particles and the column wall as the gas velocity increased depended on the balance of the two effects mentioned above.

Due to the image force, a layer of negatively charged particles was attracted to the column wall for all gas velocities and formed the first wall layer. This layer coated the entire column wall, from the distributor plate to the column exit. Although the negative charge of the bottom inner wall layer was particularly measurable at the 7.5 U_{mf} operating velocity, the results of the CPS tests showed that the bottom wall layer contained both positively and negatively charged particles for all operating conditions. After the first wall layer was formed, the negatively charged wall particles attracted positively charged particles from the bulk due to attractive Coulomb forces. In addition, the net positive space charge of the bulk contributed to the migration of the positively charged particles towards the wall and the formation of the positively charged layer.

5.4 Conclusions

The effect of the fluidizing gas velocity and fluidization flow regime on the degrees of electrostatic charge generation and particle wall fouling was studied in pre-turbulent and turbulent flow regimes. Polyethylene particles were fluidized at gas velocities of 1.5, 3, and 5 times of U_{mf} (pre-turbulent flow regime) and 7.5 times of U_{mf} (turbulent flow regime) and at the pressure of 2600 kPa, which is similar to that of commercial polyethylene reactors. The net specific charge, mass, and size distribution of particles within the bulk, wall, and fine regions, as well as the electrostatic charge distribution of bottom outer wall particles were studied in this work.

The overall results indicated that the increase in gas velocity and specially the transition to turbulent flow regime augmented the magnitude of wall fouling. The amount of fouling was approximately five times larger in turbulent flow regime (7.5 U_{mf}) in comparison to that for the lowest gas velocity examined in bubbling flow regime (1.5 U_{mf}). The wall coating covered the whole column wall and contained: a thick bottom layer which extended to a height of approximately 1 m above the distributor plate and a thin top layer which extended to the column outlet. The bottom layers had a net positive charge, while the top wall layers were negatively charged for all operating conditions. Both positively and negatively charged particles were detected in the bottom layer, with small particles being negatively charged. However, in the turbulent flow regime condition, a distinct inner negatively charged layer was found in the bottom layer.

The net specific charge of both top and bottom wall layers did not vary much with the increase in gas velocity, implying that the rise of gas velocity promoted particle charging within the bed. The mean particle size of the bottom wall layers slightly increased with the increase of gas velocity, signifying that for the same fluidization period, more of the larger particles were further charged and migrated towards the column wall. A maximum mean particle size of approximately 300 μm was reached for the top wall layer which was smaller than the fines collected.

Finally, increasing the fluidizing gas velocity improved the particle-wall contacts. Thus, the net charge of the in-bed particles was more negative. One the other hand, the larger net negative charge of entrained fines resulted in the bulk particle charge to become less negative. The effect of fluidizing gas velocity on the image force between fluidizing particles and the metallic column wall was found to depend on the balance between these two effects.

Acknowledgements

Financial support by Natural Sciences and Engineering Research Council (NSERC) of Canada, Canada Foundation for Innovation (CFI), and financial assistance and input from Univation Technologies, LLC (USA) are acknowledged with gratitude.

References

[1] G. Hendrickson, Electrostatics and gas phase fluidized bed polymerization reactor wall

sheeting, Chem. Eng. Sci. 61 (2006) 1041–1064.

[2] M.G. Goode, F.D. Hussein, K.H. Lee, T.J. McNeil, C.C. Williams, Static control in olefin polymerization, US6111034 A, 2000.

[3] R.O. Hagerty, M.E. Muhle, A.K. Agapiou, C. Kuo, M.G. Goode, F.D. Hussein, R.B. Pannell, J.F. Szul, Method for controlling sheeting in gas phase reactors, US7985811 B2, 2011.

[4] G.H. Song, A.S. Rhee, G.R. Lowder, Method for reducing sheeting and static charges during polymerization of ethylene polymers, US5391657 A, 1995.

[5] M.G. Goode, D.M. Hasenberg, T.J. McNeil, T.E. Spriggs, Method for reducing sheeting during polymerization of alpha-olefins, US4803251 A, 1989.

[6] F.J. Karol, I.J. Levine, Preparation of low and medium density ethylene polymer in fluid bed reactor, US 4011382 A, 1977.

[7] F.J. Karol, C.S. Wu, Ethylene polymerization with silane modified catalyst, US4086408 A, 1978.

[8] R.J. Jorgensen, G.L. Goeke, F.J. Karol, Catalyst composition for copolymerizing ethylene, US4349648 A, 1982.

[9] A.R. Miller, Fluidized bed reactor, US4003712 A, 1977.

[10] B.E. Wagner, G.L. Goeke, F.J. Karol, Process for the preparation of high density ethylene polymers in fluid bed reactor, US4303771 A, 1981.

[11] D. Kunii, O. Levenspiel, Fluidization Engineering, illustrate, Butterworth-Heinemann, Oxiford, 1991.

[12] J.R. Grace, Fluidized bed hydrodynamics, in: G. Hetsoroni (Ed.), Handb. Multiph. Syst., Hemisphere, Washington, DC, 1982: p. Chapter 8.1.

[13] P. Cai, S.P. Chen, Y. Jin, Z.Q. Yu, Z.W. Wang, Effect of operating temperature and pressure on the transition from bubbling to turbulent fluidization, AIChE Symp. Ser. 85 (1989) 37–43.

[14] H.T. Bi, N. Ellis, I.A. Abba, J.R. Grace, A state-of-the-art review of gas-solid turbulent fluidization, Chem. Eng. Sci. 55 (2000) 4789–4825.

[15] N. Ellis, Hydrodynamics of gas-solid turbulent fluidized beds, The university of british columbia, 2003.

[16] J. Ciborowski, A. Wlodarski, On electrostatic effects in fluidized beds, Chem. Eng. Sci. 17 (1962) 23–32.

[17] M. Bafrnec, J. Bena, Quantitative data on the lowering of electrostatic charge in a

fluidized bed, Chem. Eng. Sci. 27 (1972) 1177–1181.

[18] J. Guardiola, G. Ramos, A. Romero, Electrostatic behaviour in binary dielectric/conductor fluidized beds, Powder Technol. 73 (1992) 11–19.

[19] J. Revel, C. Gatumel, J.A. Dodds, J. Taillet, Generation of static electricity during fluidisation of polyethylene and its elimination by air ionisation, Powder Technol. 135–136 (2003) 192–200.

[20] W.O. Moughrabiah, J.R. Grace, X.T. Bi, Effects of pressure, temperature, and gas velocity on electrostatics in gas-solid fluidized beds, Ind. Eng. Chem. Res. 48 (2009) 320–325.

[21] Z. Liu, X.T. Bi, J.R. Grace, Electrostatic charging behaviour of dielectric particles in a pressurized gas-solid fluidized bed, J. Electrostat. 68 (2010) 321–327.

[22] L. Yao, H.T. Bi, A.H. Park, Characterization of electrostatic charges in freely bubbling fluidized beds with dielectric particles, J. Electrostat. 56 (2002) 183–197.

[23] M. Murtomaa, E. Räsänen, J. Rantanen, A. Bailey, E. Laine, J.P. Mannermaa, J. Yliruusi, Electrostatic measurements on a miniaturized fluidized bed, J. Electrostat. 57 (2003) 91–106.

[24] T.A. Alsmari, J.R. Grace, X.T. Bi, Effects of superficial gas velocity and temperature on entrainment and electrostatics in gas-solid fluidized beds, Chem. Eng. Sci. 123 (2015) 49–56.

[25] A. Gajewski, Investigation of the electrification of polypropylene particles during the fluidization process, J. Electrostat. 17 (1985) 289–298.

[26] V. Rojo, J. Guardiola, A. Vian, A capacitor model to interpret the electric behaviour of fluidized beds. Influence of apparatus geometry, Chem. Eng. Sci. 41 (1986) 2171–2181.

[27] J. Guardiola, V. Rojo, G. Ramos, Influence of particle size, fluidization velocity and relative humidity on fluidized bed electrostatics, J. Electrostat. 37 (1996) 1–20.

[28] R.W. Ham, P.A. Gauthier, M.A. Bergougnou, Electrostatic in an air/catalyst fluidized bed at ambient temperature and pressure, Fluid. Eng. Found. New York. (1992) 611–620.

[29] S. Beret, J.M. Jenkins, T.M. Jones, R.L. Jones, Method for fluidized bed polymerization, US4588790 A, 1986.

[30] F. Salama, D. Song, P. Mehrani, Characterizing Electrostatic Charges in High-Pressure Gas-Solid Fluidized Beds: Experimental Design and Preliminary Results, in: 14th Int. Conf. Fluid. – From Fundam. to Prod., Netherland, 2013.

[31] D. Song, F. Salama, J. Matta, P. Mehrani, Implementation of Faraday Cup Electrostatic Charge Measurement Technique in High-Pressure Gas-Solid Fluidized Beds at Pilot-Scale, Powder Technol. 290 (2016) 21–26.

[32] J. Yerushalmi, N.T. Cankurt, Further studies of the regimes of fluidization, Powder

Technol. 24 (1979) 187–205.

[33] D. Song, P. Mehrani, Mechanism of particle build-up on gas-solid fluidization column wall due to electrostatic charge generation, Powder Technol. (2017).

[34] F. Salama, A. Sowinski, K. Atieh, P. Mehrani, Investigation of electrostatic charge distribution within the reactor wall fouling and bulk regions of a gas-solid fluidized bed, J. Electrostat. 71 (2013) 21–27.

Chapter 6
Mechanism of Particle Build-up on Gas-solid Fluidization Column Wall due to Electrostatic Charge Generation

Di Song, Poupak Mehrani*

Department of Chemical and Biological Engineering, University of Ottawa
161 Louis Pasteur st., Ottawa, Ontario, K1N-6N5, Canada
*poupak.mehrani@uottawa.ca; Tel: 1-613-562-5800 Ext 6098; Fax: 1-613-562-5172

The current chapter is a manuscript in press in the journal of Powder Technology "Powder Technology, in press, 2017"

Abstract

Particle build-up on gas-solid fluidization column wall due to electrostatic charging causes significant operational challenges including reactor shutdown in industrial processes such as gas-phase ethylene polymerization to produce polyethylene. It is well acknowledged that in fluidization process electrostatic charges are generated as a result of continuous particle-particle and particle-vessel wall contacts. However, the mechanism of charged particles attraction towards the fluidization column wall and their adhesion has received minimal attention. This work proposes a mechanism for particle build-up on the column wall by experimentally investigating the fouled particles charge distribution using a charged particle separator apparatus. The experiments were carried with two types of linear low-density polyethylene resins in a pressurized pilot-scale gas-solid fluidization system. Experimental results showed that the polyethylene layer built-up on the column wall contained both positively and negatively charged particles. A mechanism was proposed indicating that charged particles migration towards the metallic column wall is due to the image and electrostatic forces. The image forces are attributed to the particle-wall contacts. It was also found that electrostatic forces between the charged particles fouled on the column wall and those oppositely charged within the bulk of the bed, as well as those between the similarly charged particles in bulk, contributed to the formation of wall fouling.

Keywords: Electrostatics, Fluidizing particle charging, Reactor wall coating mechanism, Charge measurement

6.1 Introduction

Gas-solid fluidized beds have been widely employed in many industries such as petrochemical, oil and gas, food, etc. due to their excellent characteristics of providing a high degree of heat and mass transfer, and allowing for good mixing. In such systems, there is a potential for electrostatic charge generation due to continuous contacts between the particles and between the particles and the fluidization column wall. Bed electrification could then give rise to significant problems including fluidizing particle agglomeration and their build-up on the reactor wall and other surfaces. Such occurrences could have undesirable effects on the fluidized bed hydrodynamics or even necessitating reactor shutdown for clean-up. Gas-phase ethylene polymerization in gas-solid fluidized beds to produce polyethylene is an example of an industrial process where electrostatic charge generation is known to result in operational challenges. In this process, charged particles, including catalyst and polyethylene resin, adhere to the reactor wall and dome, and form sheets of fused particles. This phenomenon is referred to as "sheeting" [1]. As the sheets grow thicker, they dislodge from the reactor wall and fall to block the distributor plate, imposing frequent reactor shutdown for clean-up. This in turn causes significant economic losses for the industry.

Although a few works have been reported in literature in relation to detecting the occurrence of electrostatic charge build up within this type of reactors, the problem still persists [1-5]. This is due to the complex nature of gas-solid fluidization process, and more importantly, the lack of a comprehensive understanding of the underlying mechanism of electrostatic charge generation, as well as fouling of charged particles on the fluidized bed walls. The majority of works reported in this area have focused on evaluating the effect of various operating parameters (e.g., fluidization time, particle and gas properties, operating pressure, etc.) on the degree of electrostatic charge generation [6-13]. However, to the author's knowledge, the mechanism of particle migration and wall fouling in gas-solid fluidized beds has not been discussed in literature. Thus, the aim of this work is to suggest a mechanism for particle build-up on the fluidization column wall. The proposed mechanism is supported by experimental work carried out in a pilot-scale gas-solid fluidized bed where the electrostatic charge distribution of particles fouled on the column wall were determined and evaluated at various operating conditions.

6.2 Experimental setup and method

A pilot plant pressurized gas-solid fluidization system previously designed and commissioned by the same research group was used for this work. The details of the fluidization system are presented elsewhere [6,10]. The system contained a three dimensional stainless steel fluidization column, 0.15 m in diameter, which housed two online Faraday cups in its top and bottom expanded sections. Both Faraday cups were connected to digital electrometers (Keithley model 6514) and enabled particles charge measurement. A filter bag was placed in the top Faraday cup in order to capture the entrained fines and to allow their cumulative charge measurement. The discharge of the fluidizing particles into the bottom Faraday cup for their charge measurement was enabled by the distributor plate which was a modified knife-gate valve.

Experiments were conducted in the bubbling flow regime and at various operating pressures ranging from atmospheric to 2600 kPa (abs). The highest operating pressure was similar to operating pressure of a commercial gas-phase polyethylene process. Minimum fluidization velocity was measured for each operating pressure, and the fluidizing gas velocity was set at 1.5 times the minimum fluidization velocity for all experiments. Compressed building air and nitrogen gas from a gas cylinder were used as sources of fluidizing gas at atmospheric and high-pressure conditions, respectively. The fluidizing gas was at 0 RH% and 25°C for all trials. For experiments conducted at high pressures, the system was first pressurized to the desired pressure and then a centrifugal compressor with a variable speed drive enabled the circulation of the gas within the system at the desired flow rate.

Two types of linear low-density polyethylene (LLDPE) resin, PE_A and PE_B, directly received from commercial reactors, were fluidized in this work. The properties of the two resins are summarized in Table 6.1. More information anout the two resins is shown in Appendix D.2.1. For all experiments, 3.2 kg of particles were placed into the fluidization column. PE_A resin was fluidized at 1600 and 2600 kPa while PE_B resin was fluidized at atmospheric and 400 kPa. Minimum fluidization velocities for each operating condition, which were obtained with bed pressure drop measurements at various superficial gas velocity, are presented in Table 6.2.

Table 6.1: Properties of polyethylene particles used in this work.

	Particle Density (kg/m^3)	**Particle Size and Mass Distribution** (wt%)			**Average Particle Size** (µm)	**Geldart Group** (-)
		< 500 µm	**500 – 700 µm**	**> 710 µm**		
PE_A	918	26.44	28.54	45.02	560	B
PE_B	915	34.03	35.22	30.75	573	B

Table 6.2: Minimum fluidization velocities under various operating pressures.

Operating Pressures (kPa)	**Minimum Fluidization Velocity (m/s)**	
	PE_A	**PE_B**
101	N/A	0.15
400	N/A	0.12
1600	0.1	N/A
2600	0.08	N/A

In each experiment, as received particles (referred to as "initial" or "initial particles") were placed in the fluidization column after measuring their mass and net charge. During fluidization, the entrained particles were captured by the filter bag and their cumulative charge was measured by the top Faraday cup. Upon the completion of 60 min of fluidization, the system was depressurized, the top of the column was opened, and the filter bag was removed to measure the mass of entrained particles (referred to as "fines" or "fine particles"). The distributor plate was then opened allowing particles in bulk of the bed (referred to as "bulk" or "bulk particles") to drop into the bottom Faraday cup to measure their net charge. The bottom Faraday cup was then removed to measure the mass of the bulk particles. After visually inspecting the inner column wall for any particle fouling, the cleaned bottom Faraday cup was placed back to collect and measure the net charge of these particles (referred to as "wall" or "wall particles"). Compressed building air was passed through a long tube inserted from the top of the column in order to dislodge the wall particles from the column wall into the bottom Faraday cup. For all experiments, samples of initial, bulk, wall, and fines were collected and analyzed for particle size distribution by a Malvern Mastersizer 2000 particle size analyzer. In this work, fluidization of both polyethylene resins resulted in a negligible amount of entrainment and thus no results have been presented for the fines. All experiments were conducted 3 times to ensure the reproducibility of the results.

In a typical experiment, the wall particles electrostatic charge was measured by the bottom Faraday cup (Figure 6.1a). However, such method only enables the measurement of the net charge of particles accumulated on the column wall. In order to investigate the electrostatic charge distribution of these particles, a charged particle separator (CPS), previously designed and built by the same research group [14], was employed. As presented in Figure 6.1b, after removing the bottom Faraday cup containing the bulk particles, the charged particle separator apparatus was placed beneath the fluidization column. The charged particle separator contained two copper plates at the top section and four Faraday cups at the bottom. One of the copper plates was connected to a high voltage power supply (Ultravolt HV Rack Model 1-250-00265) with voltage of 36 kV and charged positively. The other plate was grounded and acted as a negatively charged plate. Each Faraday cup was connected to a digital electrometer (Keithley model 6514) to measure the net charge of particles inside. As the particles slowly dislodge from the column wall and drop into the charged particle separator, positively and negatively charged particles are separated and settle in the four Faraday cups at the bottom of the separator. Faraday cups number 1 and 4 (FC1 and FC4) collect the highly negatively and positively charged particles, respectively. The four electrometers were connected to a computer, and LabView software was used for data collection.

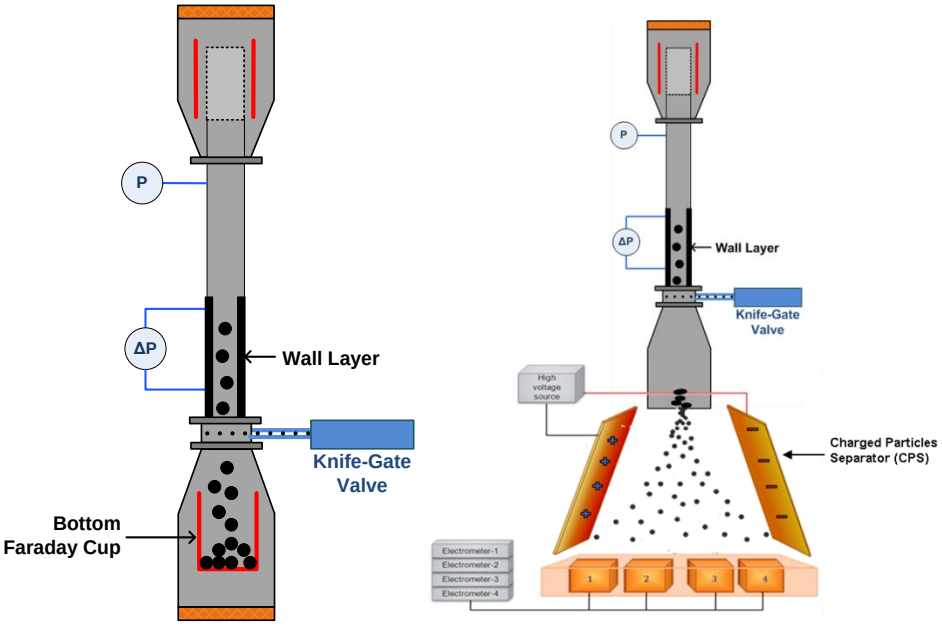

(a) (b)

Figure 6.1: Collecting the wall particles with (a) the bottom Faraday cup; and (b) the charged particle separator apparatus.

6.3 Results and discussion

For all experimental trials, the net specific charge (*q/m*) of initial particles was found to be small with a range of -0.05 to 0.05 µC/kg. After the completion of the fluidization period, more than 90% of initial particles remained in the bulk of the bed. The net specific charges of bulk particles had a range of 0.12 – 0.35 µC/kg.

6.3.1 Wall particles properties

Upon the removal of the bulk particles, the inner column wall was inspected from the bottom for any degree of particle fouling. Figure 6.2 presents examples of images obtained from the fluidization vessel inner wall before and after PE resin build up (white layer seen in the image). As can be seen in Figure 6.3, less than 6% of initial particles adhered on the column wall during fluidization. Figure 6.4 presents the net specific charges of wall particles out of the initial particles after fluidization. Results show that, after one hour of fluidization, the particles net charge was positive for both resins tested and at various pressures.

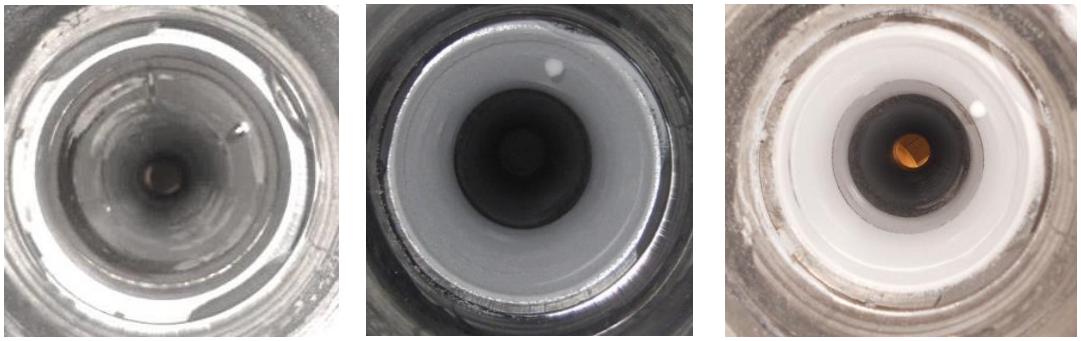

(a) (b) (c)

Figure 6.2: Typical images of the inner column wall, (a) before the fluidization; (b) after fluidization of PE_A particles; and (c) after the fluidization of PE_B particles.

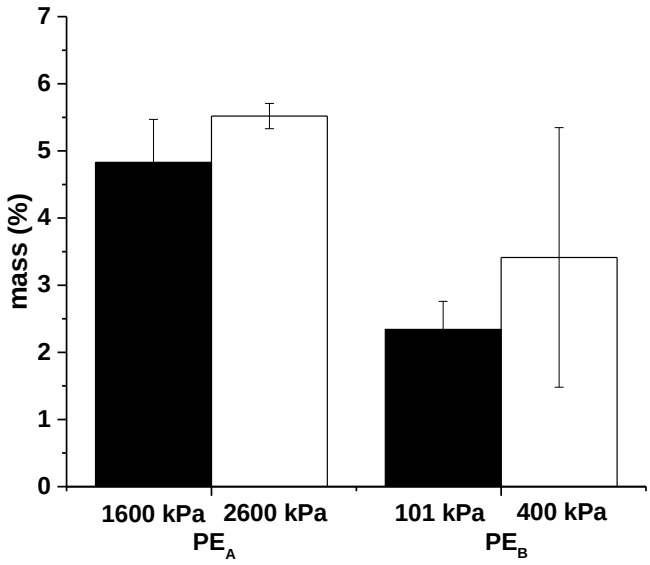

Figure 6.3: Mass percentages of PE_A and PE_B wall particles at various pressures.

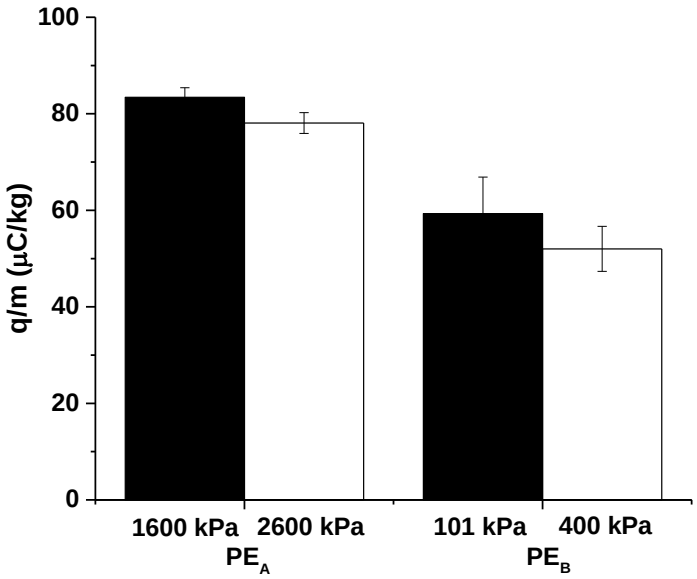

Figure 6.4: Net specific charge (*q/m*) of PE_A and PE_B wall particles at various pressures.

Similar runs were then carried out except that the charge distributions of the wall particles were measured by using the CPS unit. Results are presented in Figures 6.5 and 6.6 for mass percentage (*m%*), net specific charge (*q/m*), and the mean size (dp_{50}) of particles collected in the four Faraday cups of the CPS unit. For both types of polyethylene resin, the results indicated that particles fouled on the column wall contained both positively and negatively charged particles, although the majority of particles were positively charged. Negatively charged particles collected in FC1 and FC2 were slightly smaller than the positively charged particles settled in FC3 and FC4. This implied the existence of the size dependence of bipolar charging phenomena in gas-solid fluidization processes. "Bipolar" charging is a unique and important phenomenon observed in granular systems. Researchers have noticed that in contact charging of granules made of identical material, but having different sizes, particles tend to be charged oppositely. A number of authors [15-18] have reported that in bipolar charging, the smaller particles charge negatively and larger particles charge positively. Although, contradicting results have also been obtained by others [7,9,13,19,20].

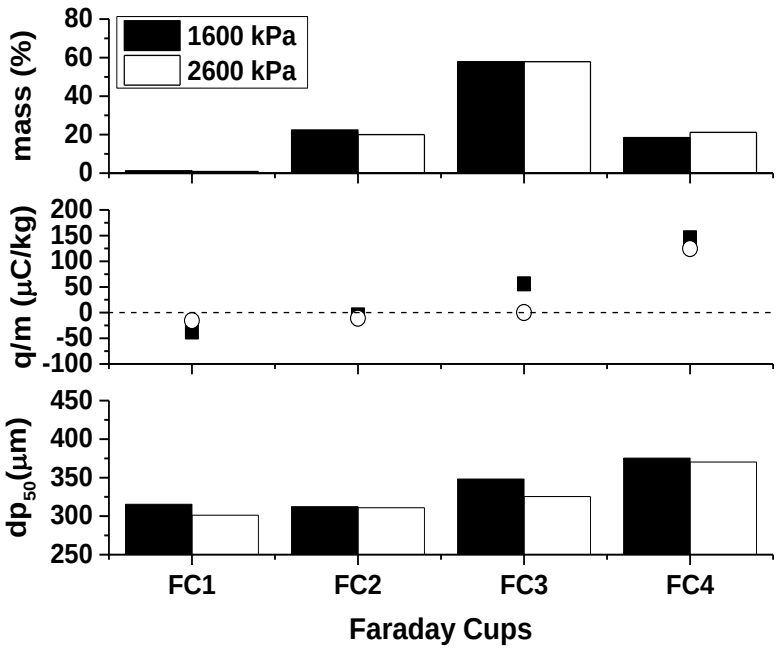

Figure 6.5: Electrostatic charge distribution of PE_A wall particles measured using the CPS unit after one hour of fluidization.

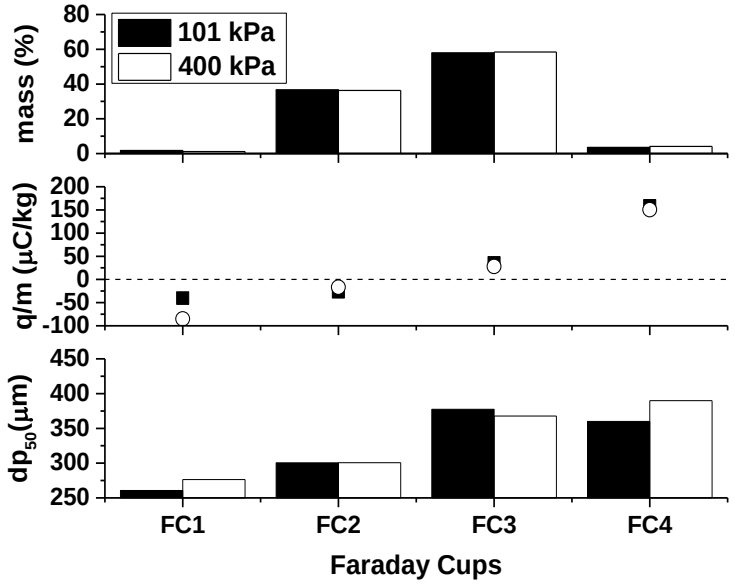

Figure 6.6: Electrostatic charge distribution of PE_B wall particles measured using the CPS unit after one hour of fluidization.

It is important to note that in all experiments, after removing the particles that could be dislodged from the column wall by using a stream of air, it was observed that a thin layer of particles remained on the column wall closer to the top of the column. These particles were dust-like with very small particle size and highly charged. It was attempted to collect these particles in the

bottom Faraday cup with the same method, however the mass collected was quite negligible. The particle charge polarity was found to be negative in all cases. Due to their negligible mass, their properties including *q/m* and particle size were not measured. Overall, after 60 min of fluidization, the net charges of the bulk and wall particles were found to be positive, while those of the dust-like wall particles were negative.

6.3.2 Mechanism of particle build-up on the column wall

According to the results, which indicate that particles fouled on the fluidization column wall composed of both positively and negatively charged particles, a mechanism for particle migration within the bed and the formation of a coating on the fluidization column wall is proposed. In the case of fluidization with negligible entrainment, the net specific charge generated within the bed is primarily the result of the contacts between fluidizing particles and the column wall because the net charge due to particle-particle contacts would be zero (Figure 6.7a). On the other hand, when entrainment is present, due to the departure of some of the charged particles, both the particle-particle and particle-wall contacts contribute to the net charge of the bed. In the present study, no entrainment was detected and thus only the particle-wall contacts were considered. When particles continuously contact with the column wall, due to the work function difference between the two materials (approximately 4.5 eV for steel and 5.3 eV for polyethylene [21]), it was found that the polyethylene particles are oppositely charged to the wall. For instance, in this work polyethylene resin and the column wall are negatively and positively charged, respectively. Since the fluidization column is made of a conductive material (stainless steel), the negatively charged particles in the bulk of the bed are being attracted towards the fluidization column wall due to image forces and deposit on the wall (Figure 6.7b). Then, the negatively charged wall layer would attract positively charged particles from the bulk of the bed while repelling the negatively charged particles due to electrostatic force. Moreover, the net positively charged bulk particles would create a field that repels some of the positive particles in the bulk of the bed towards the column wall. Therefore, some of the positively charged particles in bulk foul on the column wall and form a subsequent layer (Figure 6.7c). The polarity and the magnitude of the second and the subsequent layers would depend on the balance between the image and electrostatic forces. It is however important to note that the drag and gravitational forces also exist during the fluidization process which could dominate over the

image and electrostatic forces and consequently prevent or disturb the build-up of the charged particles on the column wall.

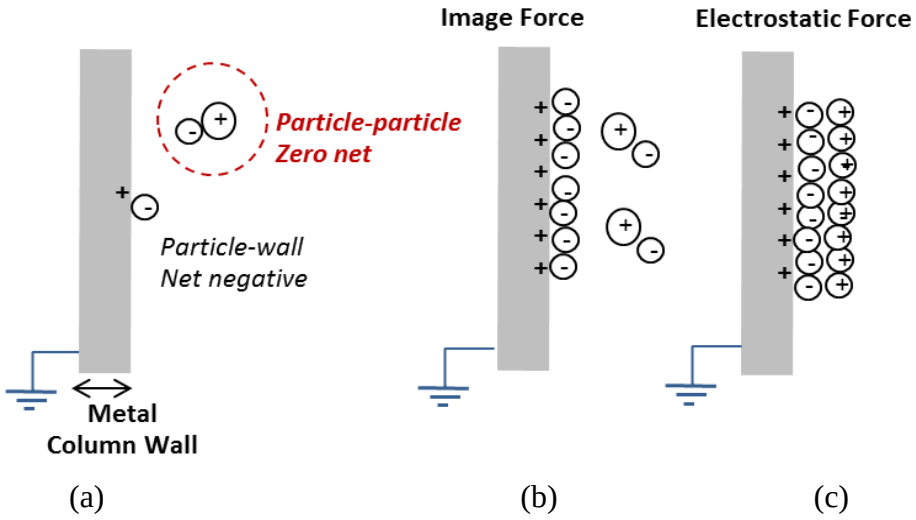

Figure 6.7: The proposed wall coating formation mechanism.

The proposed mechanism of particle build-up indicates that both image and electrostatic forces would result in migration of the charged fluidizing particles towards the column wall and consequently the formation of a coating. Since image charge is found to have a significant contribution in particle wall coating formation, the material of fluidization column should be considered as an influential parameter. In the case of the system presented in this work, fluidization was carried out in a batch operation meaning that the image and electrostatic forces were generated within the bed due to particle-particle and particle-wall contacts throughout the fluidization period. However, it is important to recognize that in the case of commercial processes such as that of polyethylene production, the reactor is operated in a continuous mode where the catalyst particles are continuously being conveyed into the fluidized bed reactor and could carry a charge with them. These charged particles would then result in the formation of image forces between the column wall and the particles in bed. In a previous work, Sowinski and Mehrani [22] examined the influence of the addition of a metallocene catalyst and its silica support on the degree of polyethylene particles fouling on a fluidized bed reactor wall. The catalyst and silica powders were injected into the fluidized bed through a 6.35 mm (1/4 inch) stainless steel tube which approximately simulated the catalyst injection process in commercial polyethylene reactors. Their work concluded that the powders gained a significant specific charge during their pneumatic conveying which then resulted in an increase in the magnitude of

reactor wall coating in comparison to the case where no powder was injected. Thus, it is critical to consider the influence of the pneumatic conveying of catalyst particles in narrow tubes which could certainly generate electrostatic charge and consequently create image forces as these charged particles enter the reactor. Therefore, the image and electrostatic forces can either be generated within the bed during fluidization of polyethylene and the catalyst particles, or the image force could be created as the charged catalyst particles enter the fluidized bed reactor. For that reason, it is important to determine the governing forces in real reactors which result in the formation of reactor wall sheeting.

6.4 Conclusions

The electrostatic charge distribution of polyethylene particles fouled on the vessel walls of a gas-solid fluidized bed was investigated in this work. Experiments were conducted in a pressurized pilot-scale gas-solid fluidization system equipped with a charged particle separator apparatus. Results showed that, although the net specific charge of particles that build-up on the vessel wall for all operating conditions was positive, the layer contained both positively and negatively charged particles. A mechanism was then proposed for the charged particles migration within the fluidized bed which was found to be due to both image and electrostatic forces generated within the bed. The combination of both forces contributed to the attraction of charged polyethylene particles towards the fluidized bed conductive walls. It was suggested that in commercial reactors, the image forces can also be created as the charged catalyst particles are pneumatically conveyed into the reactor and thus further contributing to the formation of a wall coating.

Acknowledgement:

The input and financial support from Univation Technologies LLC (Texas, USA), and the financial assistance from the Natural Sciences and Engineering Research Council of Canada (NSERC) are acknowledged with gratitude.

References

[1] G. Hendrickson, Electrostatics and gas phase fluidized bed polymerization reactor wall sheeting, Chem. Eng. Sci. 61 (2006) 1041-1064.

[2] M.G. Goode, F.D. Hussein, K.H. Lee, T.J. McNeil, C.C. Williams, Static control in olefin

polymerization, US 6111034 A (2000).

[3] R.O. Hagerty, M.E. Muhle, A.K. Agapiou, C. Kuo, M.G. Goode, F.D. Hussein, R.B. Pannell, J.F. Szul, Method for controlling sheeting in gas phase reactors, US 7985811 B2 (2011).

[4] G.H. Song, A.S. Rhee, G.R. Lowder, Method for reducing sheeting and static charges during polymerization of ethylene polymers, US 5391657 A (1995).

[5] M.G. Goode, D.M. Hasenberg, T.J. McNeil, T.E. Spriggs, Method for reducing sheeting during polymerization of alpha-olefins, US 4803251 A (1989).

[6] D. Song, F. Salama, J. Matta, P. Mehrani, Implementation of Faraday cup electrostatic charge measurement technique in high-pressure gas-solid fluidized beds at pilot-scale, Powder Technol. 290 (2015) 21-26.

[7] A. Giffin, P. Mehrani, Comparison of influence of fluidization time on electrostatic charge build-up in the bubbling vs. slugging flow regimes in gas-solid fluidized beds, J. Electrostatics 68 (2010) 492-502.

[8] Y. Tian, P. Mehrani, Effect of particle size in fluidization of polyethylene particle mixtures on the extent of bed electrification and wall coating, J. Electrostatics (2015).

[9] A. Sowinski, A. Mayne, P. Mehrani, Effect of fluidizing particle size on electrostatic charge generation and reactor wall fouling in gas-solid fluidized beds, Chem. Eng. Sci. 71 (2012) 552-563.

[10] F. Salama, D. Song, P. Mehrani, Characterizing electrostatic charges in high-pressure gas-solid fluidized beds: experimental design and preliminary results, Proceeding of The 14th International Conference on Fluidization (2013).

[11] W.O. Moughrabiah, J.R. Grace, X.T. Bi, Effects of pressure, temperature, and gas velocity on electrostatics in gas-solid fluidized beds, Ind. Eng. Chem. Res. 48 (2009) 320-325.

[12] W.O. Moughrabiah, J.R. Grace, X.T. Bi, Electrostatics in gas-solid fluidized beds for different particle properties, Chem. Eng. Sci. 75 (2012) 198-208.

[13] Z. Liu, X.T. Bi, J.R. Grace, Electrostatic charging behaviour of dielectric particles in a pressurized gas-solid fluidized bed, J. Electrostatics. 68 (2010) 321-327.

[14] F. Salama, A. Sowinski, K. Atieh, P. Mehrani, Investigation of electrostatic charge distribution within the reactor wall fouling and bulk regions of a gas-solid fluidized bed, J. Electrostatics. 71 (2013) 21-27.

[15] P. Cartwright, S. Singh, A.G. Bailey, L.J. Rose, Electrostatic charging characteristics of polyethylene powder during pneumatic conveying, IEEE Trans. Ind. Appl. IA-21 (1985) 541-546.

[16] K.M. Forward, D.J. Lacks, R.M. Sankaran, Triboelectric charging of granular insulator mixtures due solely to particle-particle interactions, Ind. Eng. Chem. Res. 48 (2009) 2309-2314.

[17] F. Sharmene Ali, M. Adnan Ali, R. Ayesha Ali, I.I. Inculet, Minority charge separation in falling particles with bipolar charge, J. Electrostatics. 45 (1998) 139-155.

[18] H. Zhao, G.S.P. Castle, I.I. Inculet, A.G. Bailey, Bipolar charging of poly-disperse polymer powders in fluidized beds, IEEE Trans. Ind. Appl. 39 (2003) 612-618.

[19] P. Mehrani, H.T. Bi, J.R. Grace, Electrostatic charge generation in gas-solid fluidized beds, J. Electrostatics. 63 (2005) 165-173.

[20] A. Sowinski, L. Miller, P. Mehrani, Investigation of electrostatic charge distribution in gas-solid fluidized beds, Chem. Eng. Sci. 65 (2010) 2771-2781.

[21] H. Masuda, K. Gotoh, K. Higashitani, S. Matsusaka, Adhesive force of a single particle, Powder Technology Handbook. Third Edition. (2006) CRC Press. Florida.

[22] A. Sowinski, P. Mehrani, Impact of addition of a catalyst or its support on reactor wall coating due to electrostatic charging during fluidization of polyethylene, Ind. Eng. Chem. Res. 54 (2015) 3981-3988.

Chapter 7
Conclusions and Recommendations

To find means to eliminate or minimize the generation of electrostatic charges in commercial gas-solid fluidized beds, it is vital to understand the underlying mechanisms of particles charging and to identify the contributing factors in such systems. To achieve this goal it is essential to carry out the electrostatic studies under industrially relevant operating conditions. Therefore, the aim of this thesis was to study the fluidized bed electrification at operating conditions similar to the commercial polyethylene reactors, a process that has been greatly impacted by operational challenges caused by electrostatics.

A pilot-scale pressurized gas-solid fluidization system was designed and built that was capable of operating at high pressures (up to 2600 kPa) and temperatures (up to 100°C), and gas velocities up to 1 m/s representing the turbulent flow regime. This new system successfully implemented an existing online electrostatic charge measurement technique consisting of two online Faraday cups that allowed the measurements of particles mass, net charge and size distribution in various regions of the fluidization system, especially those of the wall coating. This system for the first time permitted the study of the extent of fluidizing particles coating the reactor wall under the industrially relevant operating conditions. Utilizing instruments including an optical fiber probe and a differential pressure transducer, the fluidization system also enabled the investigation of bed hydrodynamics (i.e., bubble dynamics) at various operating conditions to determine their influence on the degree of bed electrification and particle wall fouling.

The system consisted of a three-dimensional gas-solid fluidization column made of stainless steel, 0.154 m in diameter and 4.5 m in total height, with a 2.5 m fluidization section. The fluidization column housed two Faraday cups located at the top and bottom of the column where the grounded top and bottom expanded sections acted as the outer cups. A filter bag was mounted at the top of the fluidized bed, inside the top inner Faraday cup, to capture the entrained particles and allowing the measurement of the net charge of these particles. A pneumatic knife gate valve was used as the distributor plate where its blade was modified to act as a perforated plate. The valve permitted the particles within the bed to be dislodged into the bottom Faraday cup for their charge to be measured without any particle handling. Due to the system's elevated

operating pressures and its scale, a mechanism was required to permit convenient access to the two Faraday ups. This was achieved in a unique way by the placement of two manways at the top and the bottom of the fluidization column.

The pilot plant facility was successfully operated where experiments were carried out to investigate the effect of operating pressure and gas velocity including the transition to turbulent flow regime on the degree of electrostatic charge generation and the extent of particle wall fouling. Linear low-density polyethylene resin directly received from commercial reactors was used for all experiments. The net charge, mass, and particle size distribution of particles settled on the column wall and in the bulk of the bed, as well as those entrained from the top of the column were measured.

For all operating conditions tested, particle wall coating was observed where the coating extended to the whole column wall, from the distributor plate to the outlet of the column. The particle coating consisted of two layers, one thicker layer at the bottom of the column extending to approximately 1 m above the distributor plate, and a second thinner layer extending to the column outlet. Bipolar charging was detected in all experiment where smaller particles tended to be negatively charged and larger particles were more likely to be positively charged.

The bed hydrodynamics were found to be significantly influenced by the elevation of operating pressure and gas velocity. The average gas bubble size and frequency were determined at 0.4 m above the distributor plate, and at the center and near the column wall. The increase in the operating pressure from atmospheric to 2600 kPa gave rise to the decline in the average gas bubble size and the increase of the frequency of smaller bubblies. This in turn resulted in more particle-particle contacts within the bed at the elevated pressures (i.e., generation of more bipolar charging), causing a larger amount of wall fouling. In contrast, the presence of larger gas bubbles and their higher frequency at the atmospheric condition was linked to more particle-wall contacts and thus the generation of more negatively charged particles in the bed. Overall, double amount of wall particles was collected by elevating the pressure to even 600 kPa, but further increase in pressure did not influence the amount of fouling.

Influence of gas velocity was examined when the system was operated at 1, 3, and 5 U_{mf} (pre-turbulent flow regime), and 7.5 U_{mf} (turbulent flow regime). Higher electrostatic charge generation was observed as the fluidizing gas velocity was increased which was attributed to the

increase in particle-particle and particle-wall contactsin the bed. The degree of wall fouling increased almost linearly with the gas velocity. The amount of fouling was approximately five times larger in turbulent flow regime (7.5 U_{mf}) in comparison to that for the lowest gas velocity examined in bubbling flow regime (1.5 U_{mf}). Increasing the fluidizing gas velocity improved the particle-wall contacts; and thus, the net charge of the in-bed particles was more negative. One the other hand, the larger net negative charge of entrained fines influenced the net charge of particles left in the bed. Both mechanisms contributor to the elevation of particle wall fouling.

Particles with sizes smaller than 400 μm were found to be more prone to foul on the column wall. The average particle size of the bottom wall layer increased with the increase of operating pressure and fluidizing gas velocity, as well as when the bed transitioned to turbulent flow regime. The particles size in the top wall layer did not vary much with the increase of operating pressure. However, it increased with the increase of gas velocity with a peak reached at 300 μm.

A possible mechanism for charged particles migration toward the column wall and their fouling was proposed. During gas-solid fluidization, particles continuously contact with each other and with the metallic column wall. In the case of fluidization with negligible entrainment, the net specific charge generated within the bed is primarily the result of the contacts between fluidizing particles and the column wall because the net charge due to particle-particle contacts would be zero. On the other hand, when entrainment is present, due to the departure of some of the charged particles, both the particle-particle and particle-wall contacts contribute to the net charge of the bed. The extent of the charged particles adherence to the column wall is influenced by the balance between the gravitational, drag, image and Column forces. The image force is formed between the charged particles and the conductive fluidization column wall. While the attractive Coulomb force is created between the charged particles accumulated on the column wall and those oppositely charged within the bulk of the bed. In the cases with entrainment, the exit of the charged fine particles leaves a net charge behind in the bulk, thus affecting the degree of image forces.

Overall, the results obtained in this work emphasized that the bed hydrodynamics, which are affected by operating conditions, considerably influenced the degree of electrostatitic charging and particles wall fouling during gas-solid fluidization processes. In addition,the particles migration and wall adherence mechanism proposed in this work signified the importance of

image force in the formation of particle wall coating in gas-solid fluidized beds. Thus, it was also suggested that in commercial reactors, the role of image forces should further be investigated since they can also be created as the charged catalyst particles are pneumatically conveyed into the reactor and thus could further be contributing to the formation of a wall coating.

7.1 Recommendations for future work

The pilot-scale pressurized gas-solid fluidization system built and operated in this work provides an excellent experimental facility to advance the research in the area of bed electrification. Thus, the following recommendations are proposed for future work:

a) In this research, all experiments were carried out at ambient temperature, 25°C. However, commercial polyethylene reactors operate at temperatures close to 80 – 110°C. Thus, it will be beneficial to study the effect of operating temperature on the degree of electrostatic charge generation.

b) In commercial UNIPOL^{TM} process, catalyst particles are pneumatically transported into the fluidized bed reactor. Thus, the catalyst particles might become highly charged during the conveying process; and thus, influencing the degree of the image forces within the bed. This consecutively could affect the degree of wall fouling. The effect of this parameter that has not been examined before can be tested in this system.

c) In this thesis, all fluidization trials were conducted with only polyethylene resin. However, in commercial processes both polyethylene and catalyst particles are present within the reactor at any given time. It is of great importance to determine the effect of presence of catalyst on the degree of bed electrification and wall coating. This parameter has not been studied before.

d) Limited number of experiments was performed by Sowinski *et al.* [1] at atmospheric condition and in bubbling flow regime to investigate the impact of adding antistatic additives on particle wall coting. This study could be repeated in the new system at operating conditions close to those of the commercial reactors to better understand the role of antistatic agents.

References

[1] A. Sowinski, P. Mehrani, Impact of addition of a catalyst or its support on reactor wall coating due to electrostatic charging during fluidization of polyethylene, Ind. Eng. Chem. Res. 54 (2015) 3981–3988.

Appendix A
Analysis of optical fiber probe data

The optical fiber probe employed in this thesis converted the intensity of light into voltage signals. Thus, dense phase in bed resulted in relatively high voltage, whereas bubble phase passing by created peaks to negative direction. An example of the signal obtained from the probe is shown in Figure A.1.

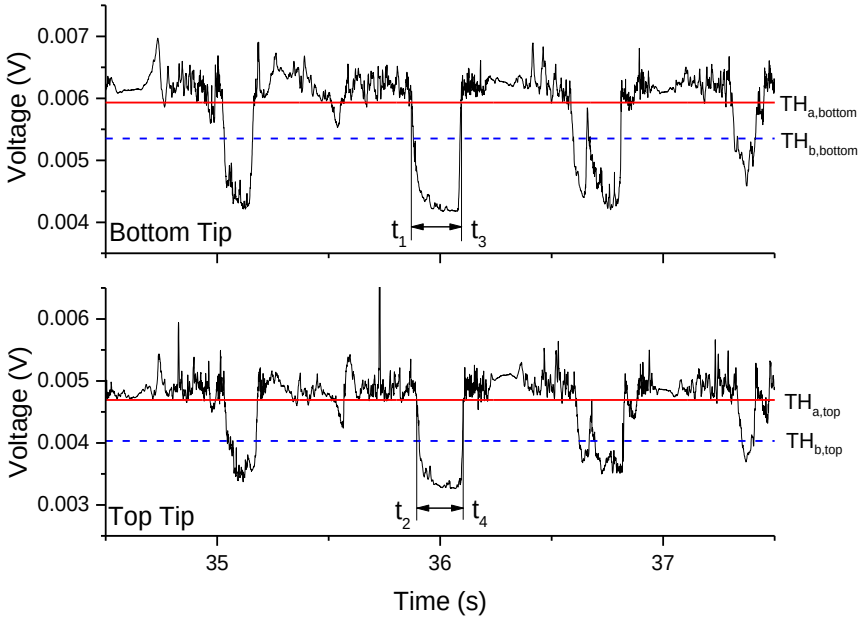

Figure A.1: Sample of voltage signals obtained from the bottom and top tips of the optical fiber probe with thresholds TH_a and TH_b.

In order to detect bubbles from the voltage signals, an algorithm was developed in-house based on the methods reported by Liu *et al*. [1] and Ruedisueli *et al*. [2]. As shown in Figure A.1 two thresholds, TH_a and TH_b were defined. TH_a was defined to indicate the starting and ending points of the signal representing the passage of the bubbles. TH_b was an indication whether a sudden decrease of signal indeed represents a local bubble passage. Sudden decreases of signal would be ascribed as bubbles only when they passed both TH_a and TH_b criteria. When a bubble passed the probe, t_1 and t_2 represented the times when the nose of the bubble reached the probe bottom and top tips, respectively, while t_3 and t_4 were the times when the bubble wake left the two probe tips. It is clear that the period spent by a bubble passing bottom and top tip were (t_3- t_1) and (t_4-

t_2), respectively. Thus, the bubble rise velocity (U_b) and bubble diameter (d_b) could be calculated by

$$U_b = \frac{D_p}{\frac{(t_2 - t_1) + (t_4 - t_3)}{2}} \quad [A.1]$$

$$d_b = U_b(t_3 - t_1) \quad [A.2]$$

where D_p is the center-to-center distance of the two tips of the optical fiber probe. Evaluation of the voltage signals showed that the signals of dense phase from the top tip were noisier that those for the bottom tip. Thus, in this work, the bubble vertical chord length was calculated from the the bottom tip signal.

Due to the fact that bubbles might split or not travel vertically as they pass the two tips of the probe, an algorithm was developed to correctly link the signals. In other words, it was necessary in decide if two paired signals described the same bubble passing through both the bottom and the top tip. Bubbles from different tips could be only considered as linked bubbles when would they satisfy all of the following criterions:

$$t_1 < t_2 \quad [A.3]$$

$$t_3 < t_4 \quad [A.4]$$

$$0 < t_2 - t_1 < 0.1 \quad [A.5]$$

$$0 < t_4 - t_3 < 0.1 \quad [A.6]$$

Different methods are proposed in literature to define TH_a and TH_b[3,4]. In this work, an approach reported by Ruedisueli *et al*. [2] was applied:

$$TH_i = q_{99} - i; \quad i = a, b \quad [A.7]$$

where q_{99} was the 99%-quantile of the the data in one trial. Upon evaluation of the signals and trying different values of *a* and *b*, *they* were set to 0 and 15% of the mean values of the signals.

A LabView program was developed to analyze the data obtained from the probe based on the mechanism introduced above. After importing a set of raw data into the program, the program recognized all the bubbles from the top and the bottom tips according to TH_a and TH_b values. Then the linked bubbles were determined based on Equations A.3 to A.6. In the end, the program calculated the bubble rise velocities and chord lengths using Equation A.1 and A.2.

Appendix B
Electrostatic charge measurement techniques

This section shows examples of Faraday cup and electrostatic probe applied to gas-solid fluidized bed in works found the literature.

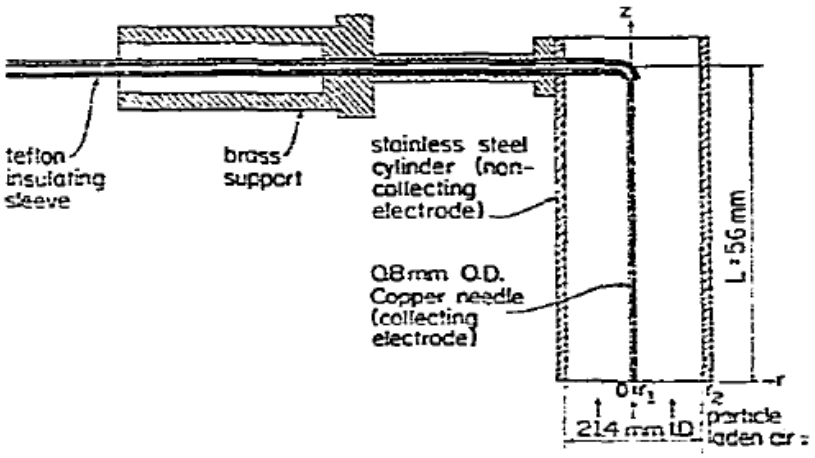

(a)

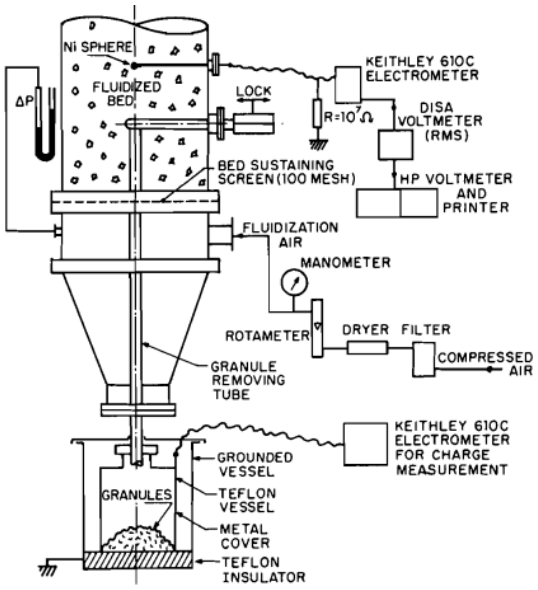

(b)

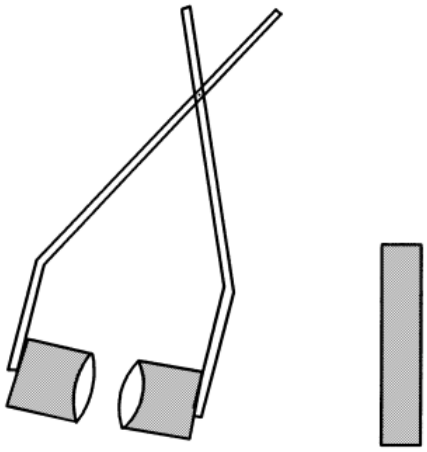

(c)

Figure B.1: Faraday cup techniques used in previous works: (a) particles removal using a vacuum pump [5]; (b) placing sampling ports with locking mechanism along the column wall [6]; (c) removing particles with a scooper after the completion of fluidization proces [7].

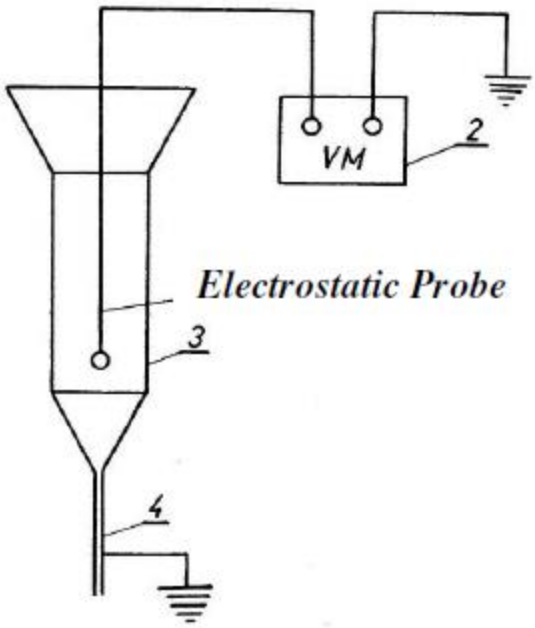

(a)

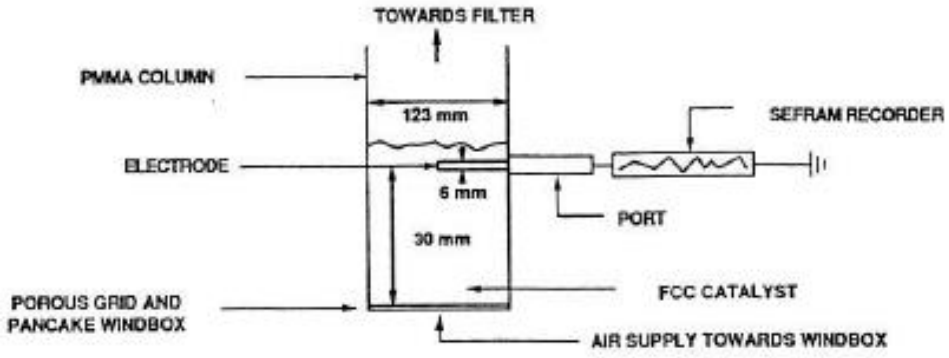

(b)

Figure B.2: Examples of electrostatic probes: (a) vertical probe [8]; (b) horizontal probe [9].

Appendix C
Experimental apparatus

This section presententsthe pilot-scale pressurized gas-solid fluidization system as well as the charged particle separator unit.

C.1 Pictures of the pilot-scale pressurized gas-solid fluidization system

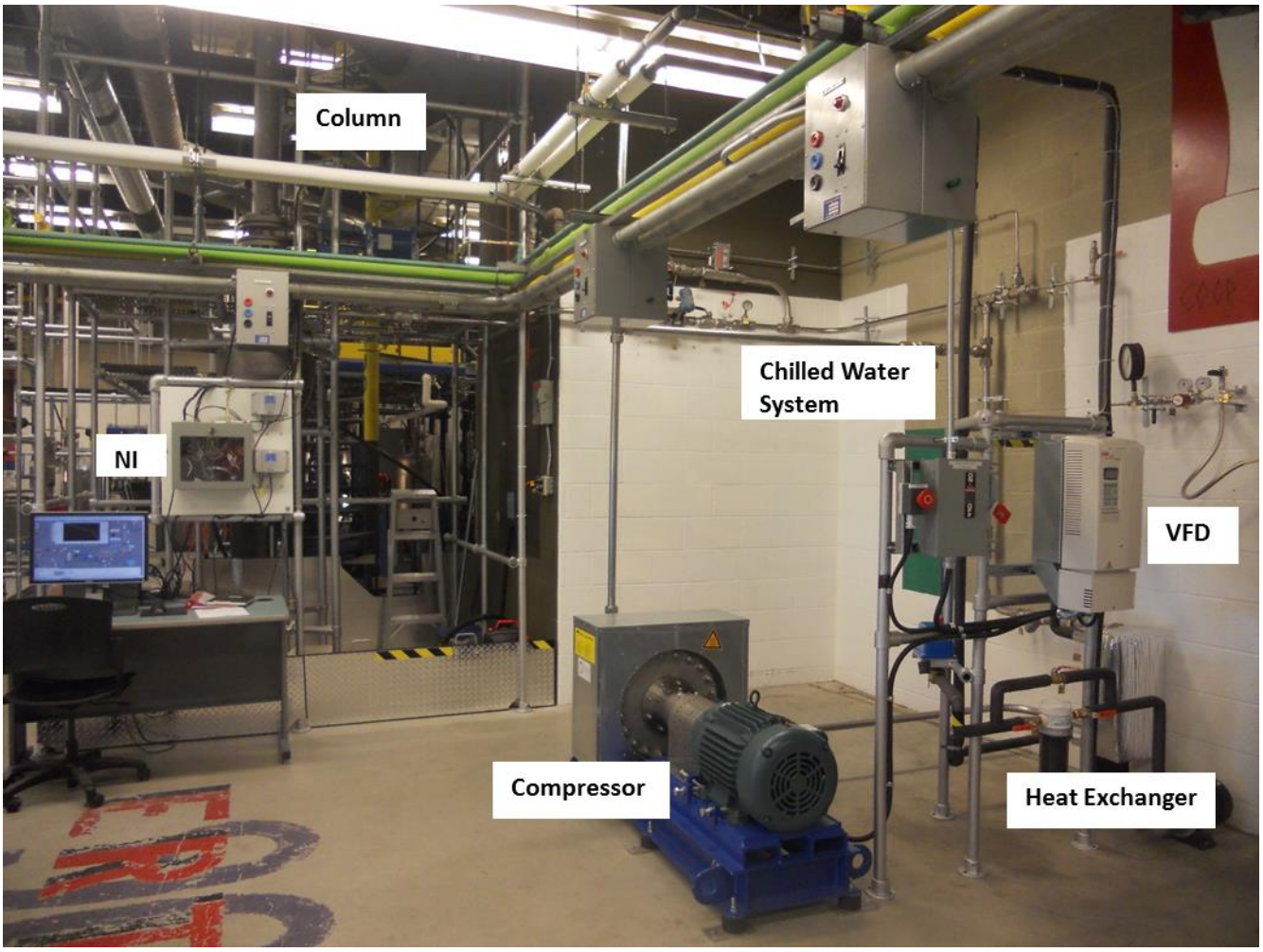

Figure C.1: Picture of pilot-scale high pressure gas-solid fluidization system laboratory.

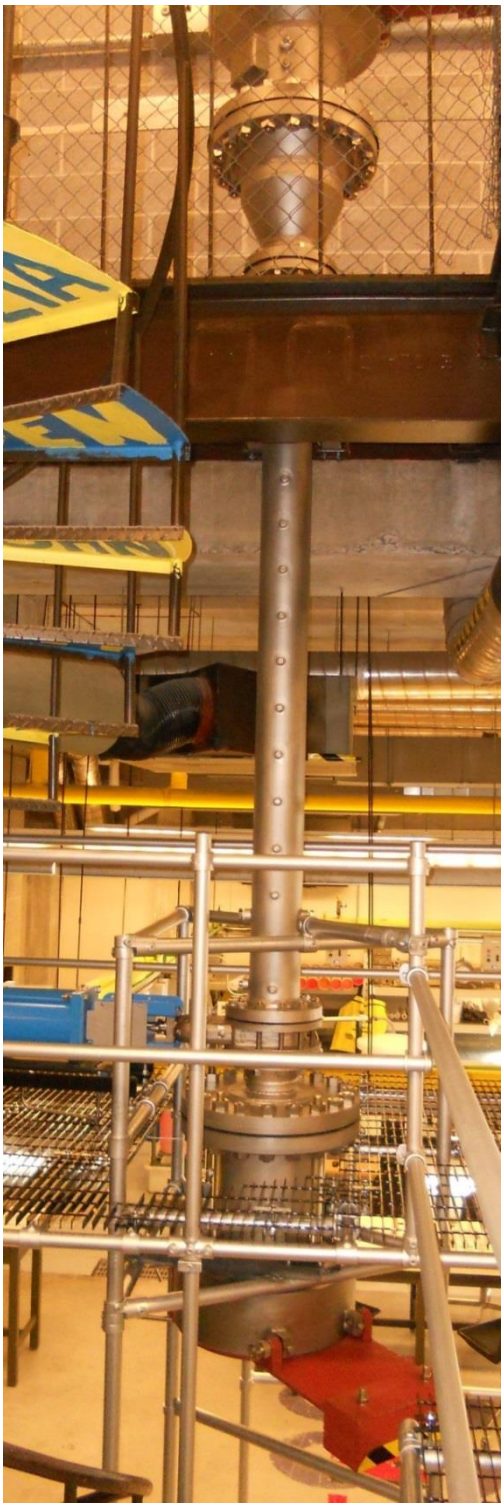

Figure C.2: Picture of the high-pressure fluidization column.

(a) (b)

Figure C.3: Pictures showing (a) the knife gate valve; (b) the modified blade of knife gate valve to serve as the perforated plate.

(a)

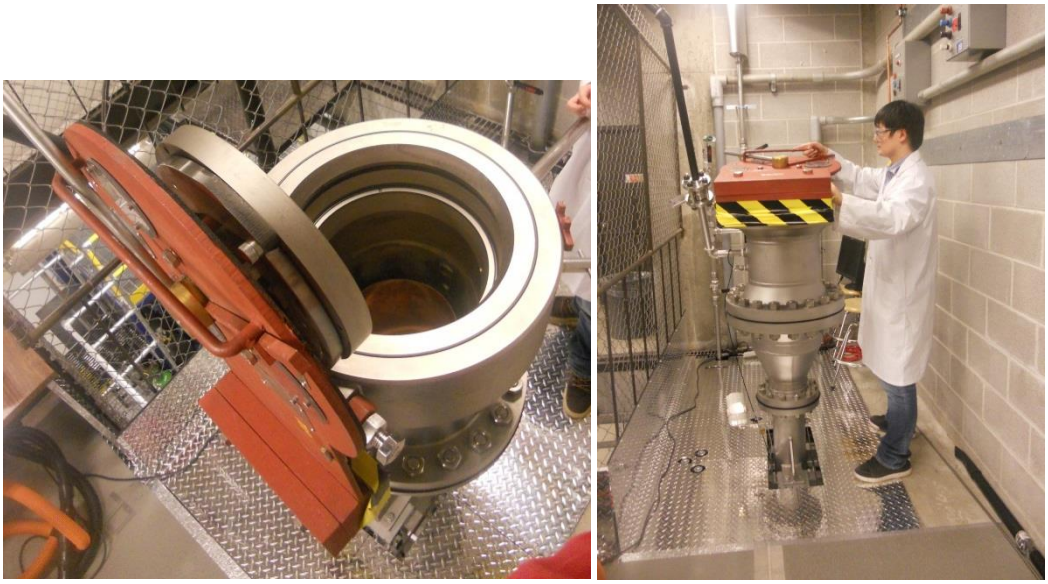

(b)

Figure C.4: Pictures of (a) bottom and (b) top manways.

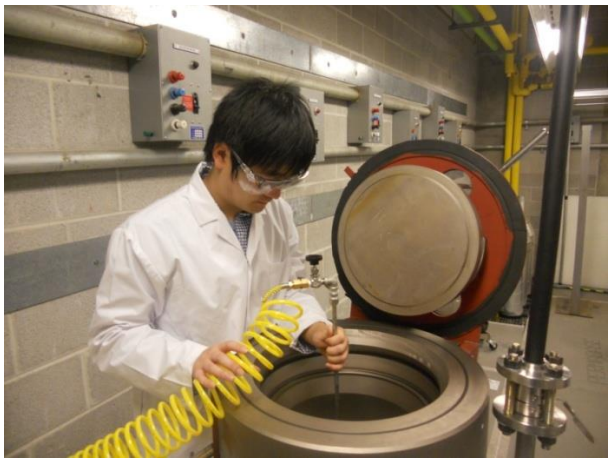

Figure C.5: Image showing the stainless steel tube held at the centre of column and attached to the building compressed air to allow the dislodge of the wall particles into the bottom Faraday cup.

C.2 Charged particle separator (CPS)

A charge particle separator developed in this research team by Salama *et al.* [10] was used in this thesis to analyze the charge distribution of particles, especially those adhered to the column wall. As shown in Figure C.6, the charged particle separator consisted of two inclined copper plate and four Faraday cups. Each of the two copper plates were 0.457 m in length and 0.305 m in width. The distance between the top of the two plates was 0.203 m, and that between the two bottoms was 0.686 m. The number 1 to 4 Faraday cups (abbreviated as FC) were placed in a row at the bottom of the separator. Each Faraday cup was connected to a Keithley digital electrometer to measure the charge of particles collected inside. The copper plates and Faraday cups were placed in a PVC box for safety reasons. An Ultravolt HV-Rack-250-00265 power source was connected to the two copper plates making one plate positively charged, and the other negatively charged. The voltage applied was varied between 15 to 45 kV. When charged particles were slowly dropped between the two plates, the negatively charged particles would be attracted towards the positively charged plate and fall into FC1 and FC2, and the positively charged particles would fall into FC3 and FC4.

The charged particle separator was modified to fit under the high-pressure pilot-scale fluidization column to analyze the charge distribution of wall particles. Although the CPS unit is portable and could be easily placed under the high-pressure column but due to the larger bottom expanded section of the column, the particles had to travel a larger distance before being dropped between

the plates of the CPS unit. Thus, as shown in Figure C.7, a 0.15 m (6 inch) diameter cardboard pipe was inserted into the bottom expanded section from the bottom of the column right below the distributor plate. The other side of the tube was place right above the CPS unit.

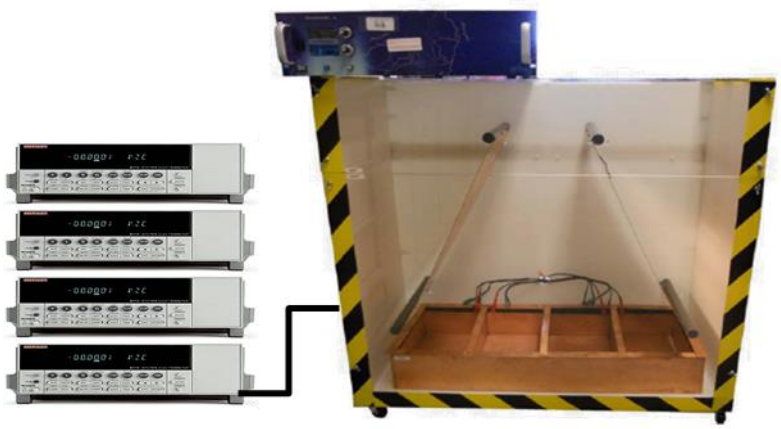

Figure C.6: Picture of the charged particle separator (CPS) unit.

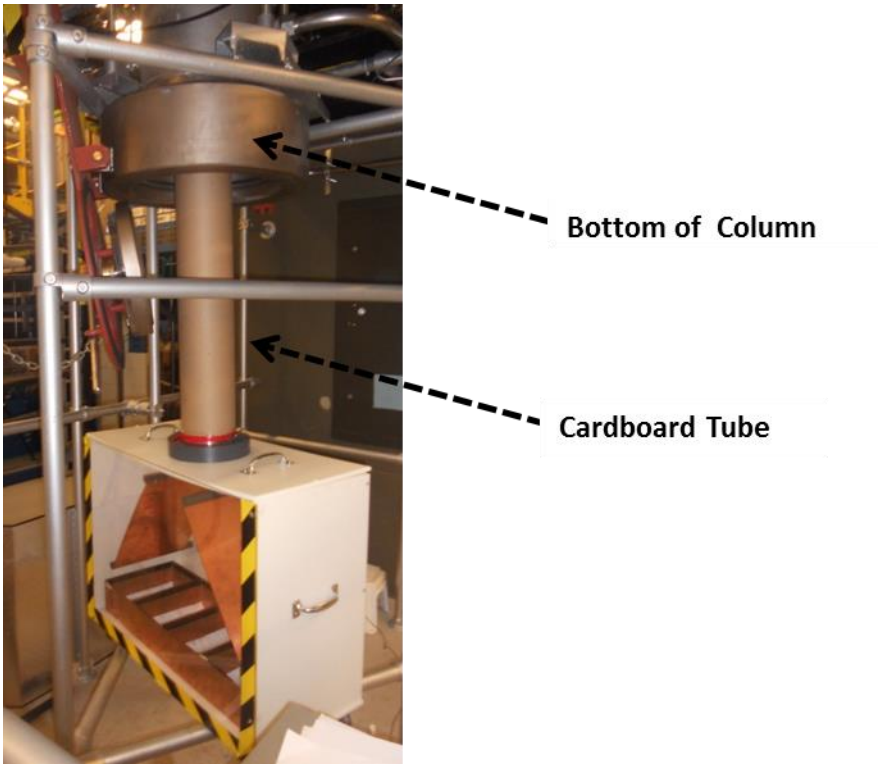

Figure C.7: Picture of modified charged particle separator placed under the high-pressure fluidization column.

C.3 Picture of the atmospheric gas-solid fluidization system

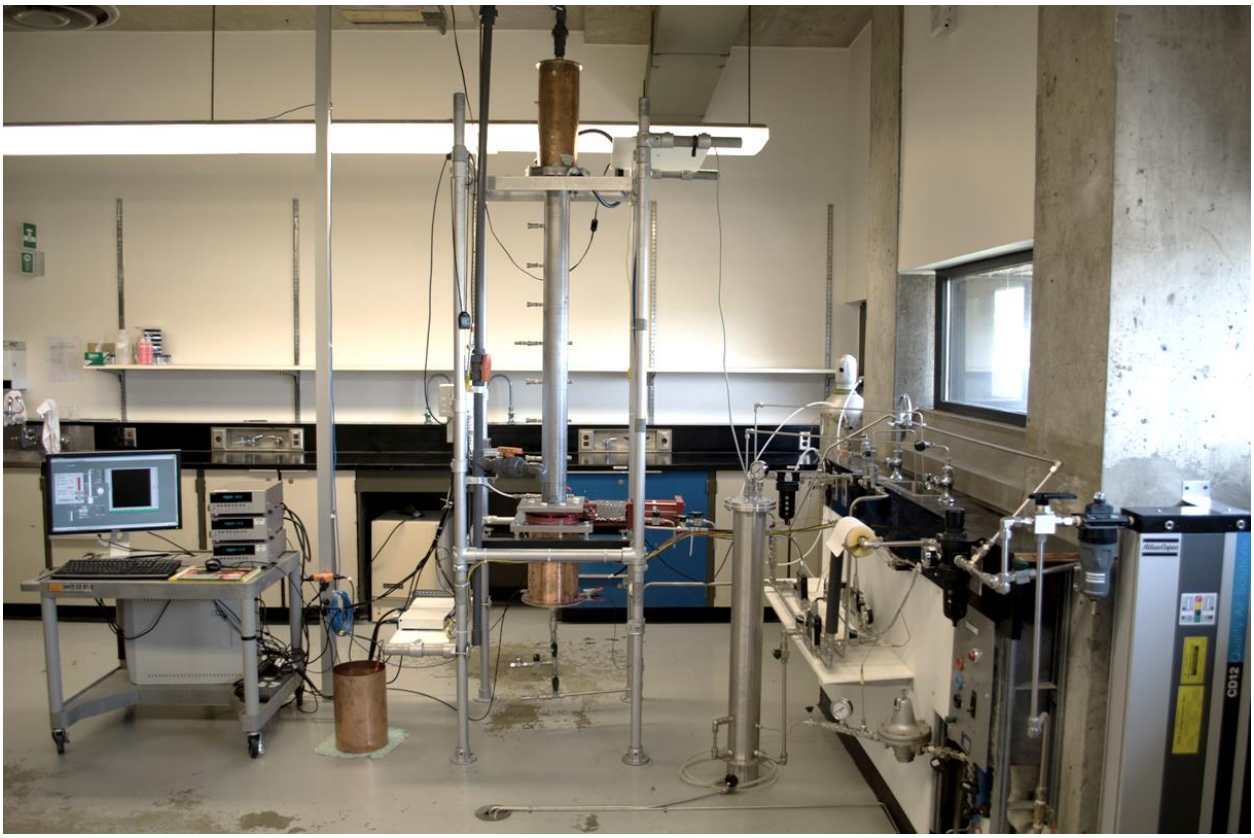

Figure C.8: Picture of the atmospheric gas-solid fluidization system.

Appendix D
Experimental materials

This section focuses on the characterization of experimental materials utilized in this thesis, including the fluidizing gas and the solid particles.

D.1 Fluidizing gas

For the open-loop atmospheric conditions, compressed building air was used as the fluidizing gas. Building air was at 891 kPa (abs), and on average at 3% relative humidity and 21.0°C.

For closed-loop experiments, nitrogen from a gas cylinder (grade 5.3 with composition shown in Table D.1) was used. Nitrogen was used since in industrial polyethylene reactors nitrogen is used for catalyst injection and using this gas from a gas cylinder allows for a clean and low humidity gas.

Table D.1: Composition of GR 5.3 nitrogen gas, supplied by Linde.

Components	Composition
N_2	100.00%
CO	< 1 ppm
CO_2	< 1 ppm
H_2O	< 1 ppm
O_2	< 2 ppm
THC	< 0.5 ppm

D.2 Fluidizing particles

Two types of linear low-density polyethylene resins and glass beads were used as fluidizing particles.

D.2.1 Polyethylene resins

Two types of linear lowdensity polyethylene resins (LLDPE) directly received from commercial gas-solid fluidized reactors, named as PE_A and PE_B, were used in this work. PE_B was utilized in experiments presented in Chapter 2 – 5, while PE_B was used in the experiments in Chapter 6.

The resins were supplied by Univation Technologies, LLC (USA), and were produced using a metallocene catalysts.

The physical and electrical properties of the two resins are shown in Table D.2. The particle densities were provided by Univation Technologies LLC (USA). Samples of the as received polyethylene resins were taken for particle size distribution measurements using a Malvern Mastersizer 2000 with a Hydro 2000S particle dispersion unit. The electrical properties of the polyethylene resins were taken from literature [11–13].

Table D.2: Polyethylene resins physical and electrical properties.

		PE_A	PE_B
Physical Properties			
Density	kg/m3	918	915
dP10	µm	334.66 ± 22.13	346.49 ± 20.02
dP50	µm	578.01 ± 69.50	588.24 ± 33.72
dP90	µm	1286.08 ± 121.06	1006.52 ± 81.31
Geldart Group		B	B
Electrical Properties			
Permittivity	F/m	2.3	
Conductivity	S/m	1.1x10-13	
Work Function	eV	5.3	

D.2.2 Glass beads

A type of commercially available glass beads was used in the experiments presented in Chapter 3. The glass beads were purchased from Potters Industries LCC. The glass beads had a density of 2500 kg/m3, with particle size range of 430 – 600 µm.

Appendix references

[1] M. Liu, Y. Zhang, H. Bi, J.R. Grace, Y. Zhu, Non-intrusive determination of bubble size in a gas–solid fluidized bed: An evaluation, Chem. Eng. Sci. 65 (2010) 3485–3493.

[2] M. Rüdisüli, T.J. Schildhauer, S.M.A. Biollaz, J.R. van Ommen, Bubble characterization in a fluidized bed by means of optical probes, Int. J. Multiph. Flow. 41 (2012) 56–67.

[3] J.F. Davidson, Symposium on fluidization: discussion, Symp. Fluid. Discuss. 39 (1961) 230.

[4] G.B. Wallis, One-dimensional waves in two-component flow (with particular referenceto the stability of fluidized beds)., UKAEA Report, 1962.

[5] L. Fasso, B.T. Chao, S.L. Soo, Measurement of electrostatic charges and concentration of particles in the freeboard of a fluidized bed, Powder Technol. 33 (1982) 211–221.

[6] G. Tardos, R. Pfeffer, A method to measure electrostatic charge on a granule in a fluidized bed, Chem. Eng. Commun. 4 (1980) 665–671.

[7] F. Sharmene Ali, M. Adnan Ali, R. Ayesha Ali, I.I. Inculet, Minority charge separation in falling particles with bipolar charge, J. Electrostat. 45 (1998) 139–155.

[8] M. Bafrnec, J. Bena, Quantitative data on the lowering of electrostatic charge in a fluidized bed, Chem. Eng. Sci. 27 (1972) 1177–1181.

[9] R.W. Ham, P.A. Gauthier, M.A. Bergougnou, Electrostatic in an air/catalyst fluidized bed at ambient temperature and pressure, Fluid. Eng. Found. New York. (1992) 611–620.

[10] F. Salama, A. Sowinski, K. Atieh, P. Mehrani, Investigation of electrostatic charge distribution within the reactor wall fouling and bulk regions of a gas-solid fluidized bed, J. Electrostat. 71 (2013) 21–27.

[11] H. Masuda, K. Gotoh, K. Higashitani, S. Matsusaka, Adhesive Force of a Single Particle, in: H. Masuda, K. Higashitani, H. Yoshida (Eds.), Powder Technol. Handb., Third, CRC Press, Florida, 2006: pp. 157–170.

[12] M. Hindermann-Bischoff, F. Ehrburger-Dolle, Electrical conductivity of carbon black–polyethylene composites, Carbon N. Y. 39 (2001) 375–382.

[13] D.W. Pryer, P.F. Gale, Cables, in: M.A. Laughton, D.F. Warne (Eds.), Electr. Eng. Ref. B., Newnes, Oxiford, 2003: pp. 31–39.